C.2

TECHNICAL REPORT
NATICK/TR-88/071

AD A 198 774

INVESTIGATION OF ALTERNATIVE FRAMING ARRANGEMENTS USING PRESSURE-STABILIZED BEAMS FOR BATTALION AID STATION SUPPORT

BY

WALTER JOSEPH KRAINSKI, JR.

SEPTEMBER 1988
FINAL REPORT
APRIL 1985 TO SEPTEMBER 1986

UNITED STATES ARMY NATICK
RESEARCH, DEVELOPMENT AND ENGINEERING CENTER
NATICK, MASSACHUSETTS 01760-5000

AERO-MECHANICAL ENGINEERING DIRECTORATE

DISCLAIMERS

The findings contained in this report are not to be construed as an official Department of the Army position unless so designated by other authorized documents.

Citation of trade names in this report does not constitute an official endorsement or approval of the use of such items.

DESTRUCTION NOTICE

For Classified Documents

Follow the procedures in DoD 5200.22-M, Industrial Security Manual, Section II-19 or DoD 5200.1-R, Information Security Program Regulation, Chapter IX.

For Unclassified/Limited Distribution Documents

Destroy by any method that prevents disclosure of contents or reconstruction of the document.

UNCLASSIFIED
SECURITY CLASSIFICATION OF THIS PAGE

REPORT DOCUMENTATION PAGE

Form Approved
OMB No. 0704-0188
Exp. Date: Jun 30, 1986

1a. REPORT SECURITY CLASSIFICATION
UNCLASSIFIED

1b. RESTRICTIVE MARKINGS

2a. SECURITY CLASSIFICATION AUTHORITY

2b. DECLASSIFICATION / DOWNGRADING SCHEDULE

3. DISTRIBUTION / AVAILABILITY OF REPORT
Approved for public release; distribution unlimited

4. PERFORMING ORGANIZATION REPORT NUMBER(S)
NATICK/TR-88/071

5. MONITORING ORGANIZATION REPORT NUMBER(S)

6a. NAME OF PERFORMING ORGANIZATION
U.S. Army Natick RD&E Center

6b. OFFICE SYMBOL *(If applicable)*
STRNC-UE

7a. NAME OF MONITORING ORGANIZATION

6c. ADDRESS *(City, State, and ZIP Code)*
Natick, MA 01760-5017

7b. ADDRESS *(City, State, and ZIP Code)*

8a. NAME OF FUNDING / SPONSORING ORGANIZATION

8b. OFFICE SYMBOL *(If applicable)*

9. PROCUREMENT INSTRUMENT IDENTIFICATION NUMBER

8c. ADDRESS *(City, State, and ZIP Code)*

10. SOURCE OF FUNDING NUMBERS

PROGRAM ELEMENT NO.	PROJECT NO.	TASK NO.	WORK UNIT ACCESSION NO.
1L162723	A427	AB	020

11. TITLE *(Include Security Classification)*
INVESTIGATION OF ALTERNATIVE FRAMING ARRANGEMENTS USING PRESSURE-STABILIZED BEAMS FOR BATTALION AID STATION SUPPORT

12. PERSONAL AUTHOR(S)
Walter Joseph Krainski, Jr.

13a. TYPE OF REPORT
Final

13b. TIME COVERED
FROM Apr 85 TO Sep 86

14. DATE OF REPORT *(Year, Month, Day)*
September 1988

15. PAGE COUNT
115

16. SUPPLEMENTARY NOTATION

17. COSATI CODES

FIELD	GROUP	SUB-GROUP

18. SUBJECT TERMS *(Continue on reverse if necessary and identify by block number)*
ARCHES, STRESSES, LIGHTWEIGHT, BEAMS(STRUCTURAL), (over)
FRAMES, MOBILE, LOADS(FORCES), PROTECTIVE EQUIPMENT,
TENTS, SUPPORTS, STRUCTURES, STRENGTH WEIGHT RATIO,

19. ABSTRACT *(Continue on reverse if necessary and identify by block number)* HOSPITALS. (JES)

This study investigates Leaning Arch and Vertical Arch framing schemes using pressure-stabilized beams for the support of a Battalion Aid Station (BAS) tent structure. Stress and displacement results are tabulated and plotted for various beam diameters and inflation pressures. Environmental conditions considered in the analysis include a snow load of 10 psf and a wind load of 30 mph directed both perpendicular and parallel to the tent axis. The use of guylines to reduce wind-induced stresses and deflections is also investigated. Based on the results obtained for the various framing arrangements, conclusions are drawn for an optimum BAS tent frame design to support varied loads.

20. DISTRIBUTION / AVAILABILITY OF ABSTRACT
☒ UNCLASSIFIED/UNLIMITED ☐ SAME AS RPT. ☐ DTIC USERS

21. ABSTRACT SECURITY CLASSIFICATION
UNCLASSIFIED

22a. NAME OF RESPONSIBLE INDIVIDUAL
Walter Joseph Krainski, Jr.

22b. TELEPHONE *(Include Area Code)*
(508) 651-5264

22c. OFFICE SYMBOL
STRNC-UE

DD FORM 1473, 84 MAR — 83 APR edition may be used until exhausted. All other editions are obsolete.

SECURITY CLASSIFICATION OF THIS PAGE
UNCLASSIFIED

18. SUBJECT TERMS (Cont'd)

PRESSURIZATION
STRUCTURAL ANALYSIS
WIND

PREFACE

This study was conducted as part of an ongoing program at the U.S. Army Natick Research, Development and Engineering Center (Natick) to develop a lightweight, highly mobile, chemically protected Battalion Aid Station (BAS) tent structure for emergency medical use in forward battle areas to replace the M51. This work was funded under the in-house work unit entitled, "Chemically Hardened Shelter System(s): BAS In-House Design Optimization." The author wishes to thank Mr. Joseph Bozluk and Dr. Earl C. Steeves for their kindly cooperation and assistance throughout the course of this study. Because units in this report refer to U.S. equipment and usage, U.S. customary units are used throughout the text.

TABLE OF CONTENTS

LIST OF FIGURES

Page

LIST OF TABLES

Page

I. INTRODUCTION

There is presently a need within the Army community for a new Battalion Aid Station (BAS) tent structure to replace the existing M51 system. In order to provide emergency medical services in the forward battle areas, a structure that is by nature both lightweight and highly mobile is required. Present mobility requirements call for three or more moves per day, which necessitates use of a lightweight tent structure of small packaged volume that can be set up and disassembled in a minimum amount of time.

One of the more promising concepts for meeting these requirements was that of a tent with support framing of highly pressurized fabric structural beam elements. These thin-walled pressurized tube elements support the lightweight fabric barrier, which in turn provides the necessary levels of chemical and biological protection. It is pressurized-beam-supported tent structures of this nature that are the focus of this study.

This report examines two alternative pressurized-arch-beam arrangements for supporting the BAS tent structure. These framing concepts are referred to as the Leaning Arch and Vertical Arch configurations throughout the text. The objective of this study was to compare these arrangements and determine the relative advantages and disadvantages of each in terms of weight, deflections, and pressure needed to support the design loads.

Analytical investigations were conducted using the Nonlinear Finite Element Structural Analysis (NONFESA) computer code.[1] This program for the analysis of stresses and deflections in frame-supported tents, as originally conceived, included both a conventional beam element and a nonlinear membrane element for modelling the fabric barrier. Research conducted by Natick over the last decade culminated in the development of a pressure stabilized beam finite element, which was incorporated into this code.[2] This member type was used almost exclusively in modelling the various support framing arrangements chosen for investigation. This study focused exclusively on the tent support framing structure. For this reason no attempt was made to model the tent skin using the nonlinear membrane element type, and only the linear elastic three-dimensional beam and pressurized beam member types were used in the analysis. Pressures resulting from wind and snow acting over the tent surface, therefore, had to be decomposed into forces and applied as point loads at the nodes connecting the various beam members comprising the structure.

Models of each of these framing schemes were constructed in two tent sizes. First, a tent 18 feet wide by 22 feet long, providing approximately 400-square feet of usable floor area, was considered. Next, consideration was given to a 300-square foot tent structure with overall width of 18 feet and length of 17 feet. Each framing arrangement was analyzed for environmental loadings of snow and wind. Design snow loads of 5 and 10 pounds per square foot (psf) were individually examined. Forces resulting from a steady wind speed of 30 miles per hour (mph) were taken as design wind conditions. Winds acting along both of the structure's major axes were separately examined. In order to determine the effects of guylines in reducing wind-induced stresses and deflections, the structures were also investigated for wind both with and without guylines included in the model.

Each framing arrangement was investigated for pressurized beam diameters of 8, 11, and 14 inches at a number of inflation pressures between 1.5 and 10 psi. Analytical results of this computer study were summarized in a series of graphs and tables. This information is shown in the Appendices of this report. These results were then used to compare the various framing configurations. Conclusions drawn from this comparison were then used to make recommendations concerning minimum weight designs that make use of as much of the available pressure as possible. Acknowledging the possibility that beam inflation pressures may have to be further restricted, general comments were also made concerning optimum designs for lower levels of maximum inflation pressure.

II. BAS STRUCTURAL ANALYSIS

A. Geometric Arrangements

Analyses were performed using the nonlinear finite element structural analysis computer code, NONFESA. As noted earlier, only the tent support framing was included in the finite element models. Therefore, all analyses assume linear, elastic material behavior throughout, since this is a basic assumption of both the beam and pressurized beam members used to model the support framing.

The pressurized arches were approximated using a series of straight beam segments to conform to the curvature of the arch. The stiffness matrix formulation of these linear elastic beam elements, similar to those used in many computer codes, as previously noted, had been further modified to account for internal pressurization effects. The relatively short length of these beam elements (<2 feet) insured both close approximation of the framing geometry as well as calculation of forces and displacements at a representative number of nodal points over the structure. This information provided a better understanding of not only the frame structures' stress state but also deflection under load.

Analytical investigations focused on two tent sizes that would respectively provide usable floor areas of approximately 300 and 400 square feet. Overall tent width in all cases was taken to be 18 feet. Overall tent structure lengths of 17 and 22 feet were assumed to satisfy the respective floor area requirements of 300 and 400 square feet. All studies were conducted with the pressurized arch beams spanning the 18 foot dimension. This greatly simplified not only the geometric construction of finite element models for the various BAS structural concepts to be investigated but also the calculation of environmental loads on each of these structures, leading to considerable savings in both the time and effort to investigate adequately a representative number of support schemes. Table 1 summarizes the various parameters investigated including tent size, framing arrangement, snow and wind loading, wind loading direction, beam diameter, beam inflation pressure, and the analyses for wind loadings both with and without guylines.

TABLE 1: Variables Involved in Analyses of Two Tent Sizes

Framing Arrangements	Tent Size (sq ft)	Loading	Guylines	Beam Dia. (in)	Beam Inflation Pressures (psi)
Leaning Arch Configuration	400	10 psf snow	-	8, 11 14	1.5,3,5,7,10 1.5,3,4,5,7.5,10
		30 mph wind	with & without	8, 11 14	1.5,3,5,7,10 1.5,3,4,5,7.5,10
		30 mph prl wind	with & without	8, 11 14	1.5,3,5,7,10 1.5,3,4,5,7.5,10
Vertical Arch Configuration	400	10 snow	-	8,11,14	1.5,3,5,7,10
		30 wind	w & w/o	8,11,14	1.5,3,5,7,10
		30 prl wd	w & w/o	8,11,14	1.5,3,5,7,10
Leaning Arch Configuration	300	10 snow	-	8,11,14	1.5,3,5,7,10
		30 wind	w & w/o	8,11,14	1.5,3,5,7,10
		30 prl wd	w & w/o	8,11,14	1.5,3,5,7,10
Vertical Arch Configuration	300	10 snow	-	8,11,14	1.5,3,5,7,10
		30 wind	w & w/o	8,11,14	1.5,3,5,7,10
		30 prl wd	w & w/o	8,11,14	1.5,3,5,7,10

The geometry of the pressurized arch span was chosen so as to provide the greatest amount of usable floor area and headroom as possible near the sides of the tent structure. As shown in Figure 1, this space allotment was accomplished by varying the radius of the pressurized arch over its 180 degree arc. Over the initial and final 19.44 degrees of the arch, the arc radius is 18 feet, providing 6 feet of head room, a distance of 12 inches in from the inside bottom edge of the tent. Over the remaining 141.12 degrees of the arch's span, the radius of the arc is 8.456 feet. Thus, at center span the distance between the floor and center line of the pressurized beam cross section is 11.632 feet.

Two framing arrangements were analyzed for each of the two tent sizes, designated the Leaning Arch (LA) and Vertical Arch (VA) configurations. The Leaning Arch structure consisted of six pressurized beam arches of circular cross section, as previously described. Pairs of these arches were inclined to each other and joined at the apex to form three distinct bays along the tent structure's longitudinal axis. Spacing of arch members was seven and one third feet at the base, with an angle of inclination to each other of 72.50 degrees for the 400 square foot structure. Comparable 300 square foot tent structure dimensions were five and two-thirds feet and 76.31 degrees, respectively.

The finite element model of the Leaning Arch structure is shown in Figure 2. The basic model consisted of 114 nodal points and 96 pressurized straight beam elements. The first 95 nodal points are used to define the tent structure geometry, while the remaining 19 node points are used to define the orientation of each of the beam element's local coordinate axes. These 19 points, therefore, have their three displacement and three rotational degrees-of-freedom deleted from the matrix of equilibrium equations.

Figure 3 illustrates use of this third nodal point in determining the local coordinate axes. The I node defines the origin of the beam's local "1" axis. The positive direction of the local "1" axis is established as being from node I to node J. The K node, as shown, may be any node in the structure contained in the local 1-2 plane that does not lie on the local "1" axis. The local "2" axis is defined along a line perpendicular to the local "1" axis and

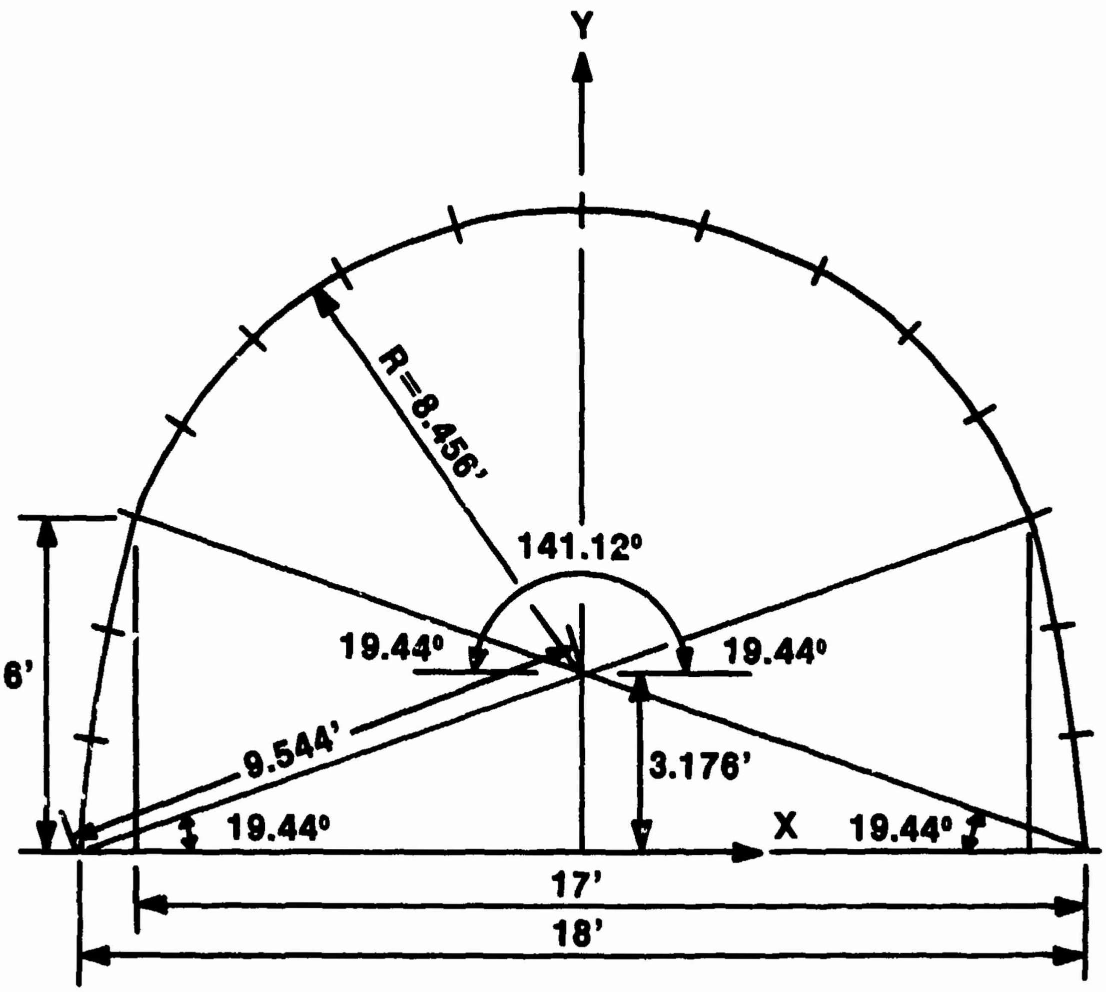

Figure 1. Vertical projection of arch geometry

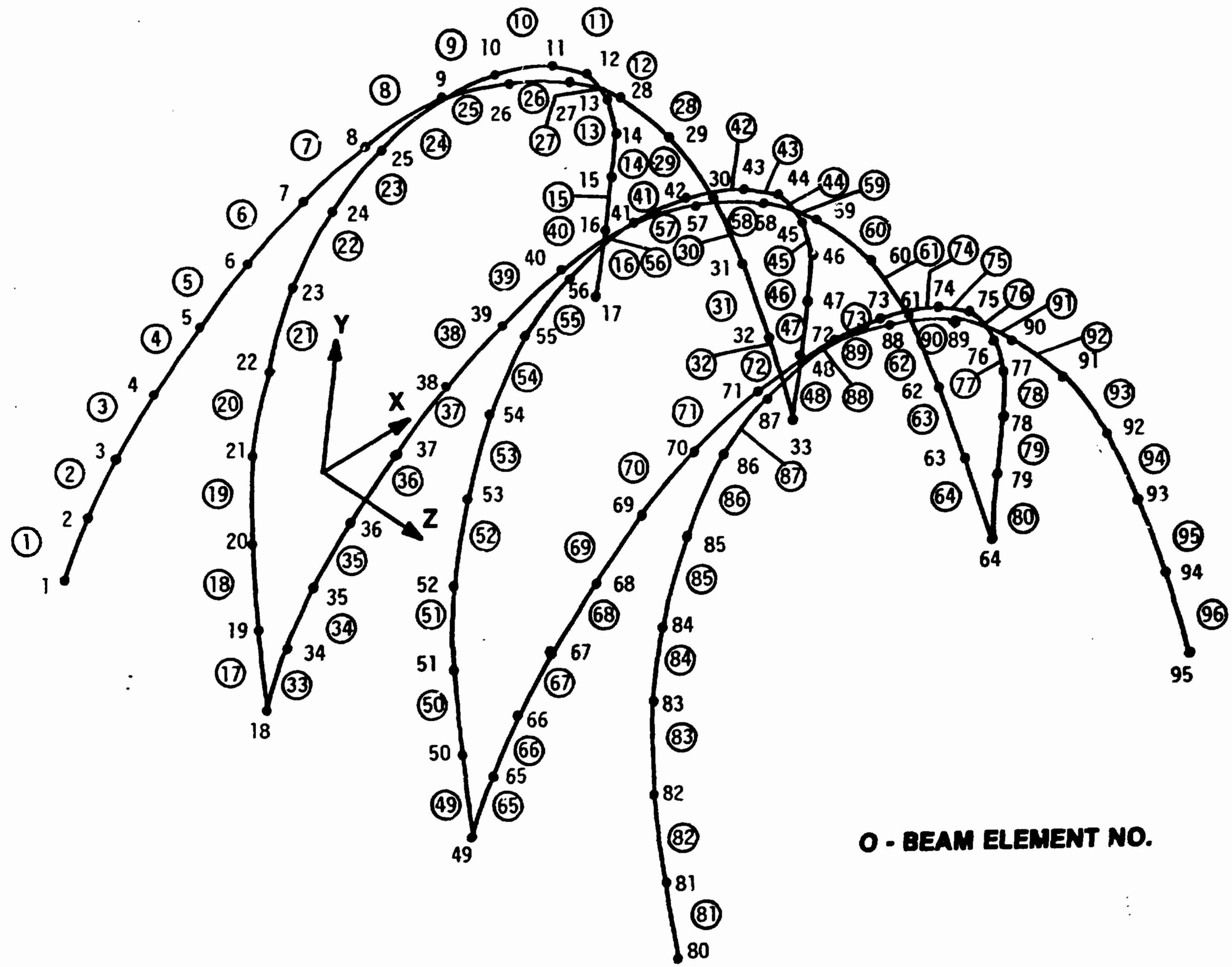

Figure 2. NONFESA model of Leaning Arch configuration showing node numbers, beam element numbers, and global coordinate axes

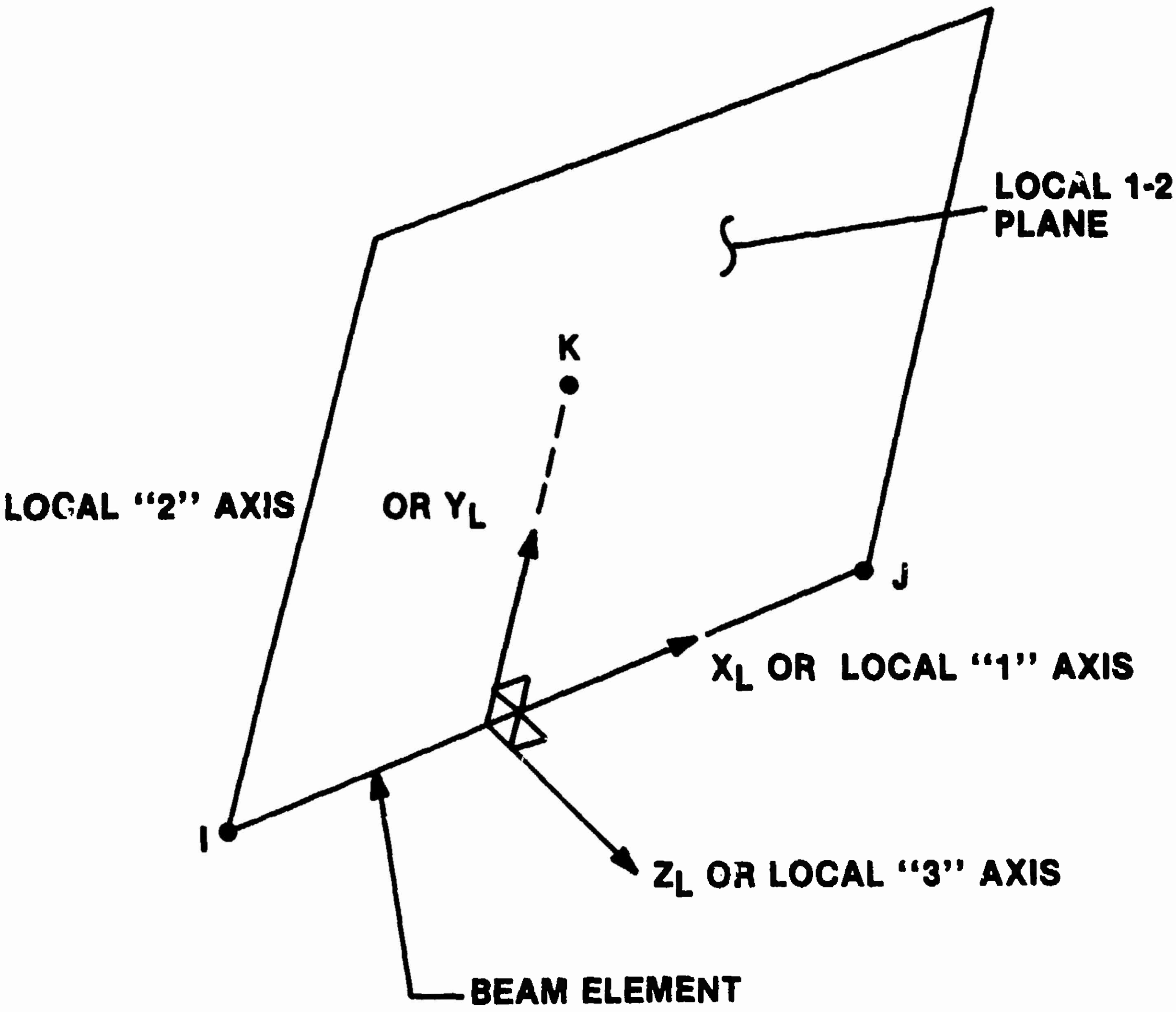

Figure 3. Use of additional node "K" to determine local coordinate axes

passing through node K. The positive local "2" direction is established as being from the local "1" axis to node K. The positive local "3" direction is then determined by the cross-product of the local "1" and "2" axes or right-hand rule.

The Vertical Arch structure analyzed consisted of five pressurized beam arches of circular cross section equally spaced along the longitudinal axis. Arch geometry in the direction of the span was as previously described. Lateral stability was provided to these arches by rigidly attaching them to another straight beam spanning the entire length of the tent structure. This longitudinal member was not assumed to be a pressurized beam element, but instead to be made of wood, specifically spruce, with a four-inch by two-inch cross section. The arch beams were attached to this member at the middle of the arch span. This spruce beam, it was felt, would provide adequate stiffness and strength for the anticipated loads, yet be relatively light in weight compared to other wood types. Location and orientation of this wood beam member in the structure is shown in Figure 4. A pressurized beam member was ruled out in this instance, since it would have made design and fabrication of the tent support structure unduly complex, and therefore, more expensive. The pressurized arch beams were spaced 5.50 feet apart for the 400-square foot tent size and 4.25 feet for the 300 square foot structure. As shown in Figure 4, the wood beam used to provide lateral stability to the five vertical arches is continuous and would be strapped to the bottom surface of the arches in one manner or another.

This eccentricity of member attachment could not be modelled in the NONFESA code, but it would not be expected to change appreciably the results obtained in this study. The finite element model of the Vertical Arch structure is shown in Figure 5. The basic model is made up of 109 nodal points and 84 beam elements. The first 85 nodal points were used to describe the geometry of the frame structure. The last 24 nodes served to establish the direction of the local coordinate axes at each of the beam elements. Beam elements 1 thru 80 were used to represent the pressurized arch beams, while elements 81 thru 84 modelled the straight wood beam used to provide stability to the structure in the longitudinal direction.

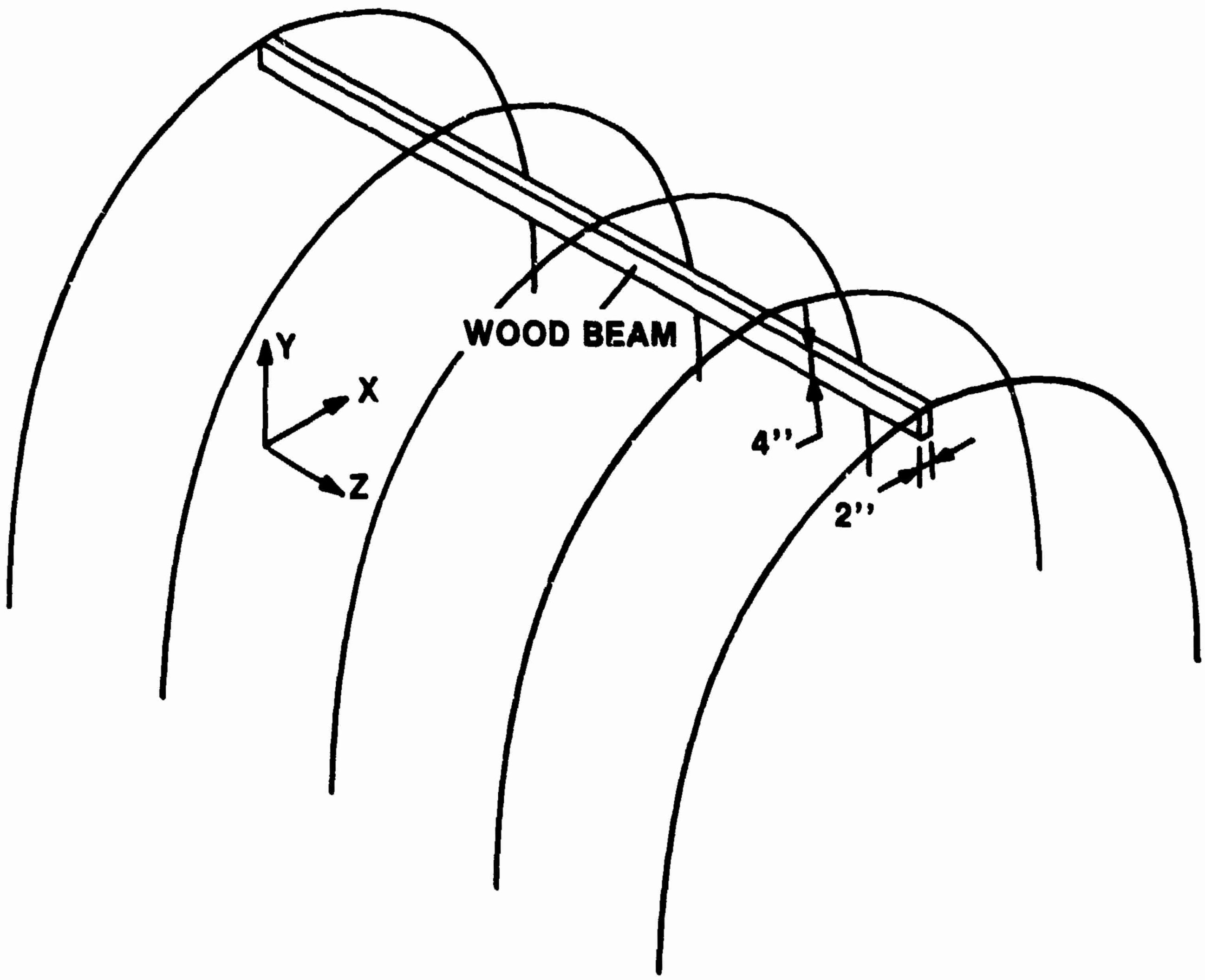

Figure 4. Orientation of 2 x 4 wood beam member in Vertical Arch configuration

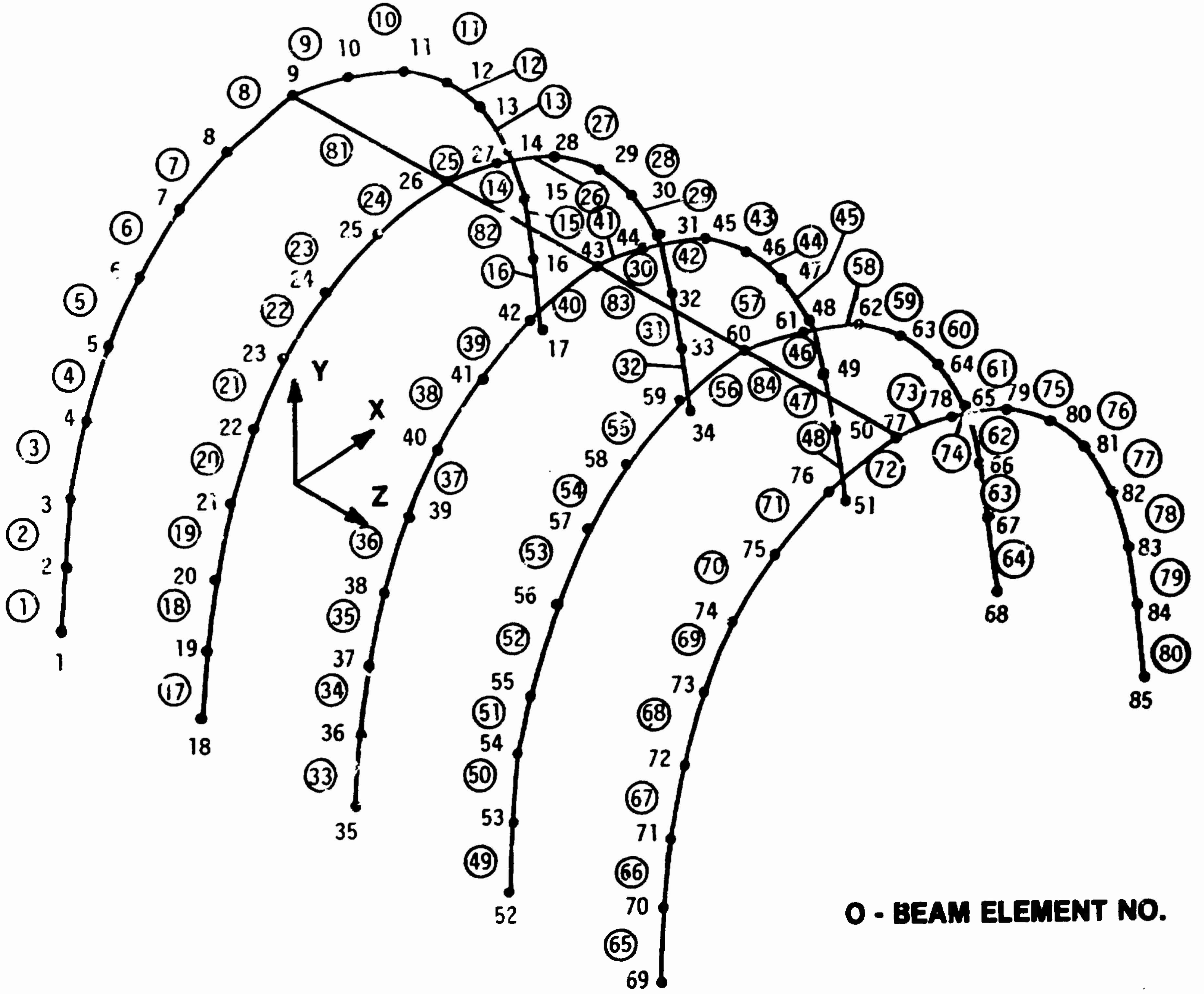

Figure 5. NONFESA model of Vertical Arch configuration showing node numbers, beam element numbers and global coordinate axes

It should be further noted that use of a solid beam member could represent a potential safety hazard in the event of a tube blow-out. Assessing this risk is beyond the scope of this study. Therefore, it is recommended that this risk be examined and weighed carefully, before this support scheme is adopted.

B. Support Boundary Conditions

The comparison of alternative framing support arrangements and the determination of minimum required pressures presume a high degree of confidence in both the accuracy and conservatism of the idealized structure analyzed. Since structural analysis results can be greatly affected by the choice of support boundary conditions, either an accurate or conservative means had to be found to model this parameter. If a knowledge of soil conditions exists and if deep, massive foundations and heavy connections are involved, reasonable assumptions about the rigidity of the support can in most instances be made. These conditions are not found in the BAS tent structure, which has a mission scenario that dictates it be lightweight and mobile, that is, easily transported, erected, taken down, and moved to a new location. Therefore, simple classification of support type or even experimental determination of the degree of fixity is virtually impossible to obtain in this case.

The rigidity of the anchorages used to secure the pressurized arch beams down to the ground surface is greatly influenced by such factors as the type of soil, moisture content, and temperature. Other factors affecting support rigidity include number, type, and diameter of stakes, depth of stake penetration, and method of attachment to the beam cloth material. At the time this study was initiated, details for securing the prototype BAS designs to the ground surface were not available. Even if they had been, however, the variation in soil parameters alone would still have precluded any rigorous attempt to model support boundary conditions.

For the above reasons it was decided instead to attempt to bound the problem, by assuming boundary conditions that would reasonably approximate beam-end conditions, yet lead to conservatively higher predictions of pressurized beam stresses and displacements. A combination hinged (X-, Z-Global Directions) and fixed end (Y-Global Direction) support was therefore chosen and adopted for use in analyses. For this type support, displacements along the three global axes were set to zero, as was rotation about the global Y-axis. Free rotation of the support, however, was permitted about the global X- and Z-axes. This effectively prevented the transfer of bending moments to the support, thus providing a more flexible pressurized arch structure to carry bending loads produced by the imposed loadings, while allowing the transfer of axial, shear, and torsional loads into the soil mass.

Use of these boundary conditions was judged conservative based on a comparison of a simply-supported beam carrying a uniformly distributed load versus a uniformly loaded beam fixed at both ends. The maximum bending moment along the simply-supported beam's span is 50 percent larger than that of the beam with fixed ends. The effect on deflections is even more pronounced, as the maximum deflection of the simply-supported beam is five times that of the beam with built-in ends. If one thinks of the individual pressurized arches as either simply-supported or built-in curved beams, the same analogy can be drawn. The arches with ends free to rotate will carry a given load at higher stress levels and deflect more than a comparable arch with fixed ends. This fact becomes more significant when one considers that bending moments are by far the single greatest contributor to stresses that cause wrinkling of the fabric.

C. Loading Conditions

As previously noted, the various BAS tent support framing arrangements were investigated for both a snow load of 10 psf, as well as a wind load of 30 mph directed along each of the two major tent axes. Internal pressurization of the tent itself was ignored in the analysis. Operations in a Chemical/Biological (CB) environment require pressures amounting to upwards of one inch of water or 5.197 psf in order to prevent infiltration by outside agents. Tent internal pressurizations of this magnitude would be very effective in offsetting stresses and deflections due to combined snow and wind loading. Pressurizing the tent would also tend to reduce sagging of the tent's fabric skin, thereby reducing pockets in which snow could accumulate. However, operational scenarios envision that the BAS tent will not be pressurized at all times, and therefore, a more critical loading condition exists when snow and wind are acting alone in the absence of this internal pressure load.

Snow and wind loads, in general, are prescribed as uniform or variable pressures acting over either the entire structure or a portion of it. Currently available research provides little information correlating snow accumulation to wind speed for various structure geometries. Nor would this cover the case in which snow accumulates on the structure, and then winds increase at a later time with the snow already present. Obviously both loads could, and quite often do, occur simultaneously. This leaves little recourse but to consider the two loads acting either simultaneously, which is the most conservative assumption, or separately at increased statistical risk. Whether or not snow and wind loads should be assumed to act simultaneously on a structure is problematical, since a high wind is likely to remove much of the snow. Moreover, one would not expect the maximum stresses resulting from snow and wind loads to occur generally at the same location on the structure. Nor would one expect peak stresses due to snow and wind at a given location to occur generally at the same orientation around the circumference of the pressurized tube. Therefore, for analysis purposes snow and wind loads were investigated separately.

This less conservative approach was logically more sound, because tent collapse cannot be considered the catastrophic event that failure of a massive, permanent structure would be. That is, of course, unless failure occurred while the tent was under attack by chemical or biological agents, and casualties resulted from the infiltration of agent(s) through tears in the tent fabric. This type of failure is highly unlikely, however, since internal tent pressurization will be upwards of 5.197 psf in a CB environment, which will add additional stiffness and strength to the structure for resisting snow- and wind-induced loads.

As noted earlier, the NONFESA computer model of the BAS tent structure included only the support framing, and not the tent fabric. This meant that snow and wind load pressures acting over the tent structure's exterior skin had to be broken down into concentrated forces in the three global coordinate directions at each nodal point. To aid in the determination of projected areas over which snow and wind pressures would be acting, plan and elevation views of the BAS tent structure were respectively drawn. These projections are shown in Figures 6, 7, and 8. Use of these projections greatly simplified load calculations by reducing the problem of three-dimensional curvature and constantly varying geometry into a two-dimensional flat plane problem. Computing nodal loads, particularly for the Leaning Arch configurations, was greatly facilitated through use of these projections.

Snow loads were assumed to act over an arc length of 60 degrees, 30 degrees to either side of the top or center line of the tent arches. As previously noted, a uniform pressure of 10 psf acting in the negative Y-global direction was used in the analyses. Figure 6 shows the actual and assumed plan view projected areas of the Leaning Arch configuration for this load. One can see that the arch members in reality are curved when viewed in this plane. Assumption of constant slope for the pressurized arch beams from the edges to the center of the tent as shown, however, greatly simplified the calculation of plan view snow load projected areas. The error introduced was minimal and on the conservative side, given the fact that the snow load was concentrated nearer the center of the tent arches. The total snow load calculated was therefore slightly greater overall, as well as slightly larger at the five nodal points on each of the end arches, than if the actual geometry had been used.

As shown on the right of Figure 6, the areas between nodes on the support framing were partitioned into triangular and trapezoidal shaped regions. Triangular regions were further broken down into three oblique angled triangles with common coordinate determined by the intersection of the medians of the three sides. Trapezoidal regions were decomposed into four oblique triangles by drawing the two cross diagonals. By knowing the projected lengths and angles of inclination between adjacent nodal points on the support framing, it was possible to calculate the length of each side of each triangle using the Law of Cosines. Having obtained the lengths of the three sides of each triangle, it then became a simple matter to calculate the projected area of each triangle using another trigonometric formula relating area to the semiperimeter and length of each of the three sides.

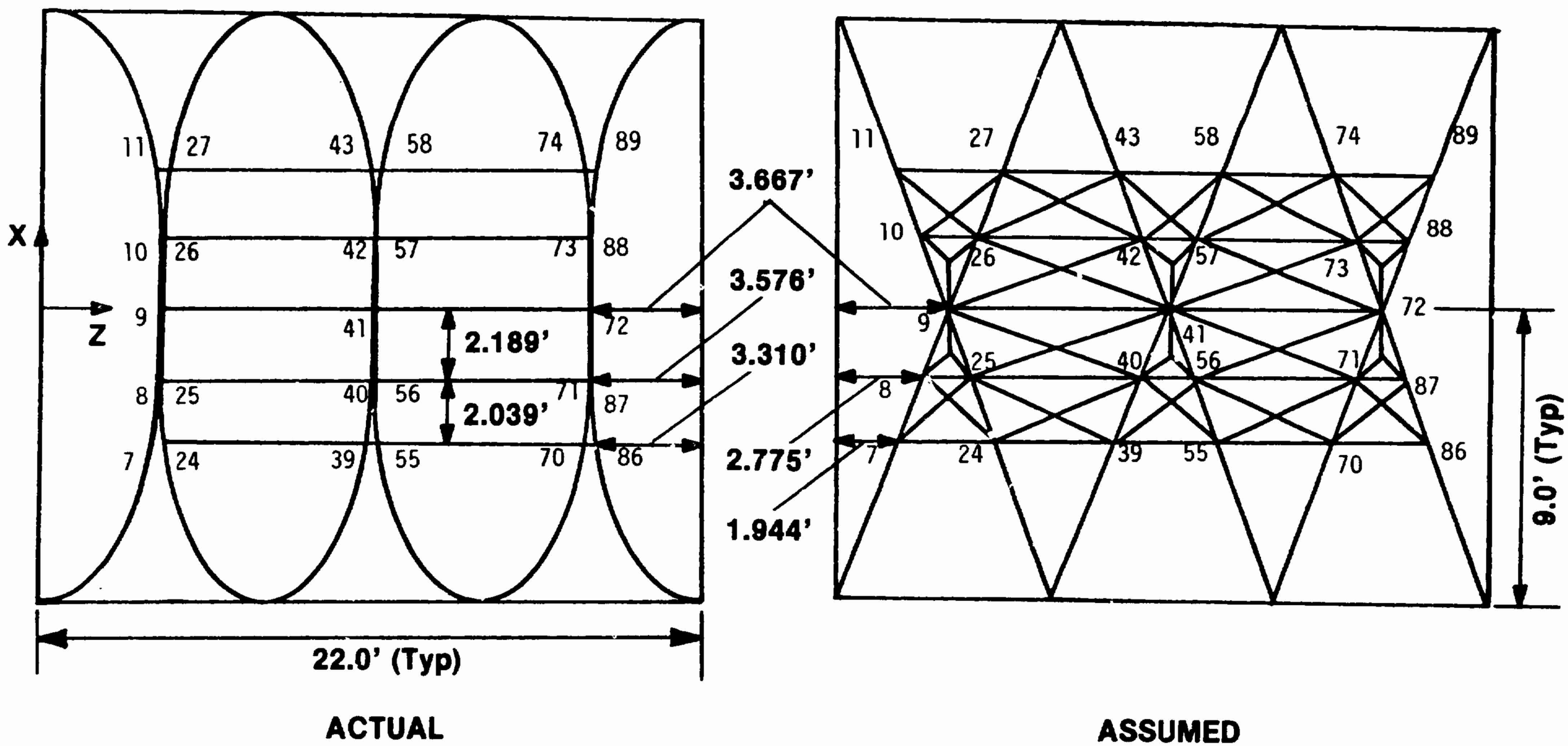

Figure 6. Actual and assumed flat plane snow load projected area - 400 sq ft Leaning Arch BAS plan view

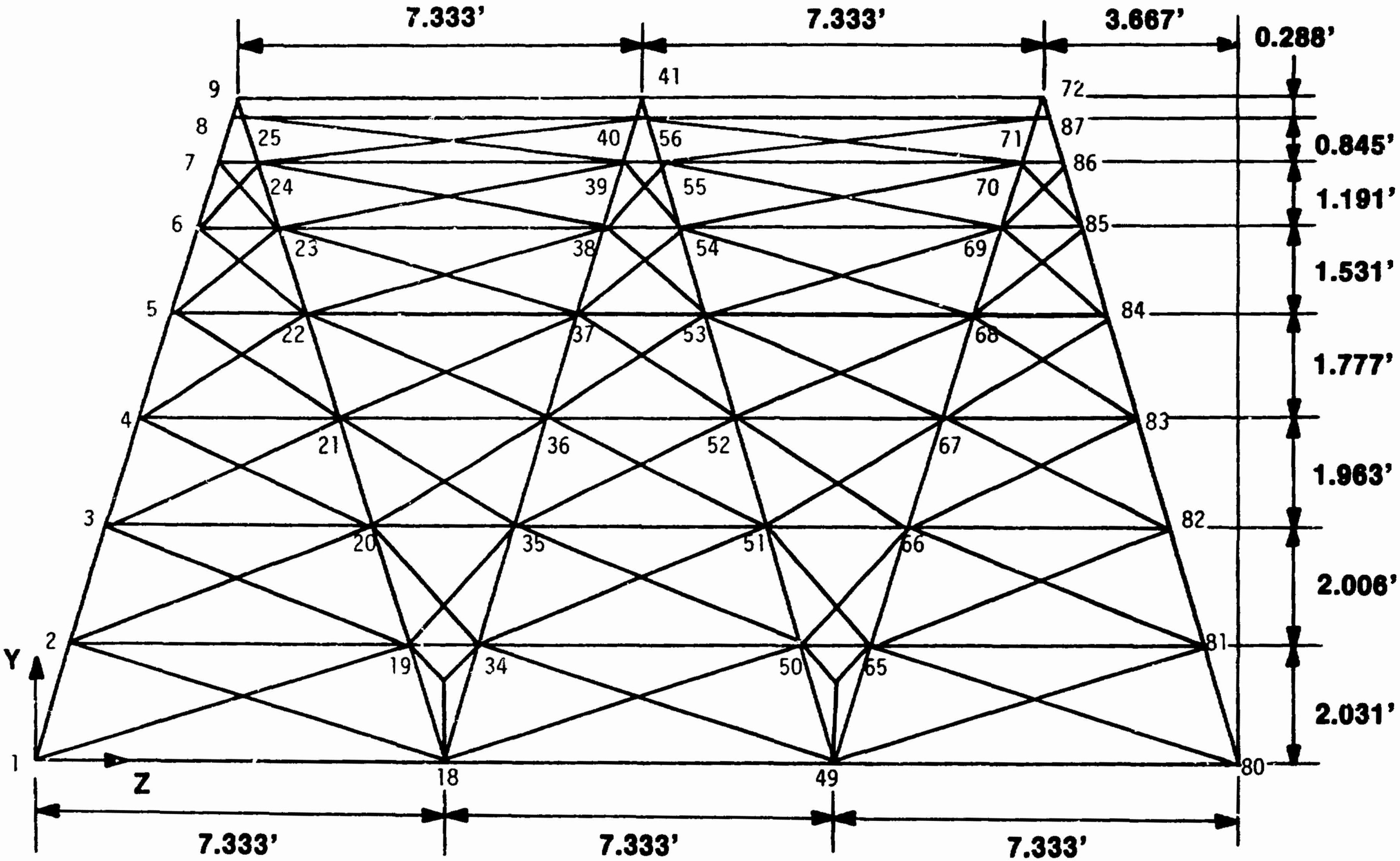

Figure 7. Flat plane wind load projected area - 400 sq ft Leaning Arch BAS side view

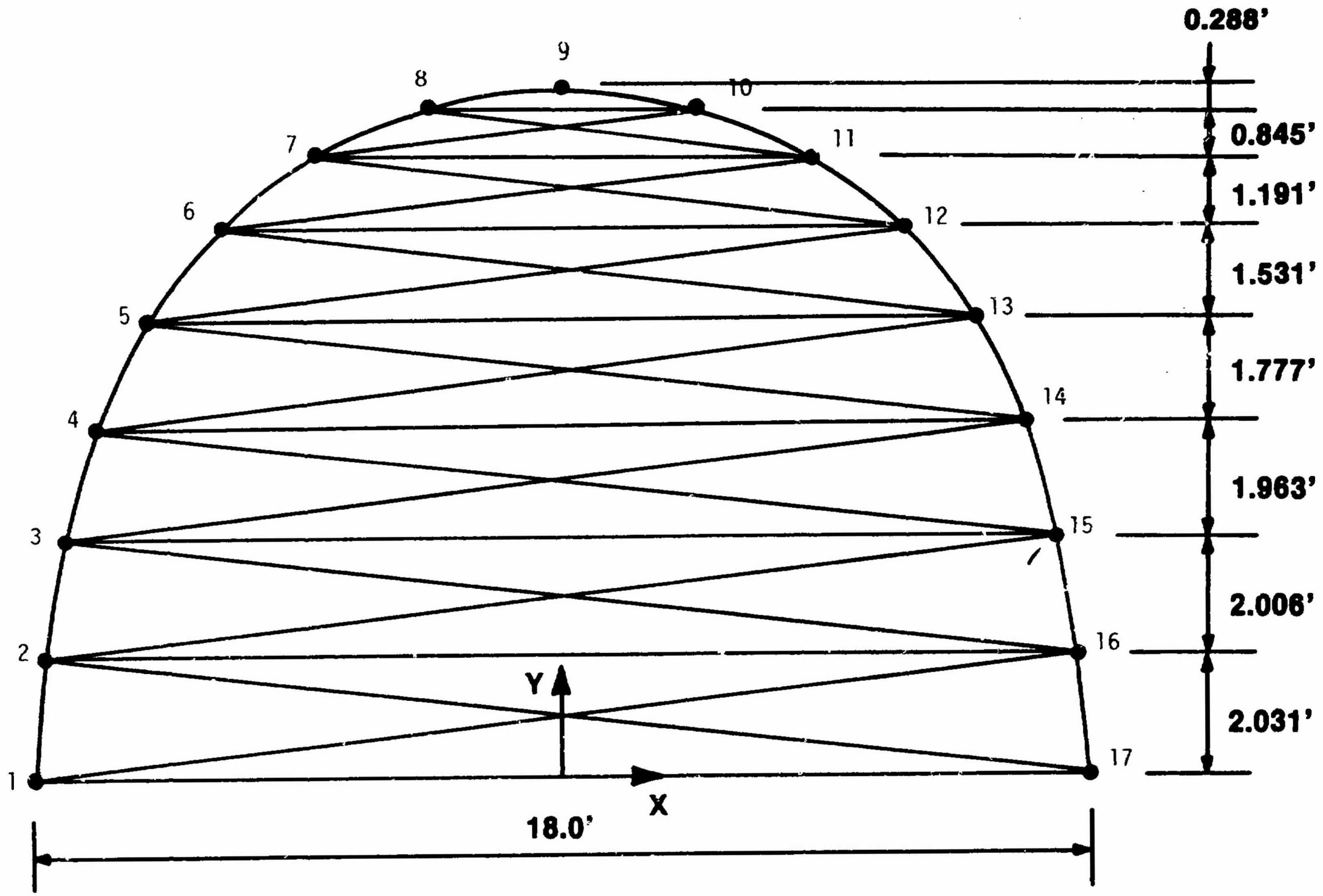

Figure 8. Parallel wind load projected area - BAS side view

The breakdown of the total projected area in this manner resulted in each of these triangles being common to two nodal points on the BAS NONFESA support framing model. Therefore, the total projected area at each nodal point was obtained by summing the areas of each triangle common to that point and dividing by two. Thus, each triangle was assumed to contribute half of its area to each nodal point, regardless of its orientation and the location of its center of gravity between these points. This approximation was judged acceptable given the number of other variables and uncertainties inherent in analysis of this nature. Having calculated the total projected area in the global-Y direction at each of the loaded nodal points, nodal forces were then calculated by multiplying the areas by the 10 psf snow load pressure.

A similar procedure was used in calculating wind load forces. Wind loadings differed, however, in that pressures are not uniform over the tent surface, but instead vary in intensity and direction depending upon the surface geometry. The method utilized in calculating wind pressures over the tent structure's curved surface was taken from Norris and Wilbur.[3] In this method wind pressures and suctions are expressed in terms of q, the velocity pressure, which is defined by the equation

$$q = 1/2\ m\ V^2,$$

where m is the mass of a unit volume of air and V is the velocity of the wind. This equation can be expressed as

$$q = 0.0025556\ V^2$$

where q is in units of pounds per square foot (psf), and V in units of miles per hour (mph). Pressures and suctions on the windward face of the structure according to this method were as follows:

1. For slopes of 20 degrees, or less, a suction of 0.7q
2. For slopes between 20 and 30 degrees, a suction of

   $$p = (0.07\ \alpha - 2.10)q$$

   in which α is the roof slope in degrees.
3. For slopes between 30 and 60 degrees, a pressure of

   $$p = (0.03\ \alpha - 0.90)q$$

4. For slopes steeper than 60 degrees, a pressure of 0.90q

Wind load on the leeward slope was taken as a suction of 0.6q for all slopes. All pressures and suctions are assumed perpendicular to the surfaces on which they act. The pressure (suction) profile calculated for the BAS tent structure is shown in Figure 9.

As noted earlier, vertical projections of the BAS tent structures were drawn to simplify calculation of wind load projected areas. The vertical projection for one of the Leaning Arch configurations is shown in Figure 7. The use of straight beam segments to model the arches meant that changes in slope occurred only at nodal points. Thus, the calculation of projected area at a given nodal point required that projected areas above and below the node be calculated separately, since pressures over the two beam segments framing into the node could vary. Global-X and -Y force components were also affected by changes in slope, pressure intensity, and load direction to either side of the node. Therefore, nodal force components had to be calculated separately for projected areas above and below the node, and then combined algebraically. Expressions for these force components given in terms of the pressure acting perpendicular to the surface, p, the vertical projected area, A, and the angle of inclination to the horizontal, θ, were as follows:

$$F_x = p\ A_v$$
$$F_y = p\ A_v \cot\theta$$

Wind loads in the direction parallel to the tent structure's longitudinal axis were calculated using an alternative method also taken from Norris and Wilbur.[3] In this procedure only wind pressures on the windward face of the structure are calculated. No attempt to account for suction on the leeward face is made. Wind pressures on inclined surfaces are calculated using the formula

$$P_n = P \frac{2 \sin i}{1 + \sin^2 i},$$

in which P_n is the intensity of normal pressure on a given surface, P is the intensity of pressure on a vertical surface, and i is the angle made by the surface with the horizontal. Note that P is analogous to q previously defined. Therefore

$$P\ (\text{psf}) = 0.0025556\ V^2\ (\text{mph})$$

Also note that for the Vertical Arch configurations investigated, i equals 90 degrees and P_n equals P. Projected areas in the vertical plane were calculated in the same manner as before using the vertical projection shown in

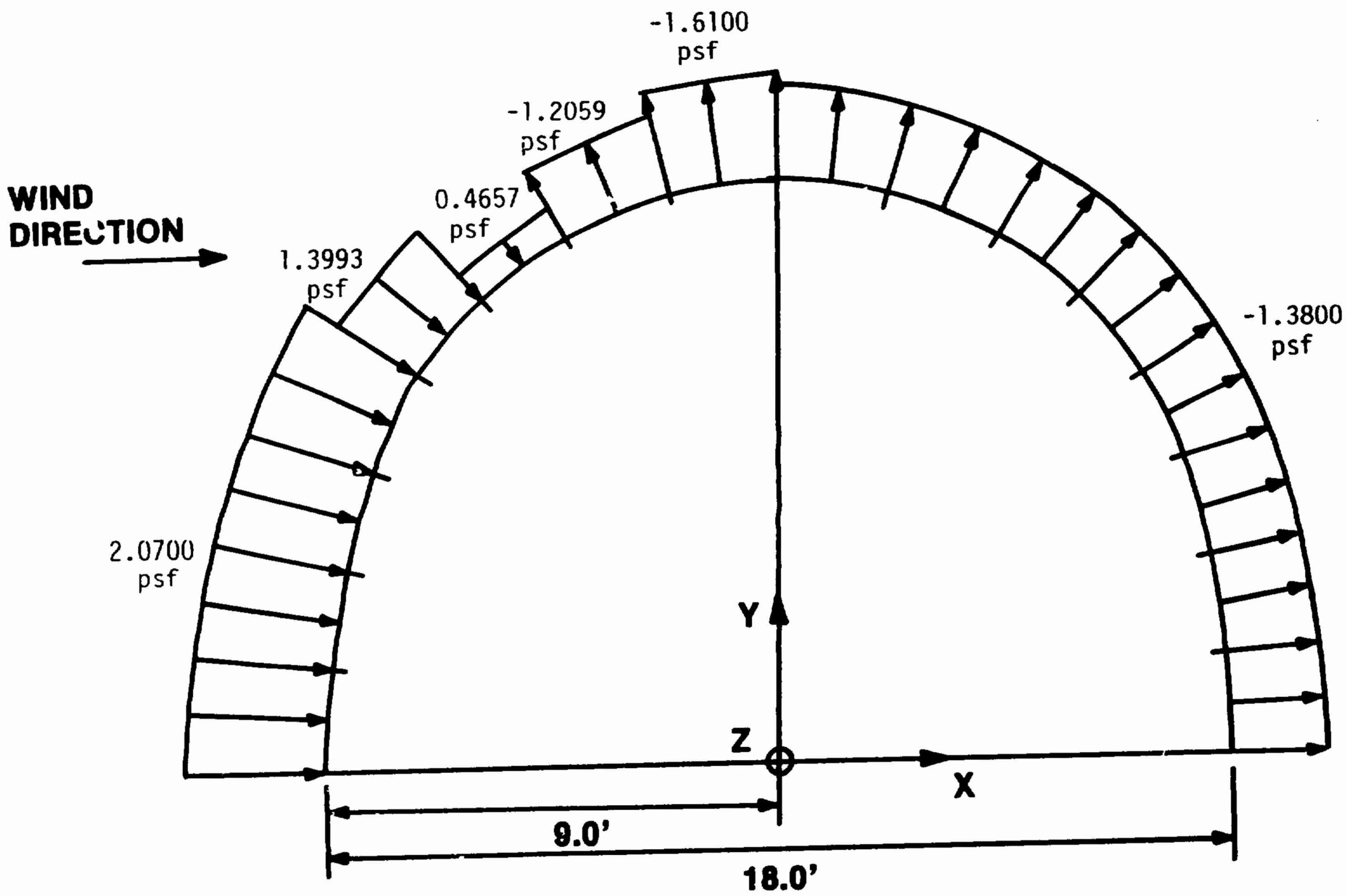

Figure 9. 30 mph wind pressure profile

Figure 8. Determination of projected areas, pressures, and nodal force components was made easy in this instance by the constant slope of the windward face of all the structures analyzed. Nodal force components in the Z- and Y-global directions were calculated using the following expressions:

$$F_z = P_n A_v$$

$$F_y = P_n A_v \cot i.$$

D. Guyline Elements

All of the BAS support framing configurations were analyzed for wind loading both with and without guylines included in the finite element model. This was done to determine the effectiveness of guylines in mitigating both stresses and deflections. Figure 10 shows the guyline patterns chosen for investigation. To resist the 30 mph wind acting over the tent structure's curved surface, a total of 12 guylines for the Leaning Arch configurations and 10 guylines for the Vertical Arch configurations were used. These guylines in all cases were taken to be tied into the pressurized beam on each side of the arch, and to be parallel to the wind direction. An additional two guylines were placed on the windward face of the computer models to resist the wind forces parallel to the tent structure's longitudinal axis. Guylines, in all instances, were assumed to frame into the pressurized beams at a point 7.777 feet above the ground surface, and to be inclined at an angle of 45 degrees to the horizontal.

Many of the same problems inherent in setting boundary conditions for the arch beam supports were also encountered in determining what stiffness to use for the guyline elements. Since the guylines are tied down both to the ground surface as well as to the sides of the pressurized tubes, the question of not only guyline stiffness but also support stiffness and local pressurized beam attachment stiffness arises. Both of these last two mentioned effects would tend to degrade the ability of the guylines to carry wind-induced tensions. Since no information on guyline stiffness was available, it was decided to determine guyline effectiveness under the most optimum condition possible, i.e., when the ground support cannot move and the guyline is virtually rigid in relation to other elements in the finite element computer model. This was accomplished by fixing the support nodes, representing the tie down to the

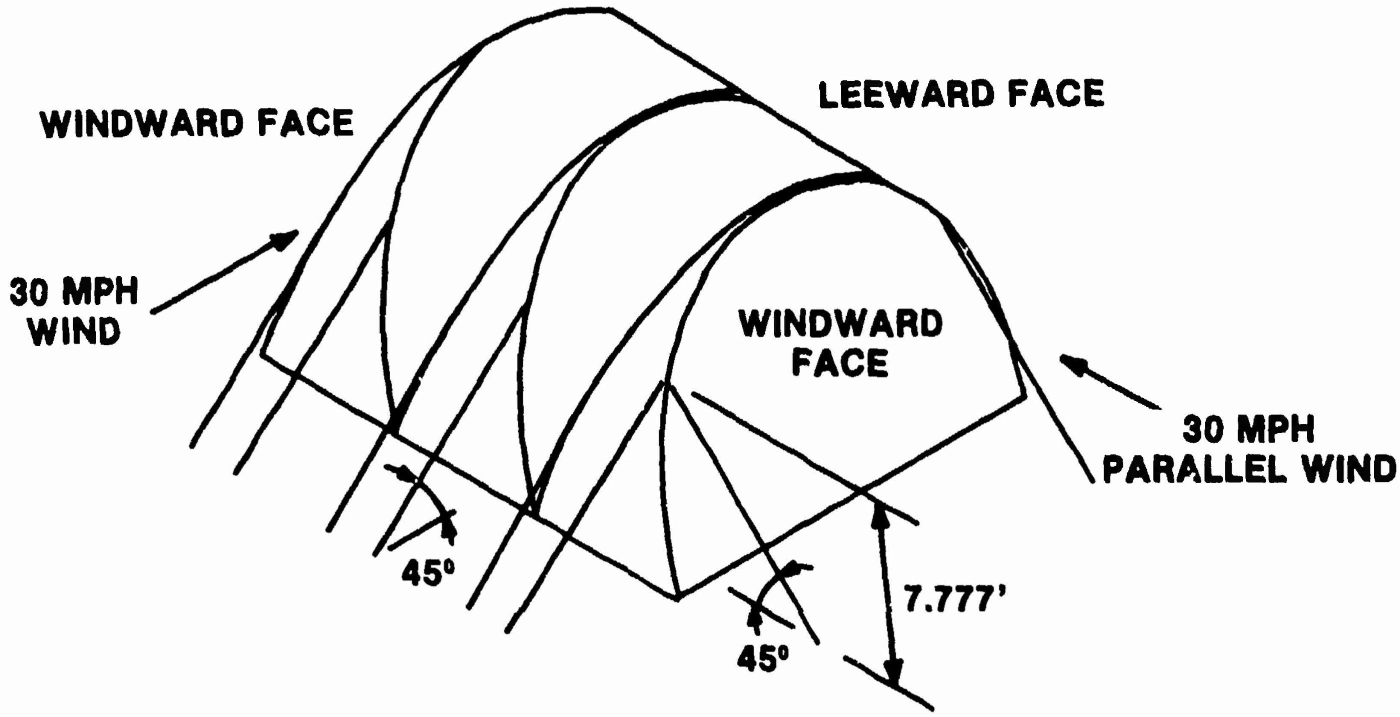

LEANING ARCH CONFIGURATION

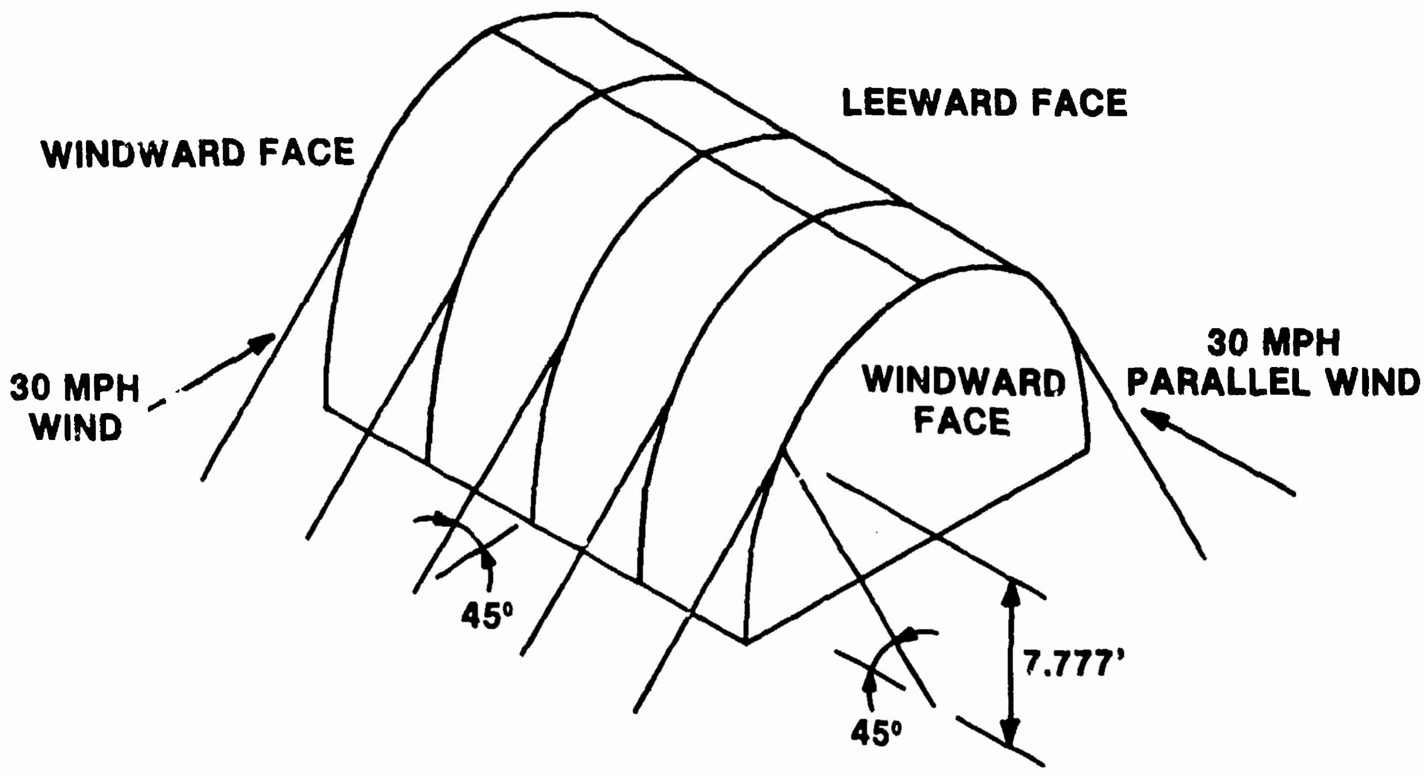

VERTICAL ARCH CONFIGURATION

Figure 10. Guyline configurations, Leaning Arch and Vertical Arch configurations

ground surface, against translation and rotation in the three orthogonal directions, as well as specifying large cross-sectional areas, A, and moduli of elasticity, E, for the guyline elements. Since the stiffness of axial elements is directly proportional to A and E, little or no elastic stretching of these elements would occur, only rigid body rotations. Therefore, guyline loads developed at attachment points to the more flexible pressurized beam frame would tend to be maximized based on general stiffness considerations for the entire structure. This degree of brace effectiveness is virtually impossible to achieve in a real world situation given the constraints previously discussed. However, by investigating both extremes, i.e., the tent structures without guylines and the tent structures incorporating these rigid brace elements, it was hoped to bound the analyses and provide a range over which stresses and deflections could be expected to fall.

The guyline element used in analyses is a special case of the truss element found in the NONFESA computer code. Its stiffness matrix and internal load vector are identical to that of the truss element. The guyline element, however, is only capable of carrying tension axial force. Therefore, at each cycle and step of the solution, the guyline resultant force is checked, and if compressive, stiffness components are reduced to approximately zero. Guylines on both the windward and leeward faces were included in the finite element models when analyzing for 30 mph winds acting over the tent structure's curved surface. Thus, each of the Leaning Arch configurations investigated had a total of 12 guylines and each of the Vertical Arch configurations 10 guylines to resist this loading. This was done because it was not immediately obvious whether the combination of pressures and suctions acting over the tent structure's curved surface would result in tensile or compressive forces in the leeward side guylines. As previously noted, wind pressures were calculated only on the windward face of the BAS tent structure for winds parallel to the frame longitudinal axis. Therefore, only the two guylines on the tent's windward face were included in the computer models, since it was obvious that leeward face guylines would be in compression, and thus ineffective in this instance.

E. Description Of Analyses

Output obtained from the NONFESA computer code consisted of beam forces, element stresses, nodal displacements, and nodal rotations. Beam forces, specified along the member's local coordinate axes, were given at both ends of each beam element. Forces included axial force and torque along the local-x axis, as well as local-y and -z axis shear and bending moment. This information was provided for both regular beam and pressurized beam elements in the finite element model. Element stresses provided by NONFESA included axial stress, as well as bending and average shear stress. Beam stresses were similarly provided at the ends of each element in local coordinates. However, the structure's global coordinate system was used to specify the total displacement and rotation at each nodal point. Axial forces and stresses were provided for guyline elements, when included in the model. Only the axial forces were of interest in this case, however, since guyline stresses were calculated using a pseudo cross-sectional area as previously described.

As noted earlier, analytical investigations focused on four BAS tent support framing arrangements; the two Leaning Arch configurations providing floor areas of 300 and 400 square feet, respectively, and the 300 and 400 square foot Vertical Arch configurations. Each of these framing schemes was analyzed for three environmental loading conditions: 10 psf snow, 30 mph wind, and 30 mph parallel wind. Wind loads along the two major tent axes, in turn, were investigated both with and without guyline braces included in the finite element model, as previously described.

The stiffness of pressurized beams is directly proportional to the beam diameter and inflation pressure. Thus, given a beam fabric with adequate tensile strength, one can in theory obtain sufficient stiffness from any size beam simply by supplying the required pressure. Based on stiffness considerations, it is apparent that larger diameter pressurized beams require lower inflation pressures to carry a given load than do smaller diameter beams. Larger beam diameters, however, imply more beam fabric, and therefore, greater weight. Hence, in the absence of other considerations, one would be driven to a design utilizing very small diameter beams at extremely high pressures in order to minimize structure weight. There are, however, practical limits to the extent to which this can be done for the BAS structure, based on mobility requirements. That is because the weight saved by using smaller diameter beams at higher internal pressure is offset by the need to transport bulkier, heavie compressors to supply these higher levels of inflation.

Investigations of the various framing schemes were, therefore, restricted to pressurized beam diameters between 8 and 14 inches and beam inflation pressures less than 10 pounds per square inch gauge. This was the maximum pressure that it was determined currently available support equipment of acceptable weight could provide. To cover adequately this range of values, each support arrangement was analyzed for beam diameters of 8, 11, and 14 inches and beam inflation pressures of 1.5, 3, 5, 7, and 10 psi. The only exception to this was the investigation of the 400 square foot Leaning Arch configuration for the 14-inch diameter beam size. This arrangement was analyzed for pressures of 1.5, 3, 4, 5, 7.5, and 10 psi.

The acceptability of each framing scheme analyzed was determined by comparing the computed peak compressive stress against the so-called wrinkle stress value. From a physical point of view the wrinkle stress allowable is equal to the initial longitudinal pretension stress given to each of the pressurized arch beams when inflated to a given pressure level. When snow or wind load is applied to the tent structure, axial and bending forces are developed in the beam elements. If at certain points along the beam cross-section's perimeter the combination of bending compressive stresses and/or compressive axial stress exceeds this initial pretension stress, wrinkling of the beam fabric will occur because the fabric cannot support compressive loads. As a result, a phenomena similar to yielding of a ductile material takes place as the beam undergoes a gradual, continual increase in deformation. At this stage the structure is near a state of collapse. It should also be noted that beyond this point NONFESA computer analyses are technically no longer valid, since large deformation nonlinear behavior violates the linear, elastic assumptions inherent to the beam elements used.

This wrinkle stress or pretension stress value is equivalent to the longitudinal stress calculated for a cylindrical thin-walled pressure vessel of radius, r, and wall thickness, t, subjected to a uniform internal pressure, p. As shown in Timoshenko and Young[4] as well as many other texts in strength of materials, the longitudinal stress, σ_1, expressed in units of force per unit area, is equal to the following:

$$\sigma_1 = \frac{pr}{2t}$$

NONFESA output for pressurized beam fabric stresses was given in units of pounds per inch (lb/in) length, since fabric thickness generally is not a known quantity, and fabric tensile strength is usually provided in units of force per unit length of material. By moving the thickness term, t, to the left side of the above equation, one obtains the following expression for the wrinkle stress in terms of the desired units:

$$\sigma_1 t = \text{wrinkle stress (lb/in)} = \frac{pr}{2} .$$

The circumferential stress or hoop stress, σ_2, for a cylindrical thin-walled pressure vessel under internal pressure is given by the following expression:

$$\sigma_2 = \frac{pr}{t} .$$

In the absence of external loading, the hoop stress is therefore equal to twice the longitudinal stress. This equation can be expressed as follows:

$$\sigma_2 t = \text{hoop stress (lb/in)} = p\ r.$$

Thus, for a beam of given radius, r, the internal pressure, p, should be such that p times r is less than the fabric tensile strength given in pounds per inch length. For a pressure of 10 pounds per square inch and radius of 7 inches, the peak hoop stress is 70 lb/in. Most fabrics under consideration for use in the BAS tent structure have tensile strengths much greater than this value. Restriction of beam inflation pressure levels to a maximum of 10 psi, therefore, insured that wrinkling would occur prior to development of tears in the material due to tensile stress. Hence, attention was directed exclusively to the determination and comparison of peak longitudinal compressive stresses to the wrinkle stress value.

F. Results

1. Interpreting NONFESA Data

Tables A.1 to A.5 shown in Appendix A summarize the results of the finite element analyses conducted on the 300 square foot Leaning Arch configuration assuming eight inch diameter pressurized arch beams. In all, a total of 60 tables of this type were generated in order to summarize NONFESA results for each of the two framing arrangements, two tent sizes, and three beam diameters investigated. Thus, Appendix A is provided primarily as an example to aid one's understanding of how the NONFESA output data were interpreted and reduced into a more useful form.

Each table in Appendix A lists critical element stress and nodal displacement values at each beam inflation pressure for a particular framing arrangement, loading condition, and beam size. Separate entries for the global-X, -Y, and -Z translational displacement components, as well as the axial and two bending components of element longitudinal stress, are provided for in the tables.

Space is also provided for entries to identify the node point, as well as the element and element end, at which displacements and stresses were respectively tabulated. Each finite element computer run was reviewed to determine the largest value of each individual displacement and stress component. All six of these maximum components were tabulated at each inflation pressure along with the other two components of stress or displacement at that location. Values underlined in the tables identify the largest value of that particular component.

Summarizing the results in this manner provided a means of quickly determining the relative magnitude, and thus importance, of each stress and deflection component. It also provided a means of identifying critical points on the structure, and to check the computer model. With regard to the latter, it was quite often intuitively obvious, due to structure and/or load symmetry, whether one would expect to find a single point or multiple points with the same deflection or stress. As a result, these tables served as a further check of model geometry, element properties, load magnitude, and load direction.

2. Peak Longitudinal Compressive Stresses and Deflections

These tables summarizing the raw output data from NONFESA represented only the first step in interpreting analytical results. Since NONFESA does not calculate resultant stresses and deflections, the element stress and nodal displacement components had to be combined to determine the peak longitudinal compressive stress and peak deflection values. This combining of stresses and deflections was required before structural acceptability at various inflation pressures could be determined and before comparisons could be made between the various framing arrangements. It should be noted that, in general, the peak compressive stress or deflection does not necessarily have to occur at a point where one of the stress or displacement components is a maximum. A number of computer runs for each framing scheme and loading condition were investigated in detail to verify whether or not this was true for the BAS concepts. It was found that stress and deflection peaks did, in fact, occur at one of the maximum component points in virtually every case for the BAS structures and loadings considered.

The peak deflection is defined by the vector sum of the three displacement components. This deflection was obtained by taking the square root of the sum of the squares of these three components. Peak compressive longitudinal stress was calculated by first taking the root mean square of the two element bending stress components. The axial stress component was then either added or subtracted, respectively, to this value, depending upon whether this stress was compressive or tensile. Appendix B, Tables B.1 to B.8, summarize peak deflections and compressive stresses calculated at each beam size and pressure for each of the framing arrangements and loadings investigated. One will notice that one additional load case not previously mentioned has been added to Tables B.1 to B.4. This loading is for a 5 psf snow load. No additional finite element computer runs were needed to investigate this loading condition. Stress results were computed instead, assuming half the values obtained in the 10 psf snow load analyses. Maximum deflection values, though not listed in Tables B.5 to B.8, could be similarly obtained. This load case was investigated to determine if savings in structure weight and required inflation pressure could be achieved by reducing the design snow load by one half.

It should be noted that both snow and wind were treated as static loads. Therefore, peak compressive stresses and deflections resulting from these loads were computed in the same manner and compared to the same allowable wrinkle stress value for a given beam radius and pressure. However, wind is in reality a dynamic load, capable of constant and sometimes sudden changes in speed and direction. Thus, the two wind conditions investigated for simplicity considered only the static portion of the wind load resulting from a steady wind speed of 30 mph. Inherent to the analysis, therefore, is the assumption that the wind speed, and thus force, builds up slowly on the tent structure to its maximum value and does not undergo sudden fluctuations. This assumption eliminates the need to consider dynamic amplification resulting from either the sudden application of the 30 mph wind or wind gusts above this load.

For suddenly applied loads of this nature, one would have to consider this amplification effect, which is a function of both the tent structure's natural frequencies, as well as the shape and duration of the load pulse. This is often done by performing either a dynamic modal analysis or equivalent static analysis of the structure. In an equivalent static analysis for wind loads, the wind forces applied to the structure are multiplied by some factor to account for dynamic effects, and the allowable stress is generally increased by one third. For dynamic or equivalent static analysis of pressurized beam structures for wind load, however, it is suggested that this increase in the wrinkle stress value not be taken.

3. Comparison of Peak Compressive Stress to Wrinkle Stress

Determining whether each framing arrangement was structurally acceptable for a particular loading, beam diameter, and inflation pressure required the comparison of the peak compressive stress to the wrinkle stress value. Therefore, using the peak stress values tabulated in Appendix B, a series of graphs comparing peak compressive stress and wrinkle stress were developed.

These graphs are shown in Figures C.1 to C.24 of Appendix C. The graph shown in each figure summarizes results for a particular framing arrangement and loading condition. Beam inflation pressure and compressive stress were, respectively, taken to be the abscissa and ordinate of the graph as shown. Stress results for the three beam diameters investigated, i.e., 8, 11, and 14 inches, were included on each graph. For each of these beam sizes, peak compressive stresses taken from Appendix B were plotted at the corresponding beam inflation pressures between 1.5 and 10 psi. A curve was then drawn through these points. These plots of the peak compressive stress, based on finite element analytical results for the three beam sizes, are represented by the three curved lines shown in the graphs. One can clearly see that stresses are greater at low inflation pressures, with the smallest diameter beam, represented by the uppermost curve, being the most highly stressed. Also, as beam inflation pressure is increased, the structure's stiffness increases, leading to a corresponding drop in stress levels, as shown.

4. Wrinkle Stress

Plots of the wrinkle stress for each of the beam sizes were also included in the graphs. As previously noted, the wrinkle stress value is defined as the beam inflation pressure, P, times the beam radius, R, divided by two. Thus, for constant beam diameter, a linear relation exists between the wrinkle stress value and the beam inflation pressure. Hence, plots of the wrinkle stress versus beam inflation pressure for the three beam sizes resulted in three straight or constant slope lines as shown in the figures. One can see from these plots that the wrinkle stress value increases with increasing beam inflation pressure. Also, for a given inflation pressure, the largest diameter beam will have the largest wrinkle stress value, as shown.

5. Adequacy of Tent Designs

Having plotted these curves of the peak compressive stress and wrinkle stress versus the beam inflation pressure, it was then possible to determine the adequacy of individual tent support designs. As an example, Figure C.1 summarizes results of the analyses conducted on the 400 square foot Leaning Arch configuration for a 10 psf snow load. If one looks at the peak compressive stress, σ_c, and the wrinkle stress curves for the beam size, D = 14 in, one can see that these two curves intersect at a beam inflation pressure of 5.6 psi and stress of approximately 19.5 lb/in. This point represents the minimum beam inflation pressure resulting in an acceptable design. For beam pressures less than this value, the peak compressive stress is greater than the wrinkle stress value. Therefore, one would expect wrinkling and structural failure to begin. For beam pressures greater than 5.6 psi, peak compressive stress is less than the wrinkle stress, and the structure is able to carry the load at some factor of safety. Thus, for a beam diameter, D = 14 in, and inflation pressure of 10 psi, the peak compressive stress and wrinkle stress are equal to 16.00 and 35.00 lb/in, respectively. The structure at this pressure, therefore, is able to carry the snow load at a factor of safety of approximately 2.19.

Similarly, for a beam diameter, D = 11 in, the minimum required pressure necessary to carry the snow load is approximately 9.3 psi, as shown. At an inflation pressure of 10 psi, this beam size is able to carry the snow load at a factor of safety of only 1.10. For a beam size, D = 8 in, the wrinkle stress curve lies entirely below the peak compressive stress curve, as shown in the graph, for beam inflation pressures between 1.5 and 10 psi. Thus, no acceptable designs exist over this range of pressures for this particular tent arrangement and beam size that can support the 10 psf snow load. This same line of logic can be similarly applied to the other figures shown in Appendix C when investigating other framing schemes and loadings.

Two other groups of graphs were put together to provide a visual comparison of stresses and deflections for the various framing arrangements and loadings investigated. These graphs are shown in Figures C.25 to C.34. Figures C.25 to C.29 provide a summary of peak compressive stress, σ_c, versus beam pressure for each of the loadings investigated. Figures C.30 to C.34 similarly summarize the maximum deflections. The graph shown in each figure is composed of 12 curves summarizing results for the four framing arrangements and three beam diameters analyzed. Thus, these graphs not only provide a comparison between different beam sizes for a particular framing arrangement, but also comparisons between various framing arrangements and beam diameters in general. The minimum required pressure, represented by the intersection of the wrinkle stress and peak compressive stress curves, as previously described, was not plotted in these figures. These values, however, can be easily obtained from Figures C.1 to C.24 and plotted in Figures C.25 to C.34, if one wishes to see a visual comparison of usable beam inflation pressure for each of the 12 designs considered.

6. Trends: Beam Size, Stress and Deflection

A number of distinct trends can be observed by examining Figures C.25 to C.34. Foremost among these trends is the spacing between curves on each of the graphs as one goes from one beam diameter to the next larger beam size. Although not previously mentioned, this trend is also quite evident if one examines the peak compressive stress curves in the graphs shown in Figures C.1 to C.24. Although the beam diameter is increased by three inches in going from both 8 to 11, and 11 to 14 inches, spacing between the 8- and 11-inch beam diameter curves is greater than that between the two larger beam sizes for a given configuration. Thus, the stress and deflection curves shown in the graphs tend to bunch up and overlap more with increasing beam size.

This behavior can be explained and could even have been predicted, based solely on stiffness considerations for the pressurized beam members. The axial and bending stiffnesses of a beam of given length and material type are functions, respectively, of the member's cross-sectional area and moment of inertia. For the thin-walled pressurized tube members the area, A, and moment of inertia, I, are given by the following expressions:

$$A = 2 \pi r t$$

$$I = \pi t r^3.$$

Thus, for a material of given thickness, t, the axial stiffness is a direct function of the beam radius, r. Similarly, bending stiffness of the member is directly proportional to the cube of the beam radius. Bending stiffness, therefore, increases much more rapidly than axial stiffness for a given increase in beam radius. This can be seen by considering the three beam sizes analyzed. By increasing the beam diameter from 8 to 11 inches, an increase of 37.5 per cent is realized in the axial stiffness and 160 per cent in the bending stiffness. Similarly, in going from 11 to 14 inches in diameter, the axial stiffness is increased by 27.3 per cent and the bending stiffness by 106 per cent. One can see that the first 3-inch increase in beam diameter resulted in a greater increase in stiffness on a percentage basis than the second. Consecutively smaller increases in stiffness would result from further increases in the beam diameter above 14 inches. This fact accounts for the closer spacing between curves for the two larger diameter beams shown in the figures.

This information would be particularly useful if one wished to fit additional curves into Figures C.1 to C.34 to obtain approximations of required pressures, stresses, and deflections for other beam diameters. Attaining additional stiffness and strength is not without cost, however. This is achieved at the expense of increased weight, which, like axial stiffness, is directly proportional to the beam radius, r.

7. Trends: Load Carrying Effectiveness

A number of other trends were observed in Figures C.25 to C.34 relative to the effectiveness of each framing arrangement to carry a given load. A study of these figures revealed that the Leaning Arch configuration was capable of supporting the 10 psf snow and 30 mph wind loads at lower peak stress and deflection levels than the Vertical Arch arrangement. This was true for both the 300 and 400 square foot tent sizes. The introduction of guylines to help carry this wind load not only leads to a reduction in stresses, and more significantly, deflections for all the configurations, but also a change in the relative effectiveness of the framing types. Thus, the Vertical Arch configurations with guylines were able to support the 30 mph wind load at lower stress and deflection levels than the corresponding Leaning Arch type structures. This trend was a complete reversal of that observed when the structures were analyzed without guylines.

This reversal is particularly interesting in view of the fact that the Vertical Arch arrangement has one less pressurized arch beam and two less guylines than the Leaning Arch configuration. Since the wood beam joining the vertical arches carries little of the wind load, it is apparent that this arrangement more efficiently transfers wind forces into the braces than the

Leaning Arch type structure. Peak guyline tension forces, therefore, are greater for the Vertical Arch arrangements for a given beam size and pressure. Stresses and deflections were also observed to be lower for the Vertical Arch structure types when subjected to the 30 mph parallel wind load. This trend was observed in both the 300 and 400 square foot tent sizes, when analyzed both with and without guylines.

Therefore, no clear-cut choice emerges from these figures as to the best of these two framing concepts. What is shown instead is that one or the other may be best from a stress/deflection and ultimately, minimum required pressure standpoint depending upon the particular loading and the presence or absence of guylines.

8. Inflation Pressures

In order to further clarify results, Tables D.1 to D.6 of Appendix D were put together. These tables summarize the minimum required inflation pressure for each beam size and framing arrangement. The maximum compressive stress and deflection at that pressure level are also tabulated. Results are shown for each of the six loading cases considered in the analyses. These tables further show how close the two framing arrangements are in terms of their load-carrying ability at a given beam diameter.

One will again observe that the 400- and 300-square foot Leaning Arch configurations can carry the snow and wind loadings at lower pressure than the corresponding 400 and 300 square foot Vertical Arch framing types. Upon closer examination of tabulated results, however, it can be seen that differences between the two arrangements in terms of minimum required pressure, maximum compressive stress, and maximum deflection are small for a given beam size. These tables also highlight instances in which pressures, stresses, and deflections are less for the Vertical Arch arrangements. This occurred, as previously noted, for the load cases of wind with guylines, and parallel wind both with and without guylines. In each instance, the minimum required pressure, as well as the maximum stress and deflection were lower for each of the Vertical Arch framing types than for the Leaning Arch structure of the same size. However, one can see that tabulated values at a given beam size are, once again, quite close for Vertical and Leaning Arch structures of equal size.

9. Guylines and Wind Forces

The tables shown in Appendix D were also used to assess the effects of guylines in resisting wind-induced forces. One is asked to focus attention first on the Leaning Arch arrangements and the 30 mph wind load acting over the tent structure's curved surface. In this case, the introduction of guylines resulted in anywhere from a 20 to 50 per cent reduction in minimum required pressure and maximum compressive stress for a given beam diameter. The effects on maximum deflection were even more pronounced. Reductions in deflection of approximately 68 and 84 per cent were realized for the 400 and 300 square foot Leaning Arch arrangements, respectively. The introduction of guylines was even more effective in bringing down pressures, stresses, and deflections in the Vertical Arch arrangements. Here, reductions of between 49 and 67 per cent were obtained in minimum required pressure and maximum stress. Once again, deflections were reduced even more. Deflection values for both the 300 and 400 square foot Vertical Arch structures with guylines were only about 15 per cent of those obtained for the same structures analyzed without braces.

Attention is directed next to results shown in the tables for the 30 mph parallel wind load, or wind acting along the tent's longitudinal axis. One can see that the inclusion of guylines generally does not result in as great a reduction in required pressure and peak stress as that obtained for wind forces acting in the other direction. By way of comparison, reductions for the two Leaning Arch configurations were between 15 and 27 per cent, while Vertical Arch results were 25 to 32 per cent lower. Once more, however, the introduction of guylines lead to a far more significant reduction in the peak computed deflections. In virtually every case, maximum deflection values tabulated average only about 15 per cent of those obtained with no braces.

It should be noted once again, however, that the reductions in required pressure, maximum stress, and maximum deflection described above assume an ideal rigid brace. Under real world conditions, reductions of this magnitude would be nearly impossible to achieve. The only statement that can be made with certainty, therefore, is that the actual pressure needed to support the structure, as well as the maximum stress and deflection with guylines, would fall somewhere between the two extremes listed in the tables.

G. Results Summary: Framing Arrangements

Table 2 provides a final summary of results for the analyses conducted on the various BAS support framing arrangements. This table, as shown, is composed of three parts. The first part provides an estimate of the framing weight in pounds for each of the tent sizes, framing types, and beam sizes investigated. Pressurized beam weights were calculated assuming fabric and bladder weights of 10.3 and 8.4 ounces per square yard respectively. These weight estimates were for the materials used by Chemfab in the construction of a prototype pressurized beam BAS tent structure for Natick. The two inch by four inch Spruce beams, comprising the top members in the two Vertical Arch arrangements, were assumed to have a weight density of 24 pounds per cubic foot. Weight estimates for the 400 and 300 square foot Vertical Arch configurations, therefore, include allowances of 29.33 and 22.67 pounds, respectively, for these members. Weight estimates shown in the chart are for the main support framing members only. Therefore, these tabulated weights do not include estimates for the entrance way and litter airlock, the tent's exterior skin, and fabric for attaching beam members. Nor do they include estimates for stakes, guylines, and other hardware used to tie down the tent structure. One can see that the support framing of each Vertical Arch arrangement, due mainly to use of this wood member, is heavier than that of the Leaning Arch structure of the same size.

Listed in the second and third parts of the table are the minimum pressures required to support all of the design snow and wind loads. Results are tabulated according to tent size, framing type, and beam diameter. Each design is considered individually both with and without guylines to help carry the wind loads. The second part lists results for a design wind load of 30 mph in both directions and a design snow load of 10 psf. The third part lists values when the design snow load is reduced to 5 psf. It should be noted that the structures' deadweight are not included in the analyses. It is

TABLE 2. Weight Estimates and Minimum Required Pressures

A. Framing Weight (lb)

Beam Diameter	400 LA	400 VA	300 LA	300 VA
8 in	56.54	74.26	55.50	67.60
11 in	77.74	91.11	76.31	84.45
14 in	98.94	107.96	97.12	101.30

B. Minimum Required Pressure (psig), 10 psf Snow & 30 mph Wind

Beam Diameter	Without Guylines				With Guylines			
	400LA	400VA	300LA	300VA	400LA	400VA	300LA	300VA
8 in	-	-	-	-	-	-	-	-
11 in	9.3	10.5	7.9	8.15	9.3	10.5	7.5	8.15
14 in	5.6	6.5	5.1	5.0	5.6	6.5	4.45	5.0

C. Minimum Required Pressure (psig), 5 psf Snow & 30 mph Wind

Beam Diameter	Without Guylines				With Guylines			
	400LA	400VA	300LA	300VA	400LA	400VA	300LA	300VA
8 in	-	-	-	-	-	-	-	-
11 in	8.2	7.3	7.9	7.3	7.0	6.25	6.45	5.5
14 in	5.2	4.55	5.1	4.55	4.0	3.75	3.7	3.15

anticipated that deadweight would result in no more than a 10 per cent increase in minimum required pressure values listed in the table. One can see that, in every instance, the minimum pressurized beam size investigated, capable of supporting the loads at a pressure of 10 psi. or less, was the 11-inch diameter beam. Also, when design loads of 10 psf snow and 30 mph wind are assumed, minimum required pressures for the 400 and 300 square foot Leaning Arch arrangements are less than those for the corresponding Vertical Arch configurations. However, just the opposite is observed when 5 psf snow and 30 mph wind design loads are considered. In this case, it is the Vertical Arch arrangements that have the lowest minimum required pressures of the two framing types considered.

III. DISCUSSION

Based on results of this study, it was concluded that both the Vertical and Leaning Arch support framing arrangements represent viable alternatives for supporting the BAS tent structure. Use of an 11-inch diameter pressurized beam in conjunction with any size and type framing scheme results in an acceptable design at some inflation pressure less than or equal to 10.5 psi. An examination of framing weights in Table 2 would lead one to conclude that the Leaning Arch arrangements are superior, and to choose this framing type for minimum weight-driven designs. One would be especially inclined to make this choice if looking at design loads of 10 psf snow and 30 mph wind, where the Leaning Arch structures also hold an advantage in terms of lower minimum required pressures. This weight advantage, however, is due entirely to use of the wood beams in the Vertical Arch framing arrangements.

Therefore, it is recommended that substitution of a lightweight glass- or carbon-fiber-reinforced composite beam for this wood member be investigated. The logical choice of cross-sectional shape for this composite member would be a hollow rectangle. However, other cross-sections should not be ruled out, particularly if advantages exist in terms of attachment to the pressurized arch beams. The wood member used in the analyses weighed one and one-third pounds per linear foot. A composite beam of half this weight would tilt the weight advantage in favor of the Vertical Arch arrangements for pressurized beam diameters between 11 and 14 inches. This fact is significant when one considers that 11 to 14 inches happens to be the approximate range of pressurized beam diameters over which acceptable, practical designs are found. The composite's effect of potentially reducing the weight becomes of even greater significance when the design snow load is reduced to 5 psf. In this case, as shown in Table 2, the Vertical Arch arrangements hold an advantage in terms of minimum required pressure over the Leaning Arch configurations. If one were able to shift the weight advantage in favor of the Vertical Arch structure through substitution of a composite member, the arguments in favor of the Vertical Arch arrangement would undoubtedly become compelling.

Of course, one would have to weigh any weight savings against the added cost of a composite beam over that of a relatively inexpensive, readily available wood member. However, these costs potentially could be offset to some degree, if the Vertical Arch structure is found to be cheaper to fabricate. There may also be further weight savings in terms of hardware needed to inflate and tie down the structure, since the Vertical Arch arrangement has one less pressurized arch beam.

It should be noted that earlier experimental work conducted by Natick[5] showed the Leaning Arch concept to be far superior to the Vertical Arch in terms of load carrying ability. Changes contributing to the improved vertical arch performance versus the leaning arch in the present study include the use of a greater number of pressurized arch beams and use of a solid, continuous member to tie the arches together. In the previous work, it was felt, the use of longer span, segmented pressurized tube members to tie the pressurized arch beams together probably contributed to reduced capacity of that frame under a simulated snow load. If one considers the relative stiffnesses of the frame members, it becomes apparent that a stiffer, longitudinal beam would transfer less moment to the arch members at each end of the tent, thus reducing out-of-plane bending of the end arches and increasing capacity. Similarly, more arch beams imply less load carried by each arch and, therefore, greater capacity for a given beam diameter and pressure.

In weight-driven designs, it was further concluded, additional weight savings might also be obtained by reducing the beam diameter of certain arrangements to less than 11 inches. Here, weight would be saved by using smaller size beams and making greater use of available pressure. This is possible for arrangements in which the minimum required pressure to support the design loads is somewhat less than 10 psi for the 11 inch diameter beam size. Arrangements shown in Table 2 fitting this description include the 300-square foot arrangements at design snow loads of both 5 and 10 psf, and the 400-square foot arrangements at a design snow load of 5 psf.

Current indications are, however, that the maximum beam inflation pressure allowed may have to be lowered to something less than the 10 psi assumed in this investigation. The reason given is that higher inflation pressures lead to an increased risk of leaks developing in the beam material. Until this question of maximum inflation pressure is resolved, only general conclusions concerning optimum beam sizes can be drawn from Table 2. About all that can be said is that, depending upon the particular tent size, framing type, and design loads, some arrangements may be adequate using an 11-inch diameter pressurized beam. For others, the optimum design from a weight and pressure standpoint would probably be at some beam diameter between 11 and 14 inches. However, information generated during the course of this study would make determination of optimum beam sizes a relatively simple task once maximum pressure levels are established.

IV. CONCLUSIONS AND RECOMMENDATIONS

An investigation of two alternative pressurized arch beam framing arrangements to support the BAS tent structure has been conducted. Based on analytical results obtained in this study, the following conclusions are reached.

1. Both the Vertical and Leaning Arch framing arrangements represent viable alternatives for supporting the BAS tent structure.

2. Use of an 11-inch diameter pressurized beam in conjunction with any configuration results in an acceptable design at some inflation pressure less than or equal to 10.5 psi.

3. For certain arrangements, further weight could be saved by using beam diameters less than 11 inches and making greater use of available pressure.

4. If maximum inflation pressure is further restricted, then the optimum pressurized beam diameter will probably fall in the range of 11 to 14 inches.

The following recommendations are also made, based on the work in this study.

1. Substitution of a lightweight composite beam in place of the wood beam member in the Vertical Arch arrangements should be investigated.

2. Stresses in the tent structure's fabric barrier should be checked.

3. A detailed investigation of deadweight stresses should be included in future analysis.

This document reports research undertaken at the US Army Natick Research, Development and Engineering Center and had been assigned No. NATICK/TR-88/071 in the series of reports approved for publication.

V. REFERENCES

1. O'Callahan, John C.; NONFESA-Nonlinear Finite Element Structural Analysis Code for the Analysis of Stresses and Deflections in Frame Supported Tents; Bolt Beranek and Newman, Inc., Report No. 2803, 1975

2. Steeves, Earl C.; Pressure Stabilized Beam Finite Element; U.S. Army Natick Research & Development Command; NATICK/TR-79/002; 1978

3. Norris, C.H. and Wilbur, J.B.; Elementary Structural Analysis, McGraw-Hill Book Company, New York, N.Y., 1960, pp. 45-47.

4. Timoshenko, S. and Young, D.H.; Elements Of Strength Of Materials, Fifth Edition, D. Van Nostrand Company, Inc., Princeton, New Jersey, 1968, pp. 50-55.

5. Steeves, Earl C.; Fabrication And Testing of Pressurized Rib Tents; U.S. Army Natick Research & Development Command; NATICK/TR-79/008; April 1979

APPENDIX A

Sample Tables of NONFESA Stress and Displacement Components vs. Pressure

TABLE A.1: Stress and Displacement Components (NONFESA) vs. Pressure for 300 sq ft Leaning Arch BAS, D = 8 in, 10 psf snow load

		Displacements (in)			Stresses (lb/in)				
P (psi)	node#	ΔX	ΔY	ΔZ	Element	End	Axial	Bnding2	Bnding3
1.5	36, 46 52, 61	11.0	.468	3.12	52 61	52 61	5.28	26.03 22.42	27.96 30.93
1.5	41	0	15.9	.004	41 57	41 41	2.24	52.61	2.51
1.5	23, 28 69, 75	3.64	2.84	5.05	40 56	41 41	2.24	19.96	48.74
3	36, 46 52, 61	9.42	.397	2.59	52 61	52 61	5.28	22.26 19.17	23.93 26.47
3	41	0	13.8	.003	41 57	41 41	2.24	46.06	2.50
3	23, 28 69, 75	3.21	2.36	3.87	40 56	41 41	2.24	17.20	42.80
5	36, 46 52, 61	7.89	.316	2.14	52 61	52 61	5.28	18.61 16.01	20.11 22.24
5	41	0	11.7	.002	41 57	41 41	2.25	39.69	2.18
5	23, 28 69, 75	2.76	1.96	3.04	40 56	41 41	2.25	14.80	36.89
7	36, 46 52, 61	6.78	.252	1.83	52 61	52 61	5.28	15.97 13.73	17.36 19.18
7	41	0	10.3	.002	41 57	41 41	2.25	34.98	1.87
7	23, 28 69, 75	2.42	1.69	2.53	40 56	41 41	2.25	13.10	32.49
10	36, 46 52, 61	5.60	.181	1.50	52 61	52 61	5.27	13.17 11.31	14.41 15.91
10	41	0	8.65	.001	41 57	41 41	2.26	29.81	1.49
10	23, 28 69, 75	2.04	1.42	2.05	40 56	41 41	2.26	11.26	27.64

TABLE A.2: Stress and Displacement Components (NONFESA) vs. Pressure for 300 sq ft Leaning Arch BAS, D = 8 in, 30 mph wind load

P	node#	Displacements (in) ΔX	ΔY	ΔZ	Stresses (lb/in) Element	End	Axial	Bnding2	Bnding3
1.5	38, 54	27.7	5.19	.419	36 52	36 52	1.42	22.61	28.91
1.5	43, 58	25.8	6.81	.377	35 51	36 52	1.33	26.96	24.90
1.5	29, 76	17.5	3.95	1.52	37 53	37 53	1.37	20.44	29.61
3	38, 54	20.5	3.68	.414	36 52	36 52	1.30	17.41	22.35
3	43, 58	18.9	5.13	.290	35 51	36 52	1.19	20.77	19.26
3	29, 76	12.8	2.89	1.07	37 53	37 53	1.26	15.51	22.60
5	37, 38 53, 54	15.3	2.66	.363	36 52	36 52	1.20	13.45	17.30
5	43, 58	13.9	3.89	.243	35 51	36 52	1.09	16.05	14.92
5	29, 76	9.40	2.13	.803	36 52	36 52	1.20	13.45	17.30
7	37, 38 53, 54	12.2	2.10	.316	36 52	36 52	1.15	11.02	14.18
7	43, 58	11.0	3.14	.214	35 51	36 52	1.03	13.15	12.23
7	29, 76	7.42	1.69	.650	36 52	36 52	1.15	11.02	14.18
10	37, 53	9.42	1.59	.187	36 52	36 52	1.10	8.71	11.22
10	43, 58	8.40	2.44	.184	35 51	36 52	0.97	10.39	9.68
10	29, 76	5.64	1.30	.511	36 52	36 52	1.10	8.71	11.22

TABLE A.3: Stress and Displacement Components (NONFESA) vs. Pressure for 300 sq ft Leaning Arch BAS with guylines, D = 8 in, 30 mph wind load

		Displacements (in)			Stresses (lb/in)				
P (psi)	node#	ΔX	ΔY	ΔZ	Element	End	Axial	Bnding2	Bnding3
1.5	45, 60	<u>3.38</u>	.786	.792	36 52	37 53	<u>2.94</u>	10.25	4.65
1.5	38, 54	2.44	<u>2.04</u>	3.69	40 56	41 41	1.31	<u>12.38</u>	1.03
1.5	37, 53	1.69	1.69	<u>4.74</u>	37 53	38 54	1.27	1.39	<u>6.63</u>
3	45, 60	<u>2.74</u>	.633	.615	36 52	37 53	<u>2.88</u>	9.18	3.89
3	39, 55	2.21	<u>1.66</u>	1.69	40 56	41 41	1.30	<u>10.15</u>	0.72
3	37, 53	1.33	1.33	<u>3.66</u>	37 53	38 54	1.27	1.25	<u>5.82</u>
5	45, 60	<u>2.22</u>	.519	.496	36 52	37 53	<u>2.82</u>	8.02	3.20
5	39, 55	1.80	<u>1.35</u>	1.35	40 56	41 41	1.29	<u>8.36</u>	0.42
5	37, 53	1.07	1.07	<u>2.90</u>	37 53	38 54	1.26	0.97	<u>5.04</u>
7	45, 60	<u>1.88</u>	.446	.421	36 52	37 53	<u>2.77</u>	7.14	2.73
7	38, 39 54, 55	1.54	<u>1.15</u>	1.87	37 53	37 53	1.26	<u>7.28</u>	2.33
7	37, 53	.909	.907	<u>2.43</u>	37 53	38 54	1.26	0.75	<u>4.47</u>
10	45, 60	<u>1.54</u>	.374	.347	36 52	37 53	<u>2.71</u>	6.14	2.24
10	38, 54	1.15	<u>.949</u>	1.50	37 53	37 53	1.25	<u>6.26</u>	1.89
10	37, 53	.749	.747	<u>1.96</u>	37 53	38 54	1.25	0.51	<u>3.85</u>

TABLE A.4: Stress and Displacement Components (NONFESA) vs. Pressure for 300 sq ft Leaning Arch BAS, D = 8 in, 30 mph parallel wind load

		Displacements (in)			Stresses (lb/in)				
P (psi)	node#	ΔX	ΔY	ΔZ	Element	End	Axial	Bnding2	Bnding3
1.5	21, 30	10.3	8.44	29.7	20 29	21 30	4.28	17.02 13.16	30.52 32.37
1.5	5, 13	7.41	16.6	66.2	25	9	2.27	80.72	19.68
1.5	6, 12	5.14	15.4	68.9	8	9	1.80	28.86	68.57
3	21, 30	7.07	5.59	19.6	20 29	21 30	3.43	11.86 9.26	20.61 21.91
3	5, 13	4.84	11.8	47.1	25	9	1.83	59.55	19.77
3	6, 12	3.39	10.9	48.6	8	9	1.37	25.93	48.50
5	21, 30	4.99	3.84	13.5	20 29	21 30	2.89	8.70 6.91	14.16 15.12
5	5, 13	3.26	8.74	34.9	25	9	1.55	45.29	17.80
5	6, 12	2.31	8.10	35.7	3	4	2.03	18.85	40.87
7	21, 30	3.83	2.90	10.2	20 29	22 29	2.59	6.10 4.63	11.72 12.38
7	5, 13	2.43	6.99	28.0	25	9	1.39	37.01	15.93
7	6, 12	1.74	6.49	28.4	2	3	1.71	12.55	33.81
10	21, 30	2.82	2.11	7.43	20 29	22 29	2.32	4.81 3.73	8.55 9.07
10	5, 13	1.73	5.40	21.7	25	9	1.25	29.37	13.74
10	6, 12	1.25	5.02	21.9	2	3	1.47	11.09	27.46

TABLE A.5: Stress and Displacement Components (NONFESA) vs. Pressure for 300 sq ft Leaning Arch BAS with guylines, D = 8 in, 30 mph parallel wind load

		Displacements (in)			Stresses (lb/in)				
P (psi)	node#	ΔX	ΔY	ΔZ	Element	End	Axial	Bnding2	Bnding3
1.5	5, 13	1.94	2.11	2.11	2 15	3 15	8.10	24.04 29.27	16.96 3.00
1.5	5, 13	1.94	2.11	2.11	14	15	8.07	29.36	1.76
1.5	3, 15	1.02	1.56	5.78	1	2	8.04	16.00	20.10
3	5, 13	1.75	1.97	1.97	2 15	3 15	7.96	22.14 26.89	15.53 2.82
3	5, 13	1.75	1.97	1.97	14	15	7.93	26.98	1.68
3	3, 15	.966	1.41	5.20	1	2	7.91	14.72	18.53
5	5, 13	1.56	1.82	1.82	2 15	3 15	7.80	20.00 24.30	14.04 2.54
5	5, 13	1.56	1.82	1.82	14	15	7.77	24.38	1.51
5	3, 15	.883	1.28	4.66	1	2	7.75	13.27	16.82
7	5, 13	1.42	1.69	1.70	2 15	3 15	7.66	18.22 22.18	12.84 2.28
7	5, 13	1.42	1.69	1.70	15	15	7.66	22.18	2.28
7	3, 15	.805	1.18	4.24	1	2	7.60	12.07	15.42
10	5, 13	1.25	1.54	1.55	2 15	3 15	7.47	16.07 19.62	11.42 1.94
10	5, 13	1.25	1.54	1.55	14	15	7.44	19.68	1.11
10	3, 15	.704	1.06	3.76	1	2	7.42	10.61	13.74

APPENDIX B

Tables of Computed Peak Compressive Stress and Maximum Deflection vs. Beam Inflation Pressure

TABLE B.1 Peak compressive stress vs. beam inflation pressure for 400 sq ft Leaning Arch BAS, All loads, beam diameters, D = 8, 11, 14 inches

σ_c (lb/in)

D	P (psi)	snow 10 psf	wind 30 mph	30 mph wind w/guyline	11 wind 30 mph	30 mph 11 wind w/ guyline	snow 5 psf
8 in	1.5	74.55	46.14	21.27	83.78	40.89	37.28
	3	65.55	35.24	19.08	65.63	38.08	32.77
	5	56.85	26.95	16.80	52.12	34.99	28.43
	7	50.43	21.87	15.12	43.74	32.46	25.22
	10	43.40	17.05	13.29	35.69	29.41	21.70
11 in	1.5	40.73	25.83	11.91	46.06	23.65	20.37
	3	36.35	20.38	10.88	36.56	22.20	18.17
	5	31.96	15.96	9.71	29.30	20.56	15.98
	7	28.64	13.12	8.82	24.68	19.18	14.32
	10	24.90	10.35	7.80	20.16	17.51	12.45
14 in	1.5	25.62	16.34	7.68	28.79	15.73	12.81
	3	23.00	13.14	7.08	22.96	14.82	11.50
	4	21.59	11.62	6.70	20.43	14.27	10.80
	5	20.36	10.43	6.37	18.48	13.77	10.18
	7.5	17.89	8.29	5.69	15.04	12.67	8.95
	10	16.00	6.87	5.17	12.75	11.77	8.00

TABLE B.2: Peak compressive stress vs. beam inflation pressure for 400 sq ft Vertical Arch BAS, All loads, beam diameters, D = 8, 11, 14 inches

σ_c (lb/in)

D	P (psi)	snow 10 psf	wind 30 mph	30 mph wind w/guyline	11 wind 30 mph	30 mph 11 wind w/ guyline	snow 5 psf
8 in	1.5	80.84	59.54	14.48	59.69	31.29	40.42
	3	71.30	46.61	13.68	49.71	29.08	35.65
	5	61.80	36.49	12.84	40.93	26.69	30.91
	7	54.67	30.13	12.18	34.91	24.75	27.33
	10	46.77	23.95	11.38	31.83	22.41	23.38
11 in	1.5	45.33	33.94	8.40	33.25	17.80	22.67
	3	40.95	27.35	7.97	28.32	16.67	20.48
	5	36.45	21.87	7.50	23.78	15.41	18.23
	7	32.97	18.28	7.11	20.56	14.37	16.49
	10	28.99	14.68	6.65	17.14	13.10	14.50
14 in	1.5	30.09	21.78	5.55	21.17	11.68	15.05
	3	27.36	17.82	5.26	18.25	10.98	13.68
	5	24.50	14.42	4.95	15.50	10.17	12.25
	7	22.26	12.12	4.70	13.49	9.50	11.13
	10	19.67	9.79	4.40	11.33	8.68	9.84

TABLE B.3: Peak compressive stress vs. beam inflation pressure for 300 sq ft Leaning Arch BAS, All loads, beam diameters, D = 8, 11, 14 inches

σ_c (lb/in)

D	P (psi)	snow 10 psf	wind 30 mph	30 mph wind w/guyline	11 wind 30 mph	30 mph 11 wind w/ guyline	snow 5 psf
8 in	1.5	54.91	35.37	14.20	85.35	37.52	27.45
	3	48.37	27.14	12.85	64.58	35.00	24.18
	5	42.00	20.82	11.45	50.21	32.24	21.00
	7	37.28	16.93	10.41	41.68	29.96	18.64
	10	32.11	13.23	9.25	33.68	27.19	16.05
11 in	1.5	30.03	19.78	8.00	47.25	21.62	15.01
	3	26.86	15.66	7.36	36.27	20.33	13.43
	5	23.66	12.31	6.65	28.48	18.86	11.83
	7	21.23	10.13	6.09	23.74	17.64	10.62
	10	18.47	8.02	5.44	19.20	16.13	9.24
14 in	1.5	18.92	12.49	5.19	29.59	14.35	9.46
	3	17.03	10.09	4.84	22.88	13.55	8.52
	5	15.11	8.03	4.39	18.09	12.60	7.55
	7	13.62	6.68	4.04	15.11	11.81	6.81
	10	11.92	5.30	3.64	12.25	10.82	5.96

TABLE B.4: Peak compressive stress vs. beam inflation pressure for 300 sq ft Vertical Arch BAS, All loads, beam diameters, D = 8, 11, 14 inches

σ_c (lb/in)

D	P (psi)	snow 10 psf	wind 30 mph	30 mph wind w/guyline	11 wind 30 mph	30 mph 11 wind w/ guyline	snow 5 psf
8 in	1.5	65.02	45.13	11.03	59.67	31.31	32.51
	3	57.58	35.27	10.42	49.69	29.09	28.79
	5	50.14	27.58	9.78	40.94	26.71	25.07
	7	44.55	22.75	9.27	36.58	24.77	22.28
	10	38.31	18.09	8.67	31.86	22.41	19.16
11 in	1.5	33.81	25.58	6.40	33.21	17.81	16.91
	3	30.29	20.60	6.06	28.30	16.67	15.15
	5	26.67	16.47	5.71	23.79	15.42	13.34
	7	23.89	13.76	5.42	20.57	14.37	11.95
	10	20.71	11.06	5.07	17.15	13.11	10.36
14 in	1.5	21.68	16.37	4.22	21.13	11.69	10.84
	3	19.69	13.40	4.02	18.25	10.97	9.85
	5	17.62	10.84	3.78	15.51	10.17	8.81
	7	16.01	9.13	3.59	13.50	9.51	8.01
	10	14.24	7.38	3.36	11.34	8.68	7.12

TABLE B.5: Maximum deflection vs. beam inflation pressure for 400 sq ft Leaning Arch BAS, All loads except 5 psf snow, beam diameters, D = 8, 11, 14 inches

δ (in)

D	P (psi)	snow 10 psf	wind 30 mph	30 mph wind w/guyline	11 wind 30 mph	30 mph 11 wind w/ guyline
8 in	1.5	21.60	37.63	8.89	60.76	6.92
	3	18.70	27.73	6.86	44.83	6.23
	5	15.90	20.61	5.42	34.01	5.58
	7	13.90	16.44	4.53	27.55	5.08
	10	11.70	12.67	3.65	21.62	4.51
11 in	1.5	10.10	16.87	4.17	29.26	3.66
	3	8.91	12.99	3.28	21.85	3.32
	5	7.74	9.92	2.64	16.73	2.99
	7	6.87	8.06	2.23	13.81	2.74
	10	5.89	6.30	1.82	10.96	2.43
14 in	1.5	5.94	9.34	2.42	17.35	2.37
	3	5.31	7.36	1.93	13.06	2.15
	4	4.96	6.44	1.72	11.39	2.05
	5	4.66	5.74	1.56	10.08	1.94
	7.5	4.06	4.52	1.28	7.94	1.74
	10	3.61	3.73	1.10	6.58	1.58

TABLE B.6: Maximum deflection vs. beam inflation pressure for 400 sq ft Vertical Arch BAS, All loads except 5 psf snow, beam diameters, D = 8, 11, 14 inches

δ (in)

D	P (psi)	snow 10 psf	wind 30 mph	30 mph wind w/guyline	11 wind 30 mph	30 mph 11 wind w/ guyline
8 in	1.5	24.10	43.75	3.42	56.20	4.80
	3	21.20	32.92	3.03	37.00	4.29
	5	18.30	25.08	2.58	26.90	3.85
	7	16.10	20.30	2.27	21.50	3.50
	10	13.70	15.93	1.94	16.70	3.09
11 in	1.5	11.80	20.03	1.74	27.70	2.51
	3	10.50	15.74	1.54	18.20	2.27
	5	9.26	12.28	1.35	13.30	2.04
	7	8.29	10.15	1.21	10.80	1.86
	10	7.20	8.07	1.05	8.44	1.66
14 in	1.5	7.17	11.28	1.08	16.30	1.62
	3	6.47	9.05	0.97	10.80	1.47
	5	5.74	7.21	0.86	7.94	1.32
	7	5.17	6.02	0.77	6.43	1.20
	10	4.52	4.85	0.68	5.08	1.07

TABLE B.7: Maximum deflection vs. beam inflation pressure for 300 sq ft Leaning Arch BAS, All loads except 5 psf snow, beam diameters, D = 8, 11, 14 inches

δ (in)

D	P (psi)	snow 10 psf	wind 30 mph	30 mph wind w/guyline	11 wind 30 mph	30 mph 11 wind w/ guyline
8 in	1.5	15.90	28.19	5.31	70.79	6.07
	3	13.80	20.83	4.12	49.92	5.47
	5	11.70	15.53	3.27	36.68	4.91
	7	10.30	12.38	2.75	29.18	4.47
	10	8.65	9.56	2.23	22.50	3.97
11 in	1.5	7.41	12.61	2.50	34.21	3.20
	3	6.57	9.73	1.97	24.55	2.91
	5	5.72	7.46	1.60	18.29	2.62
	7	5.08	6.07	1.35	14.79	2.41
	10	4.36	4.76	1.12	11.50	2.14
14 in	1.5	4.37	6.97	1.46	20.34	2.08
	3	3.91	5.51	1.16	14.69	1.90
	5	3.44	4.31	0.95	10.99	1.71
	7	3.08	3.55	0.81	8.89	1.56
	10	2.67	2.82	0.67	6.96	1.39

TABLE B.8: Maximum deflection vs. beam inflation pressure for 300 sq ft Vertical Arch BAS, All loads except 5 psf snow, beam diameters, D = 8, 11, 14 inches

δ (in)

D	P (psi)	snow 10 psf	wind 30 mph	30 mph wind w/guyline	11 wind 30 mph	30 mph 11 wind w/ guyline
8 in	1.5	18.10	33.06	2.63	56.30	4.30
	3	15.80	24.79	2.28	37.00	4.29
	5	13.60	18.79	1.94	26.90	3.85
	7	12.00	15.22	1.71	21.50	3.50
	10	10.20	11.87	1.46	16.70	3.10
11 in	1.5	8.68	15.05	1.31	27.70	2.51
	3	7.76	11.78	1.16	18.20	2.27
	5	6.81	9.18	1.02	13.30	2.04
	7	6.09	7.56	0.91	10.70	1.86
	10	5.28	6.00	0.79	8.43	1.66
14 in	1.5	5.25	8.43	0.81	16.30	1.62
	3	4.74	6.74	0.72	10.80	1.47
	5	4.20	5.37	0.64	7.94	1.32
	7	3.79	4.47	0.58	6.43	1.20
	10	3.31	3.60	0.51	5.08	1.07

APPENDIX C

Plots of Peak Compressive Stress, Wrinkle Stress and Maximum Deflection vs. Beam Inflation Pressure for Each Load and Arrangement

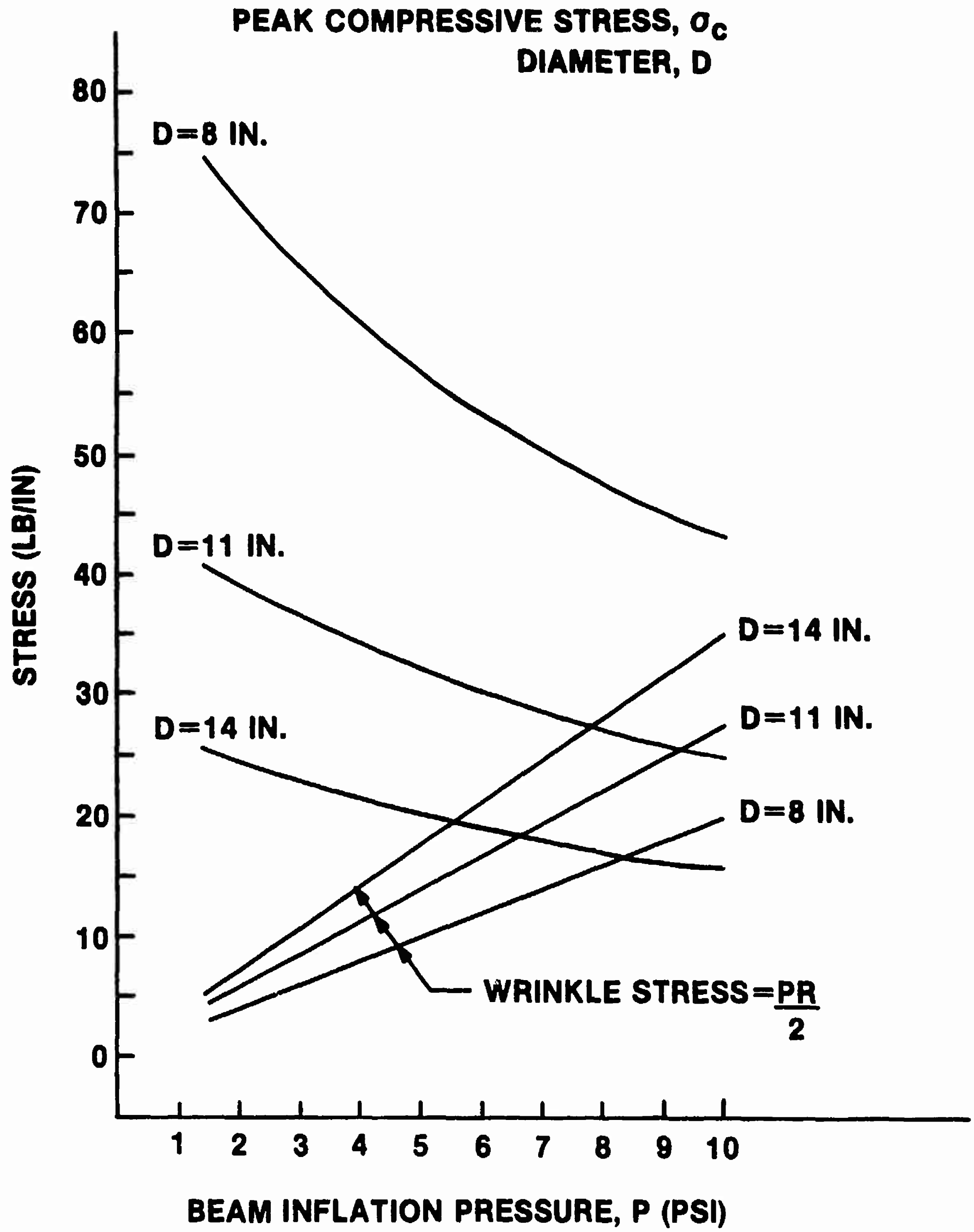

FIGURE C.1: Peak compressive and wrinkle stress vs. inflation pressure for 400 sq ft Leaning Arch BAS, 10 psf snow load

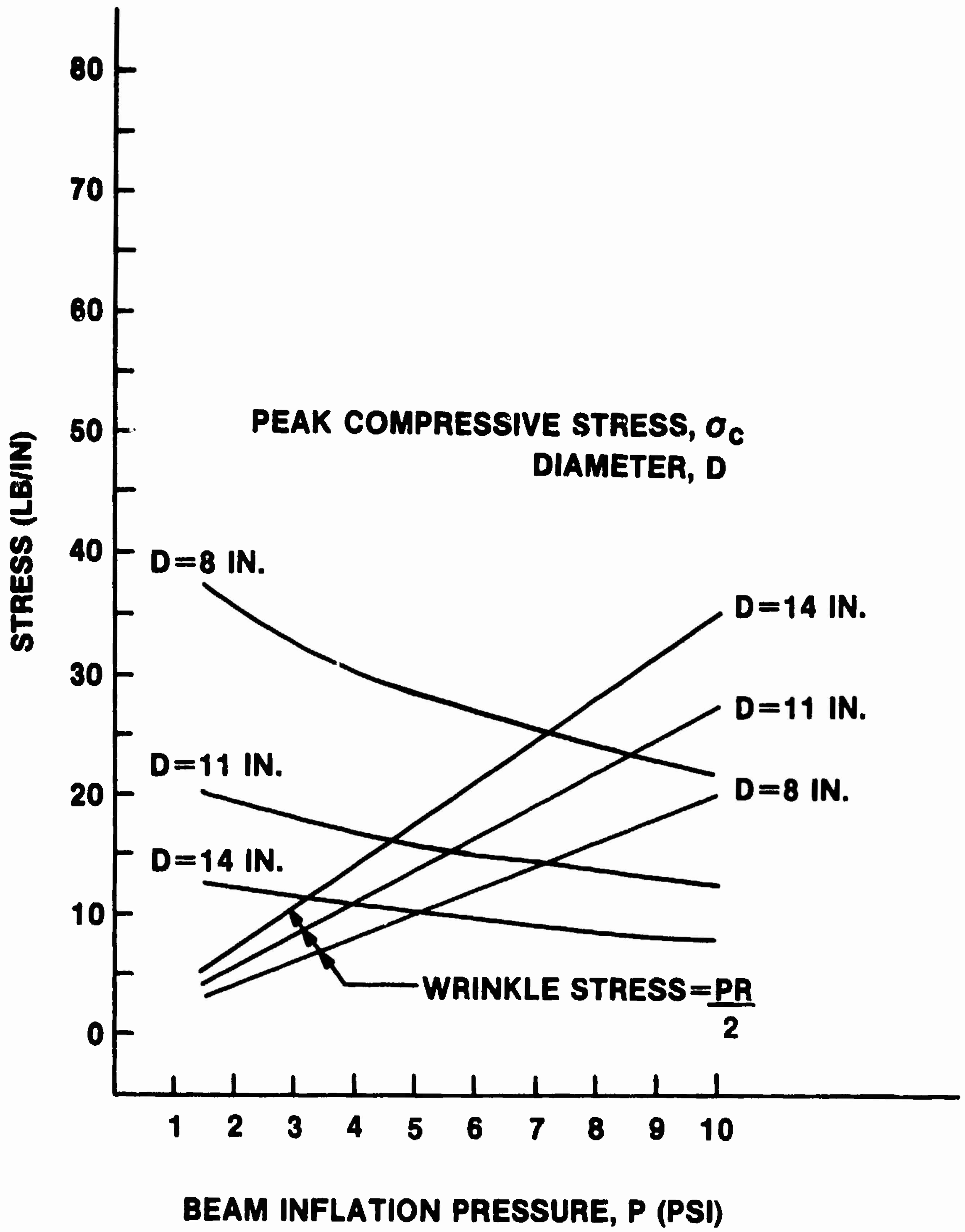

FIGURE C.2: Peak compressive and wrinkle stress vs. inflation pressure for 400 sq ft Leaning Arch BAS, 5 psf snow load

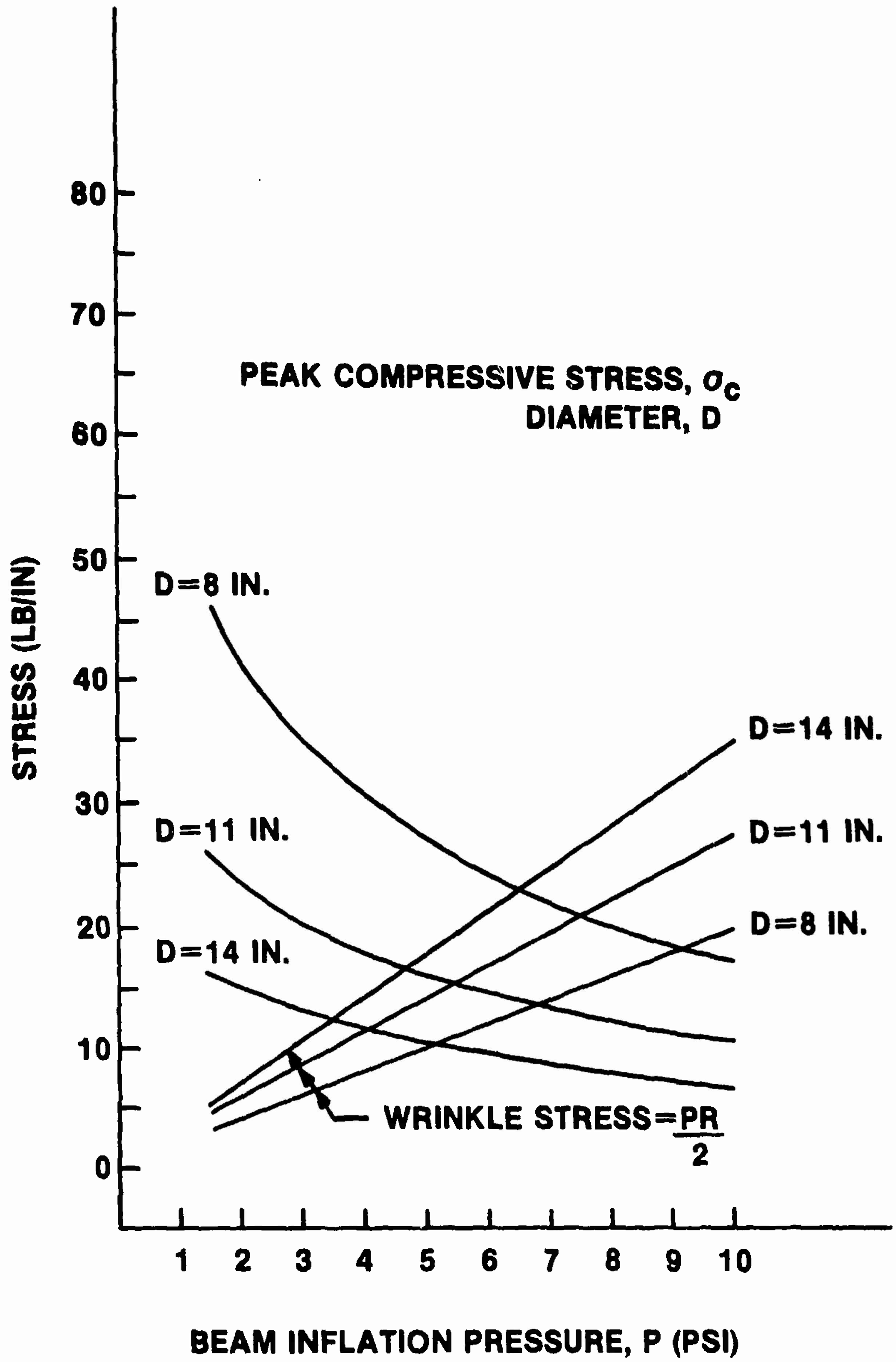

FIGURE C.3: Peak compressive and wrinkle stress vs. inflation pressure for 400 sq ft Leaning Arch BAS, 30 mph wind load

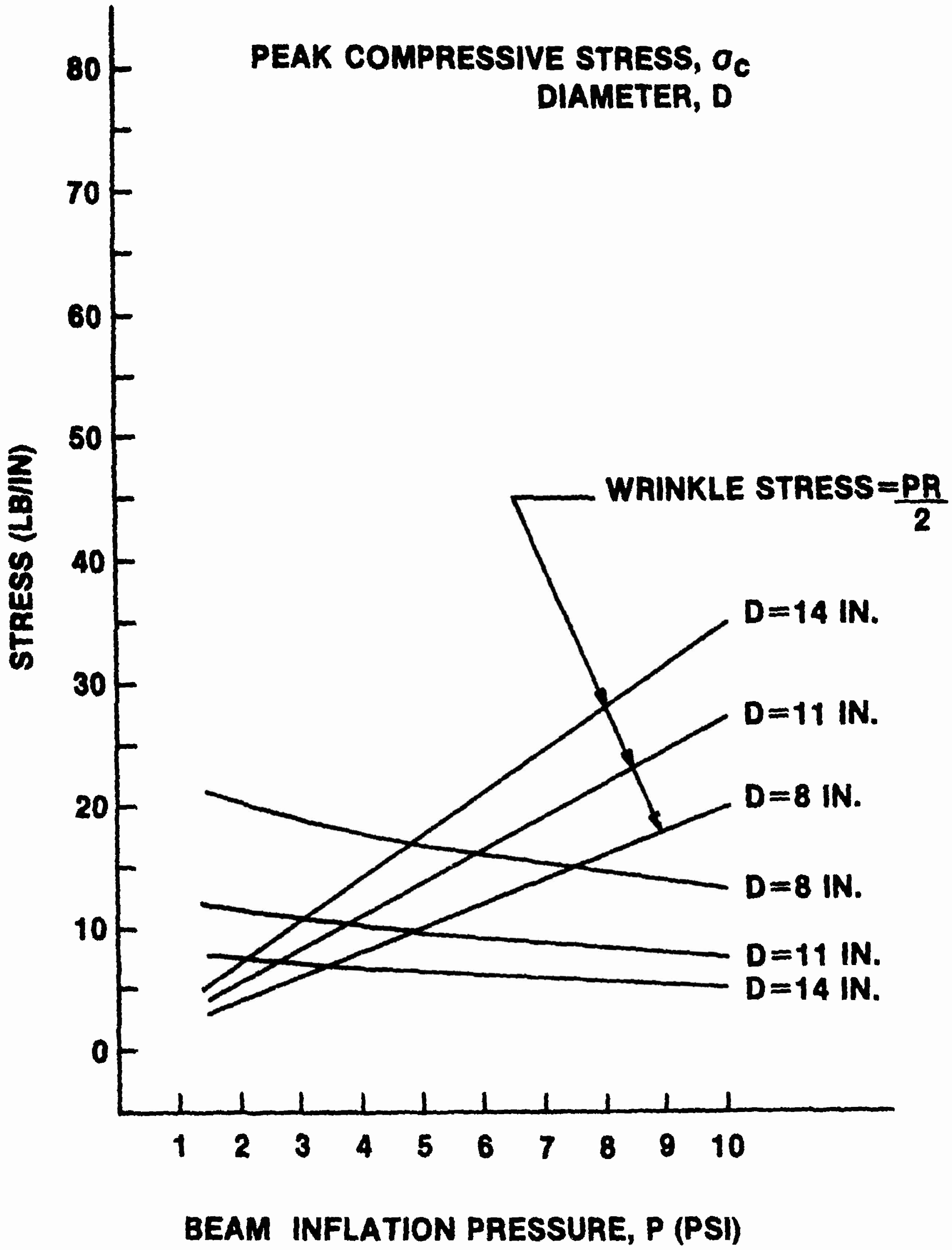

FIGURE C.4: Peak compressive and wrinkle stress vs. inflation pressure for 400 sq ft Leaning Arch BAS with guylines, 30 mph wind load

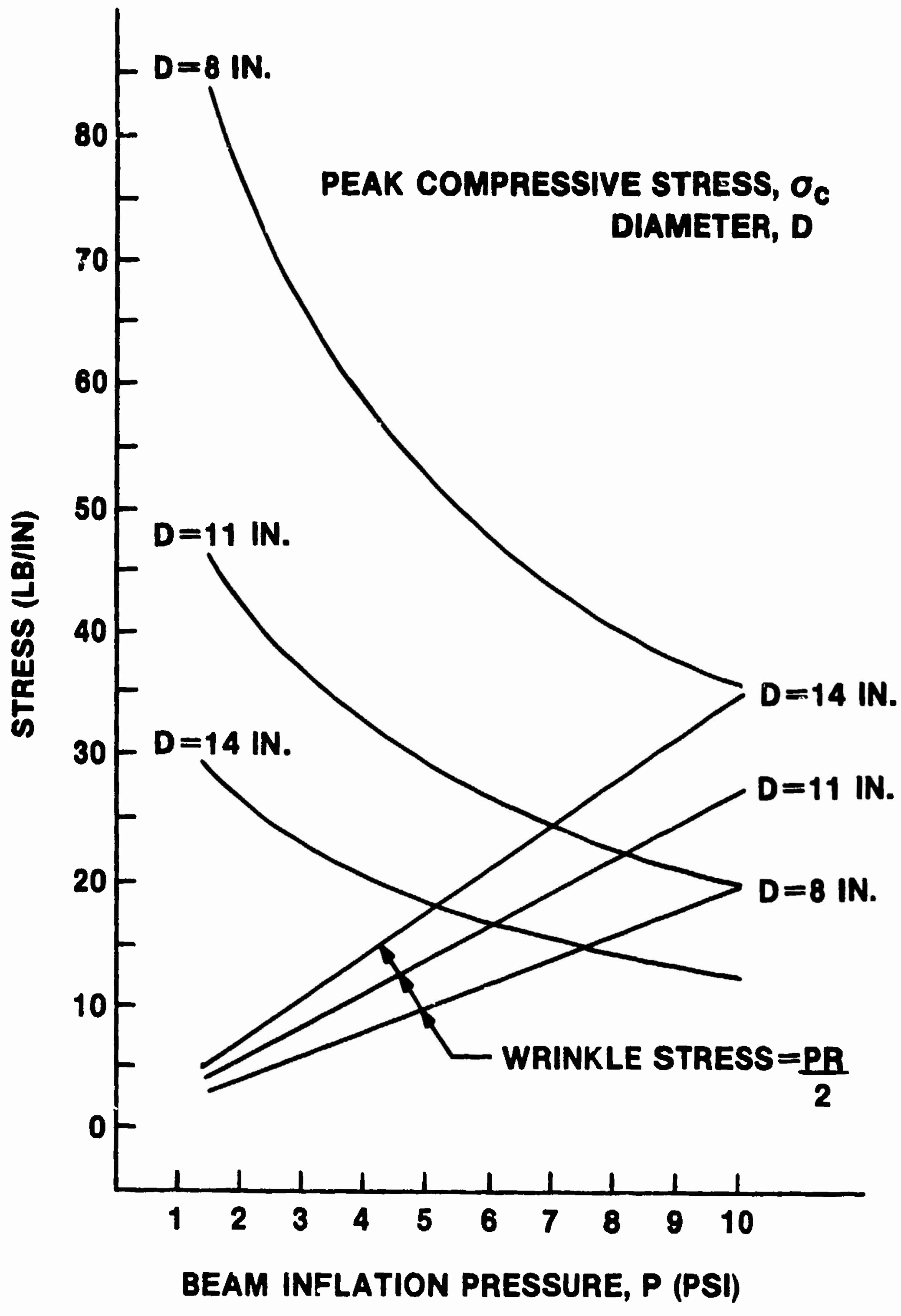

FIGURE C.5: Peak compressive and wrinkle stress vs. inflation pressure for 400 sq ft Leaning Arch BAS, 30 mph parallel wind load

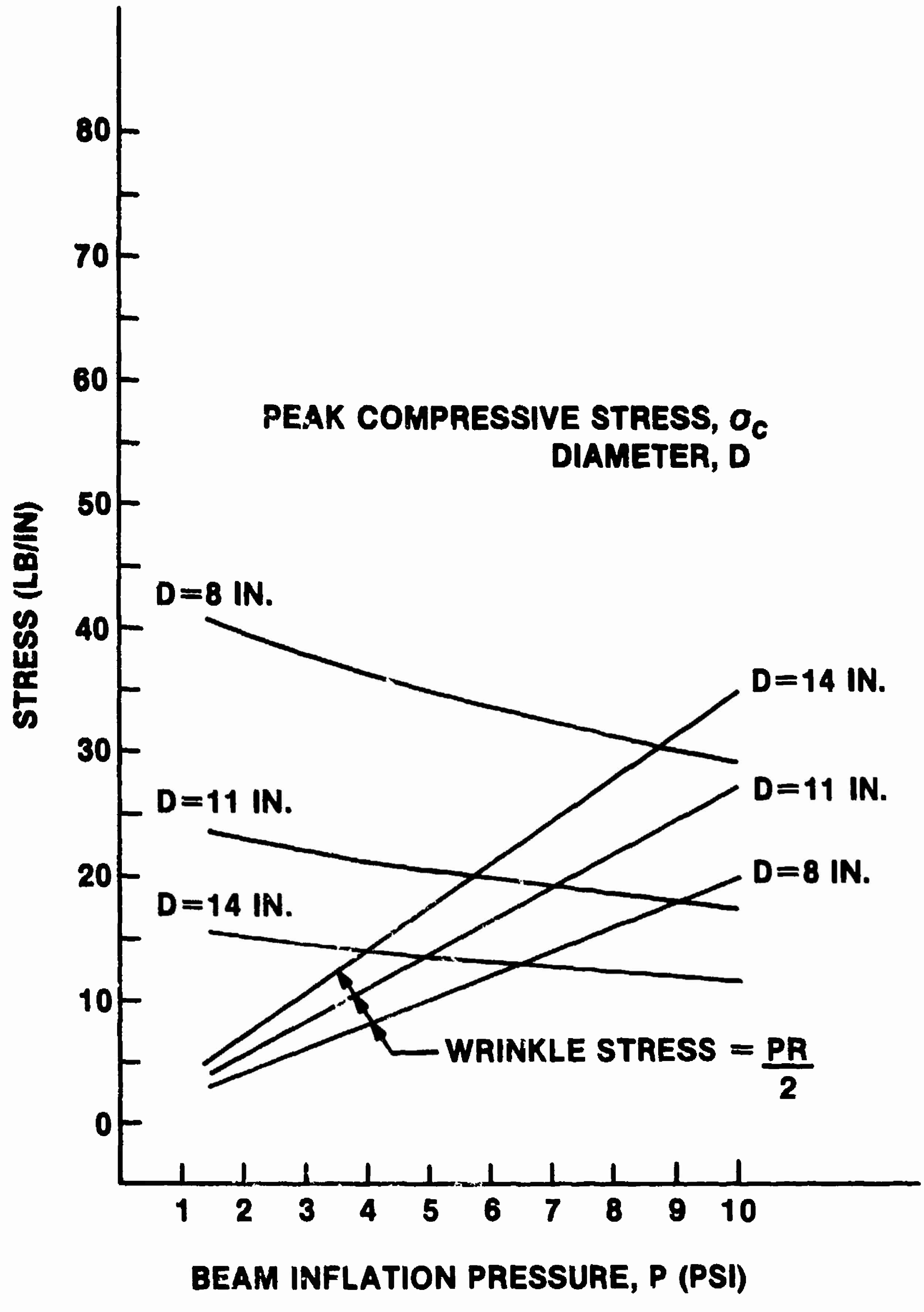

FIGURE C.6: Peak compressive and wrinkle stress vs. inflation pressure for 400 sq ft Leaning Arch BAS with guylines, 30 mph parallel wind load

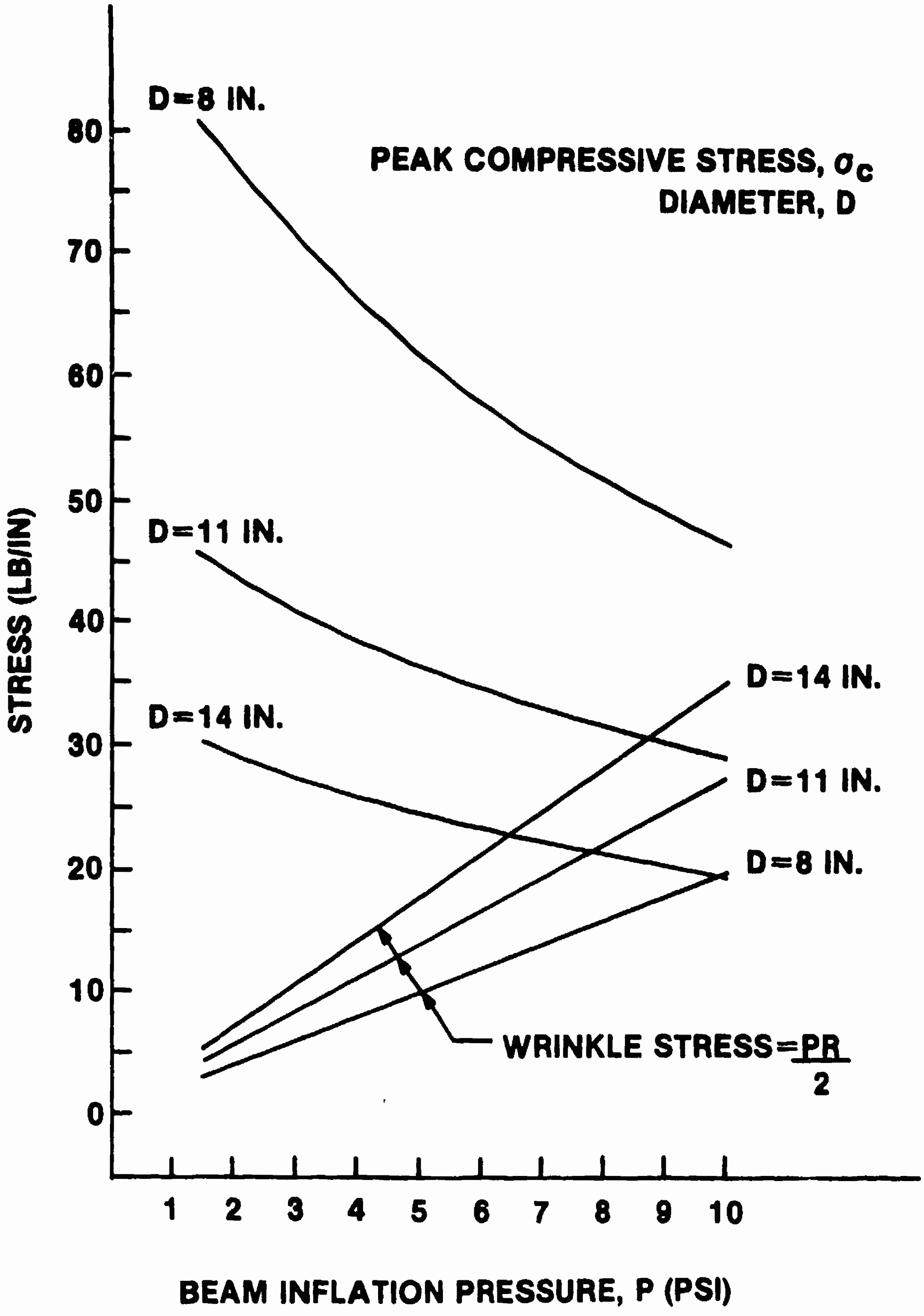

FIGURE C.7: Peak compressive and wrinkle stress vs. inflation pressure for 400 sq ft Vertical Arch BAS, 10 psf snow load

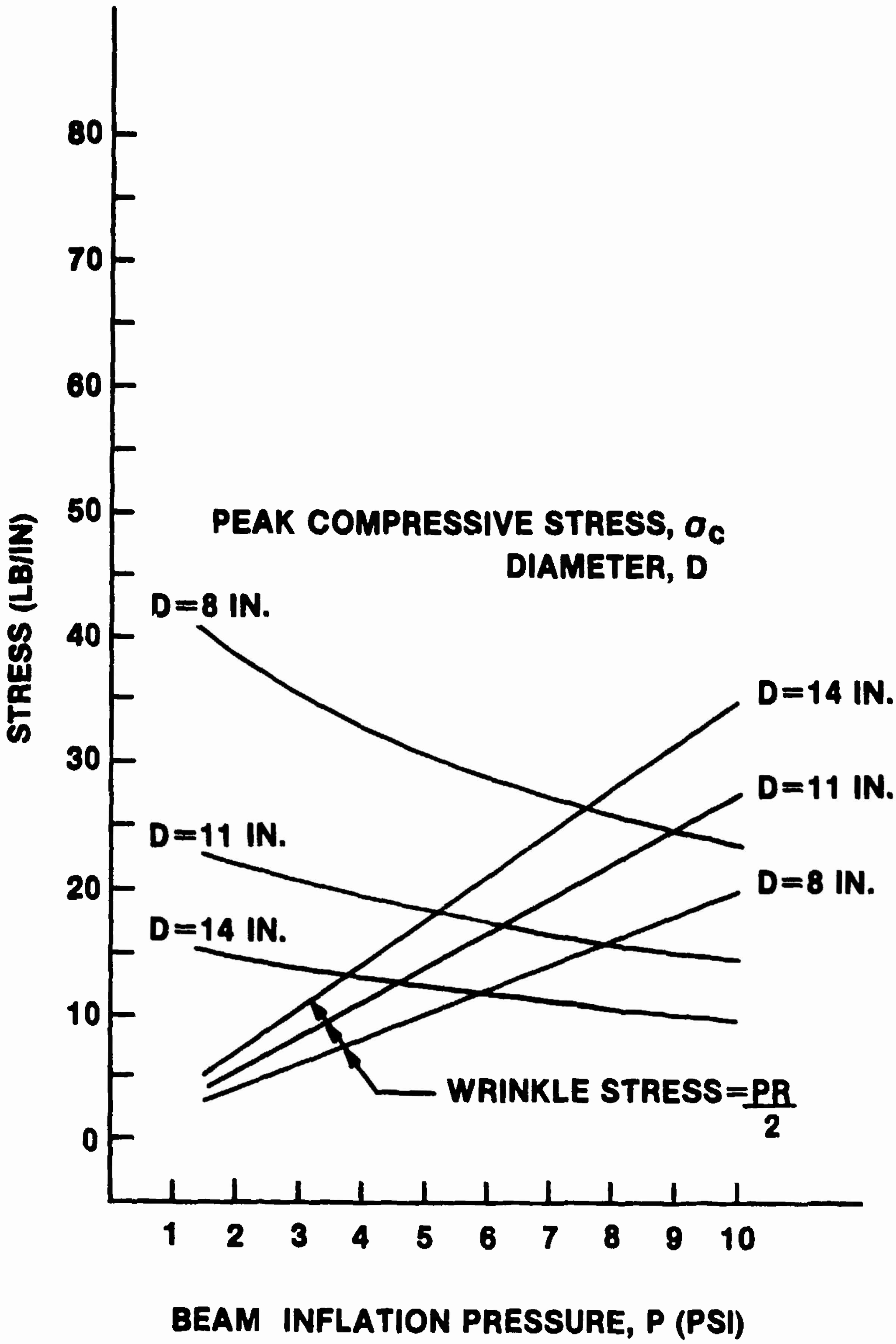

FIGURE C.8: Peak compressive and wrinkle stress vs. inflation pressure for 400 sq ft Vertical Arch BAS, 5 psf snow load

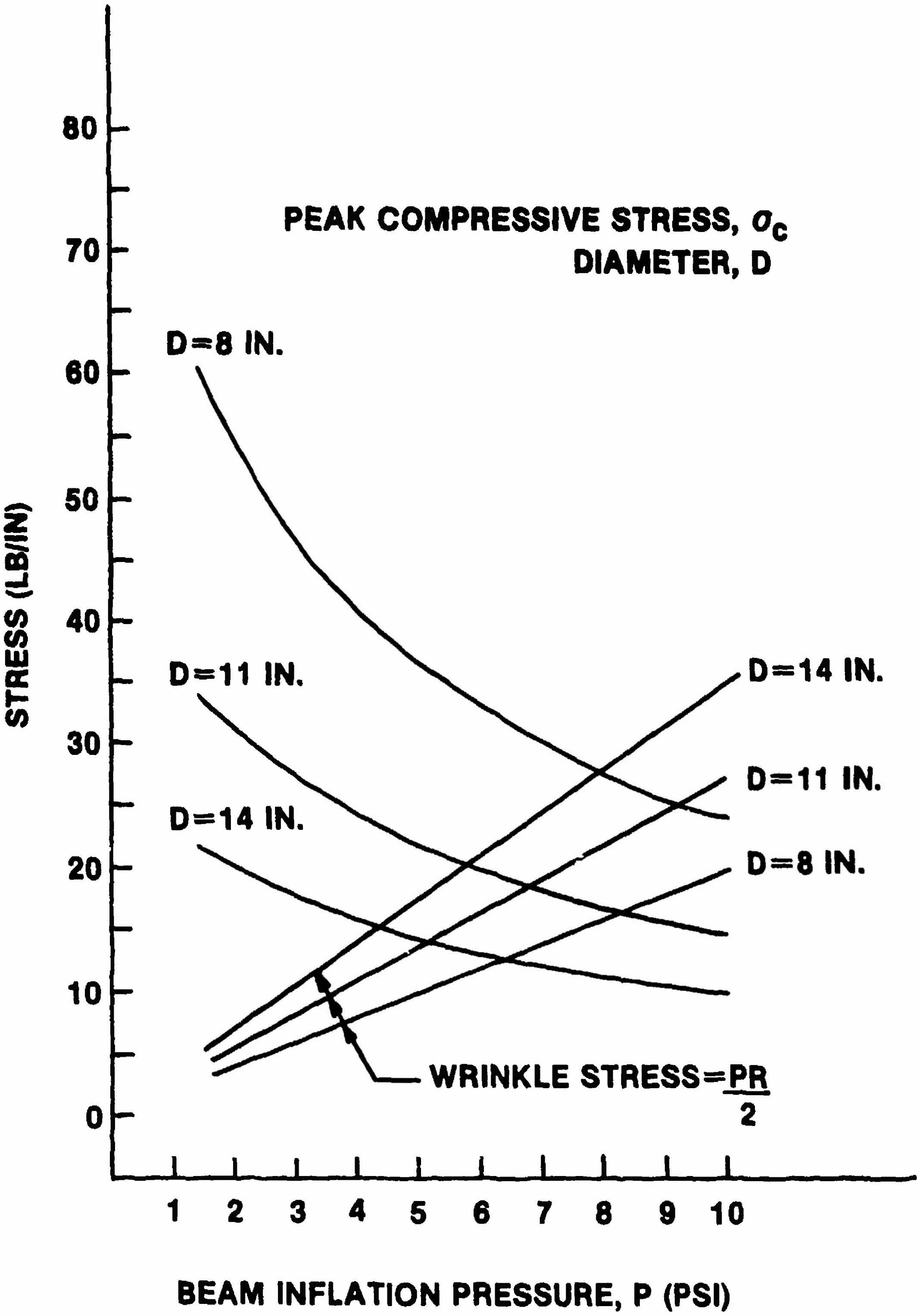

FIGURE C.9: Peak compressive and wrinkle stress vs. inflation pressure for 400 sq ft Vertical Arch BAS, 30 mph wind load

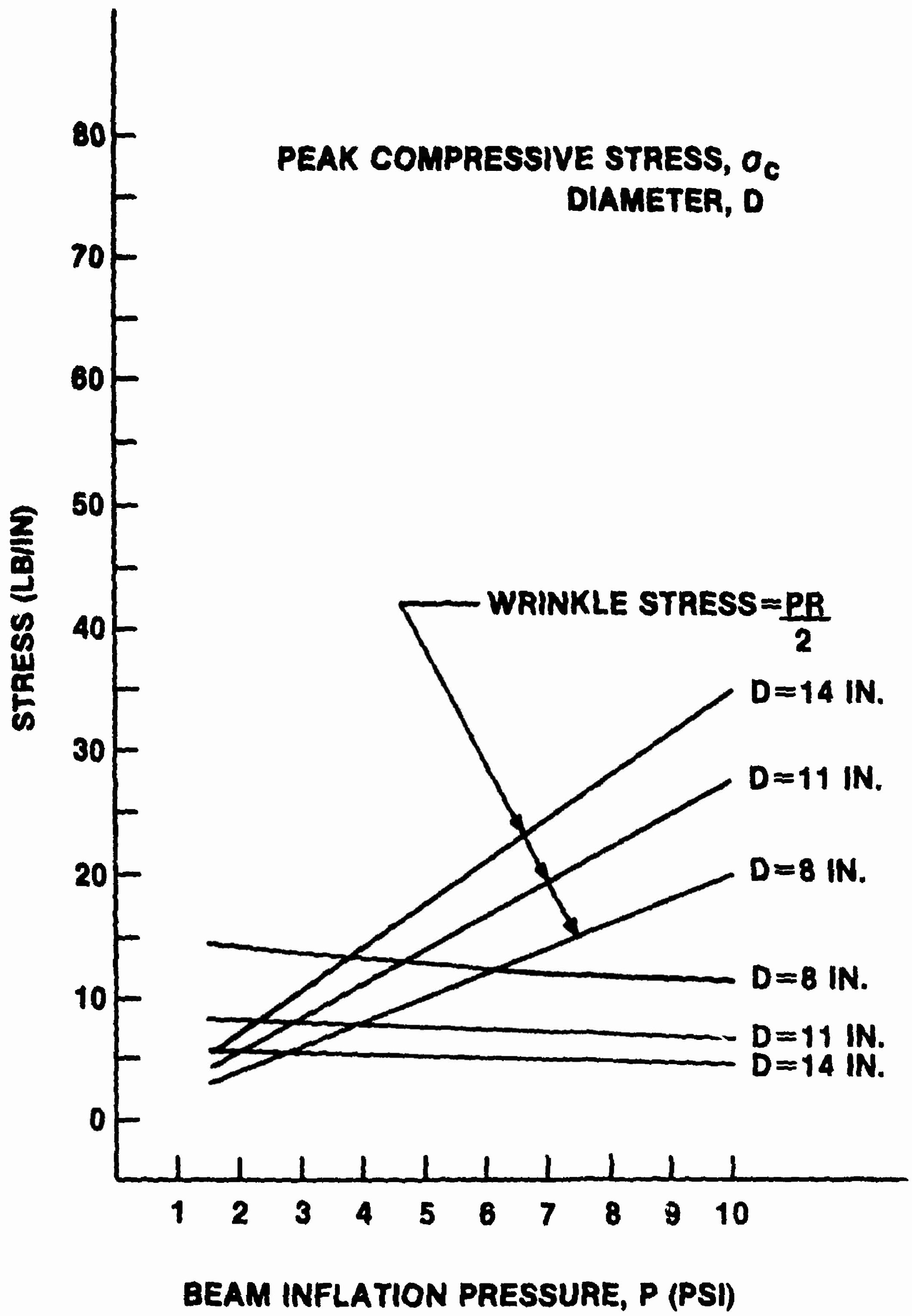

FIGURE C.10: Peak compressive and wrinkle stress vs. inflation pressure for 400 sq ft Vertical Arch BAS with guylines, 30 mph wind load

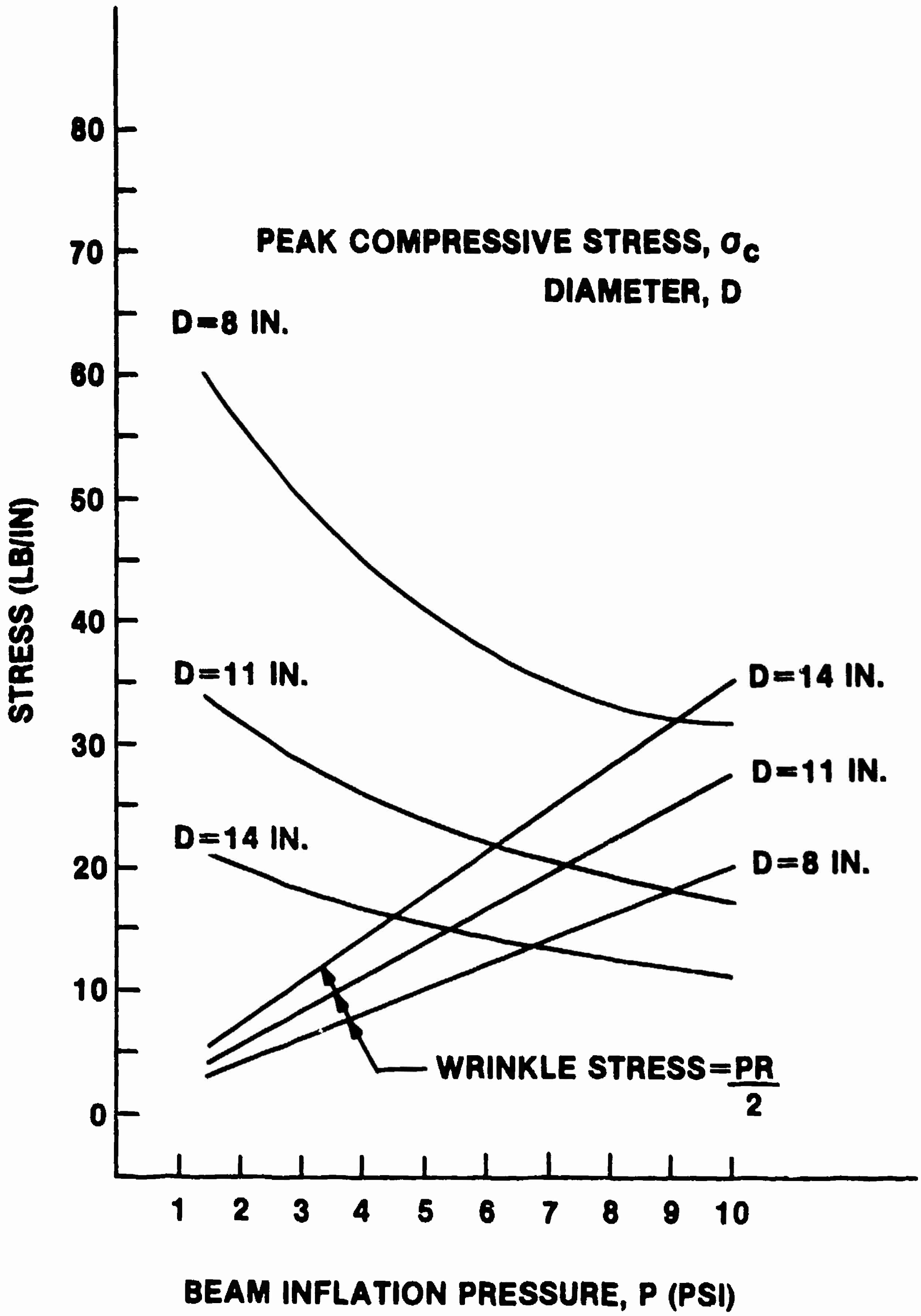

FIGURE C.11: Peak compressive and wrinkle stress vs. inflation pressure for 400 sq ft Vertical Arch BAS, 30 mph parallel wind load

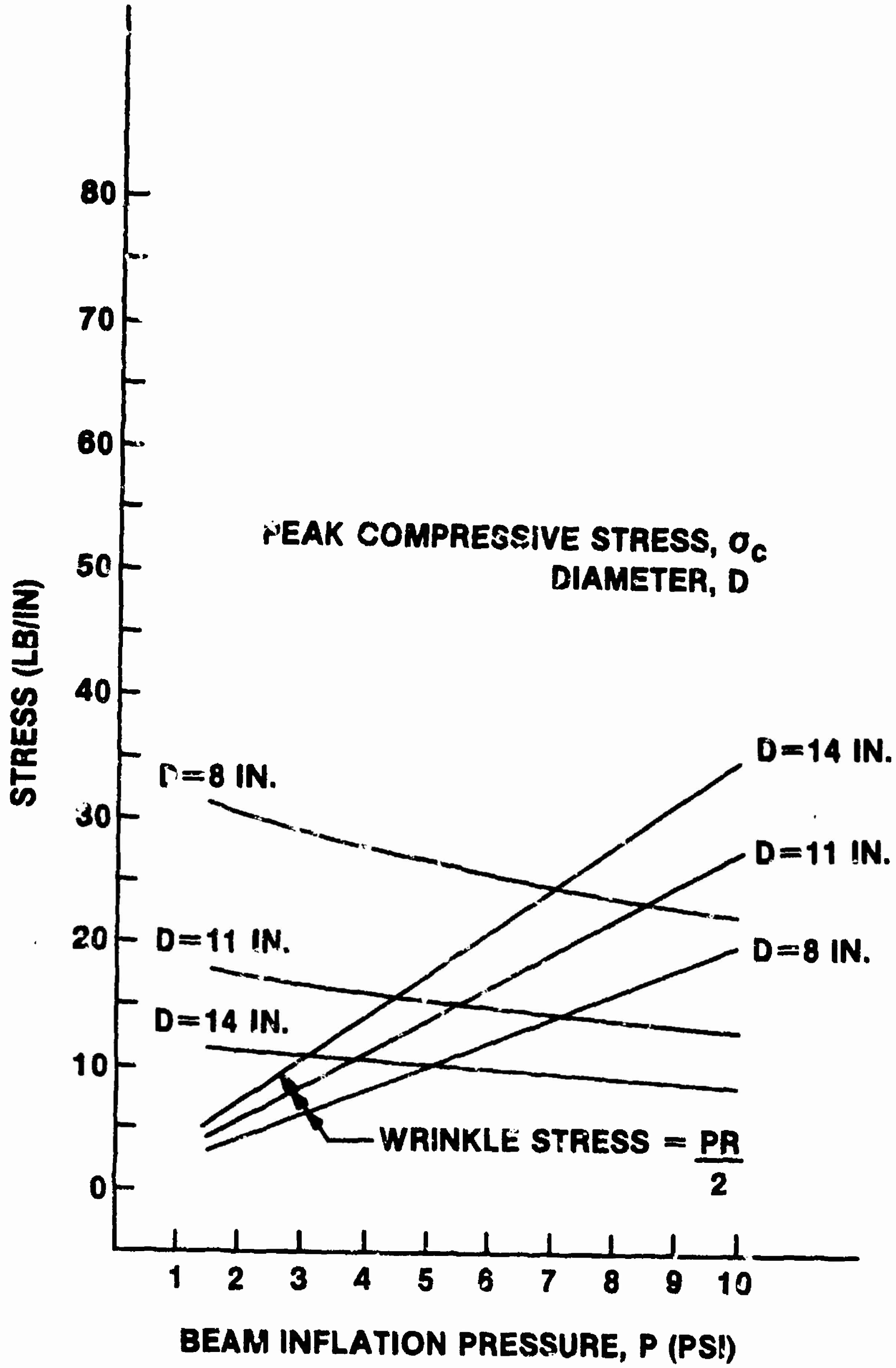

FIGURE C.12: Peak compressive and wrinkle stress vs. inflation pressure for 400 sq ft Vertical Arch BAS with guylines, 30 mph parallel wind load

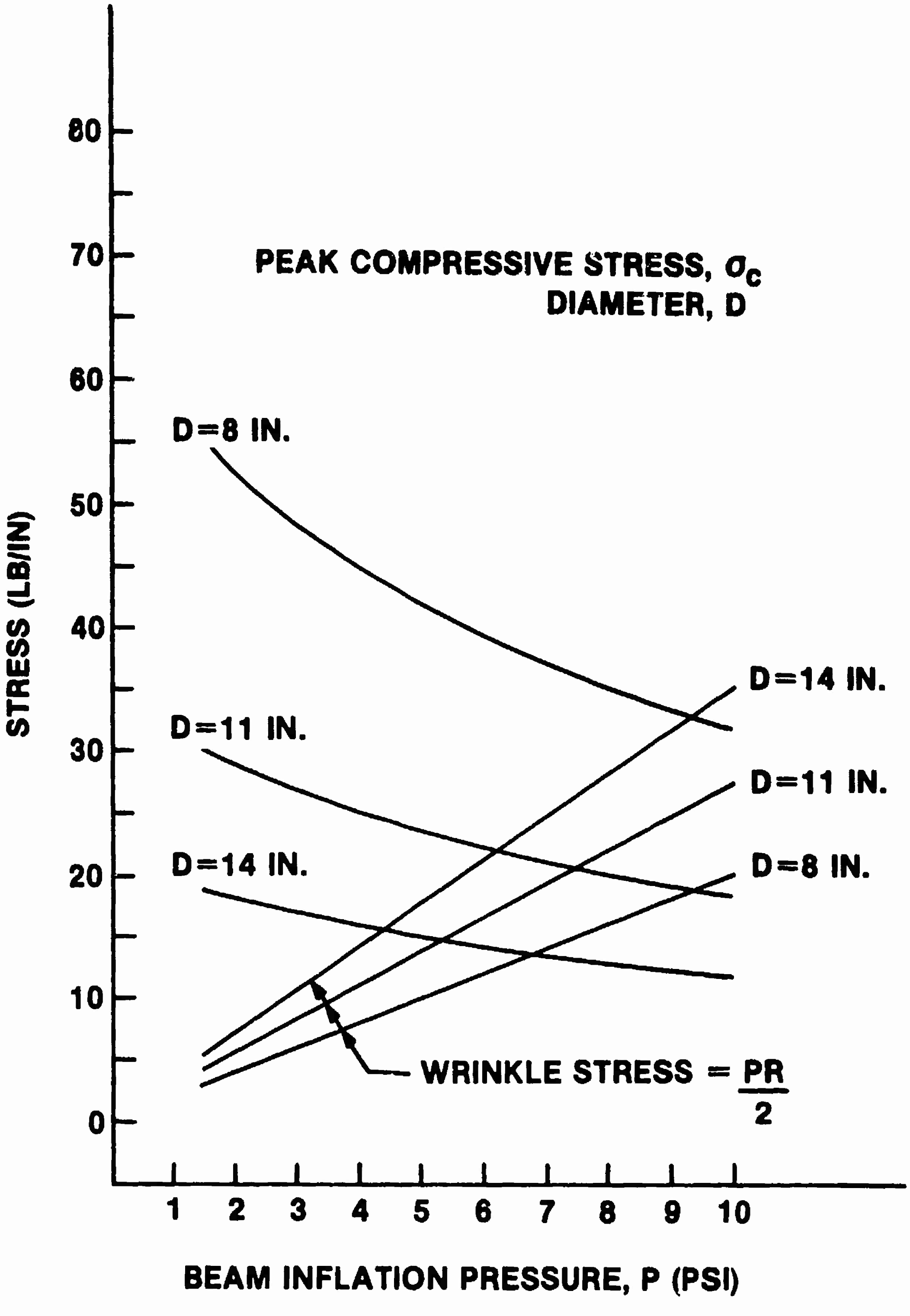

FIGURE C.13: Peak compressive and wrinkle stress vs. inflation pressure for 300 sq ft Leaning Arch BAS, 10 psf snow load

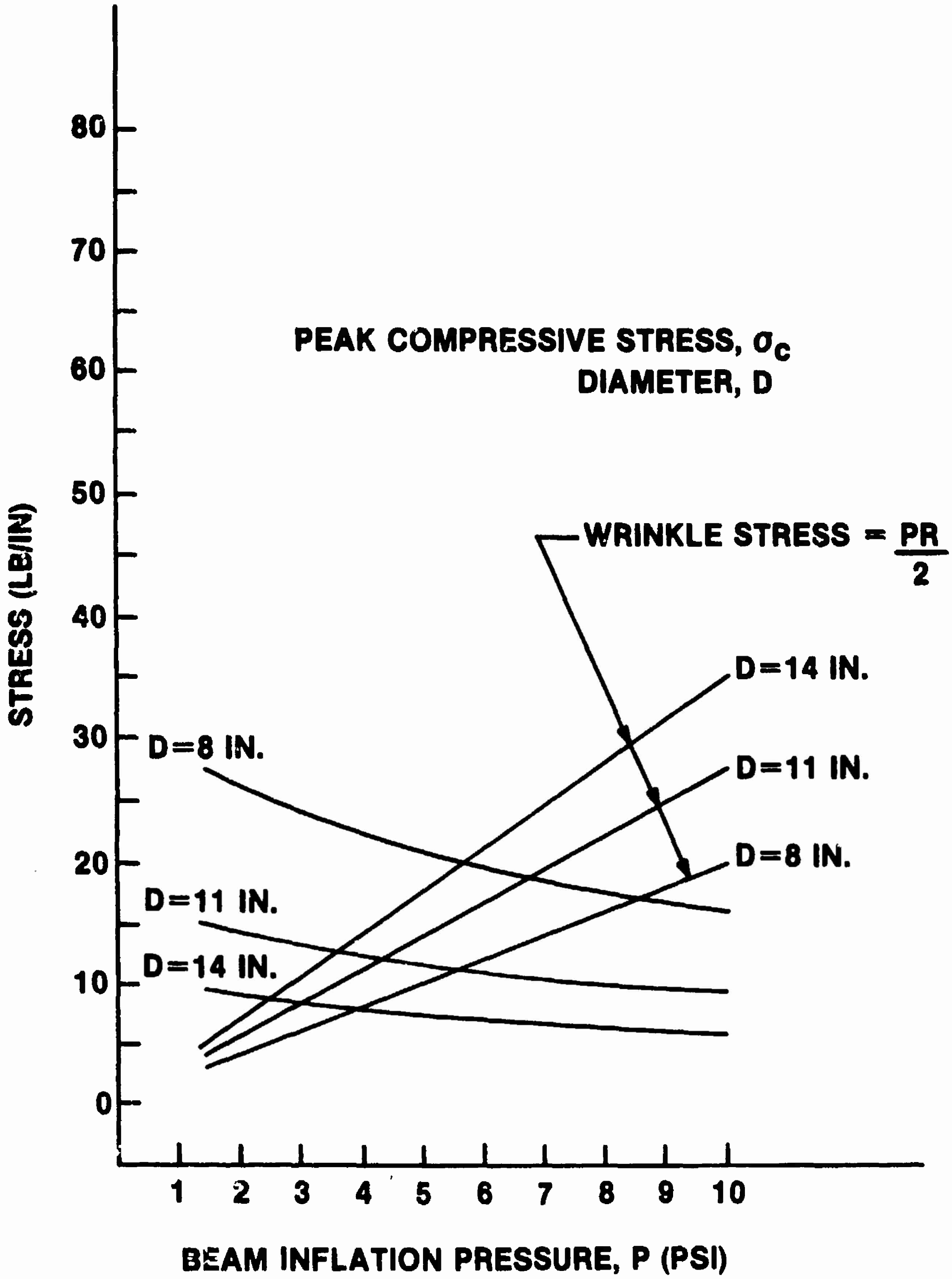

FIGURE C.14: Peak compressive and wrinkle stress vs. inflation pressure for 300 sq ft Leaning Arch BAS, 5 psf snow load

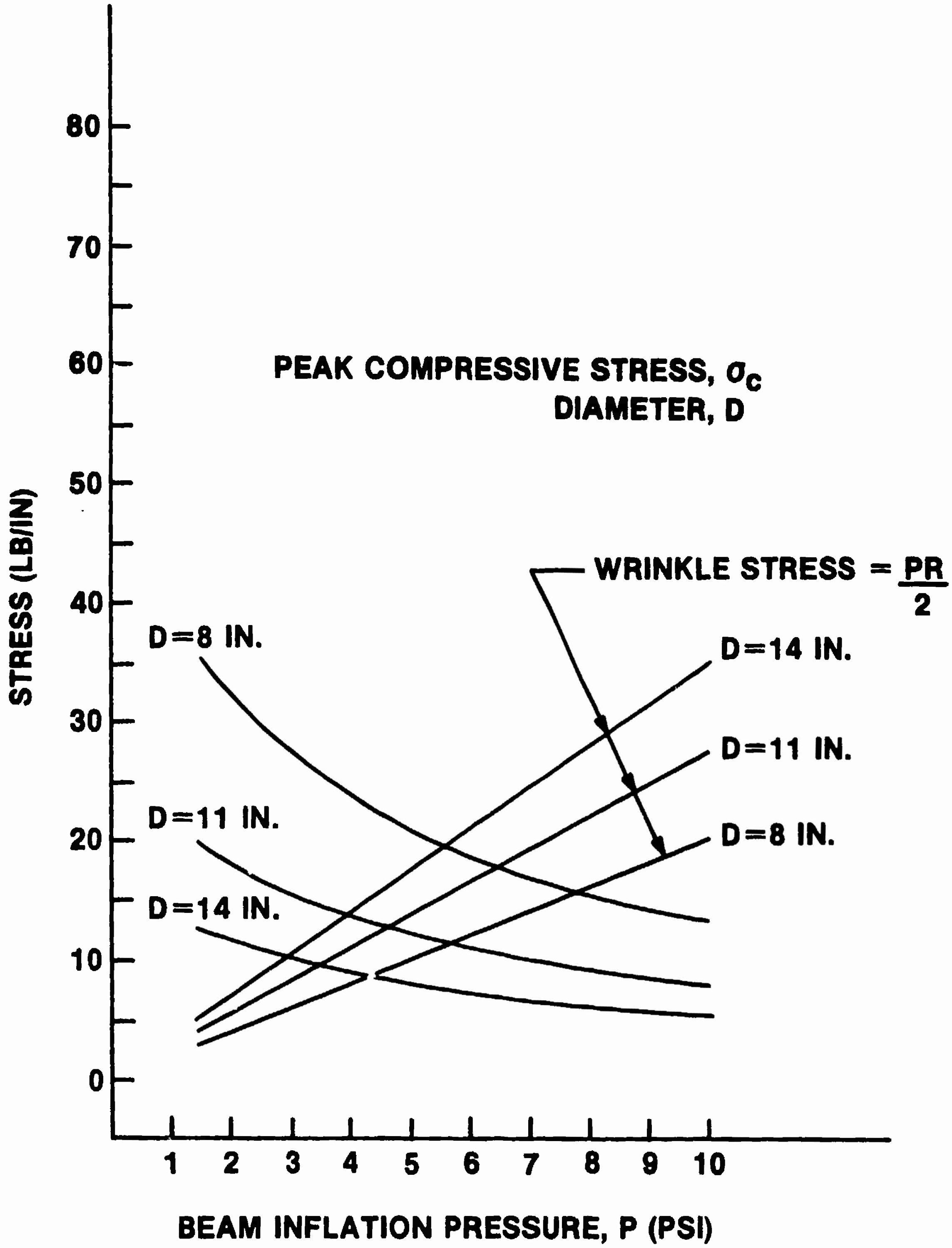

FIGURE C.15: Peak compressive and wrinkle stress vs. inflation pressure for 300 sq ft Leaning Arch BAS, 30 mph wind load

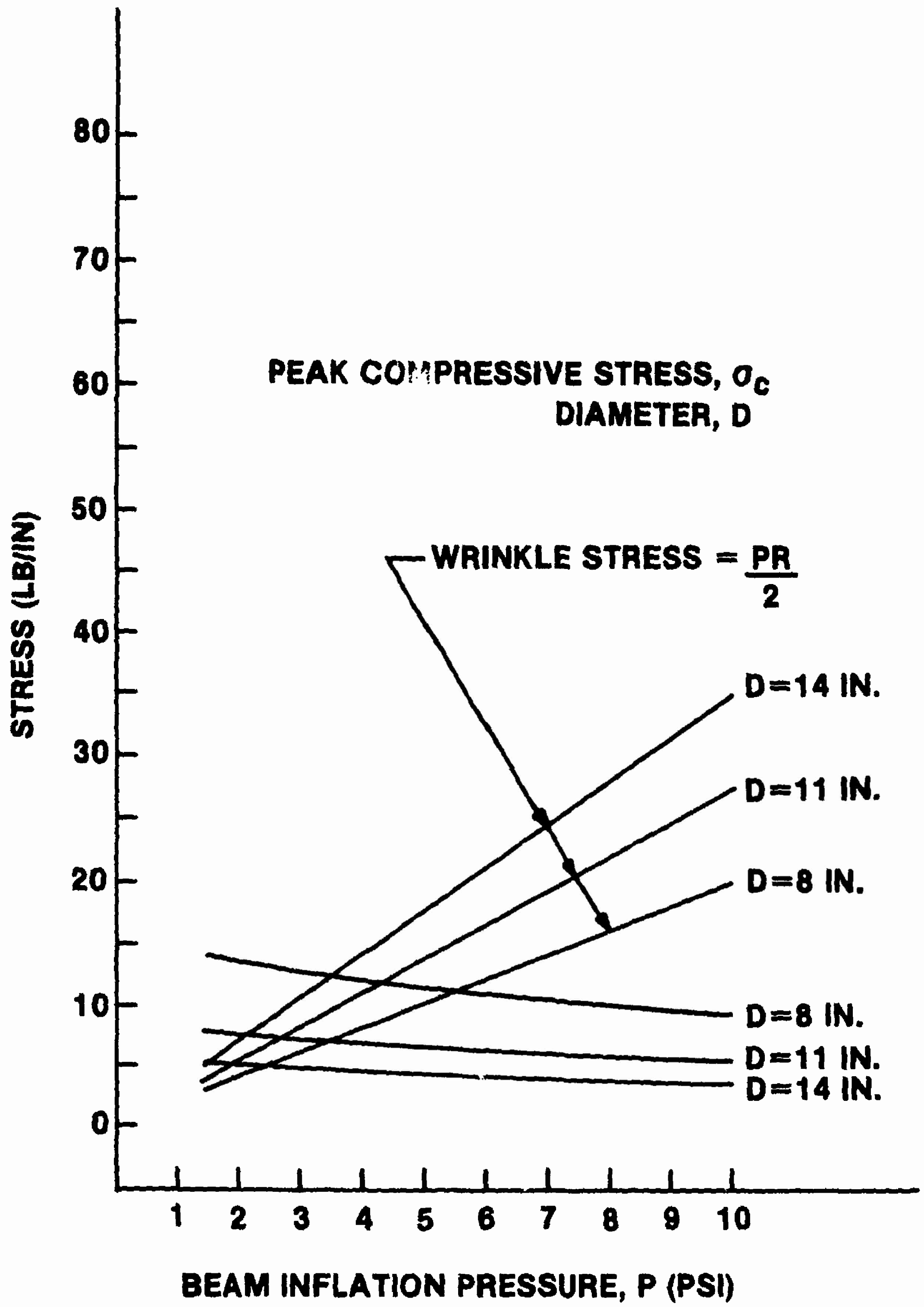

FIGURE C.16: Peak compressive and wrinkle stress vs. inflation pressure for 300 sq ft Leaning Arch BAS with guylines, 30 mph wind load

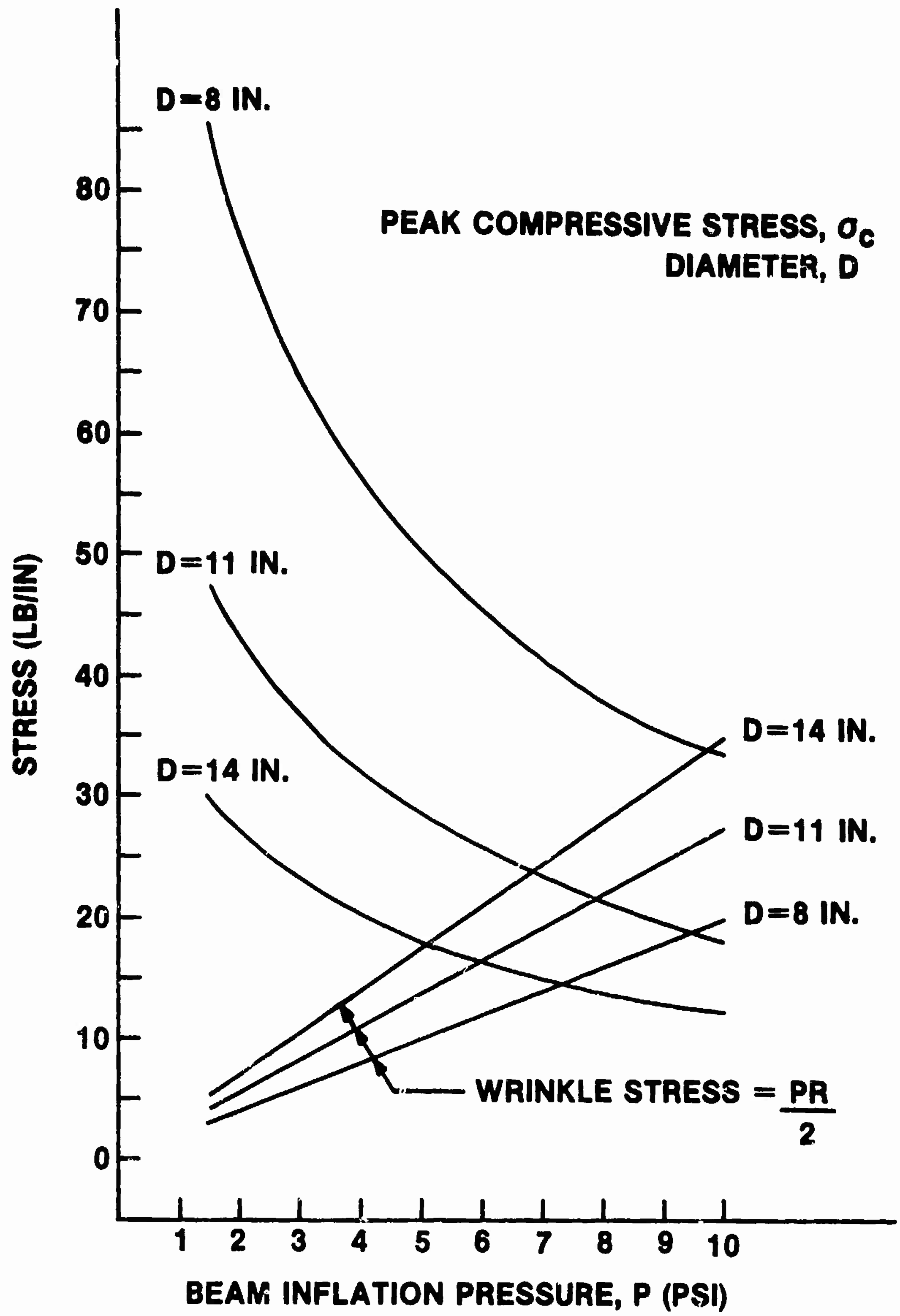

FIGURE C.17: Peak compressive and wrinkle stress vs. inflation pressure for 300 sq ft Leaning Arch BAS, 30 mph parallel wind load

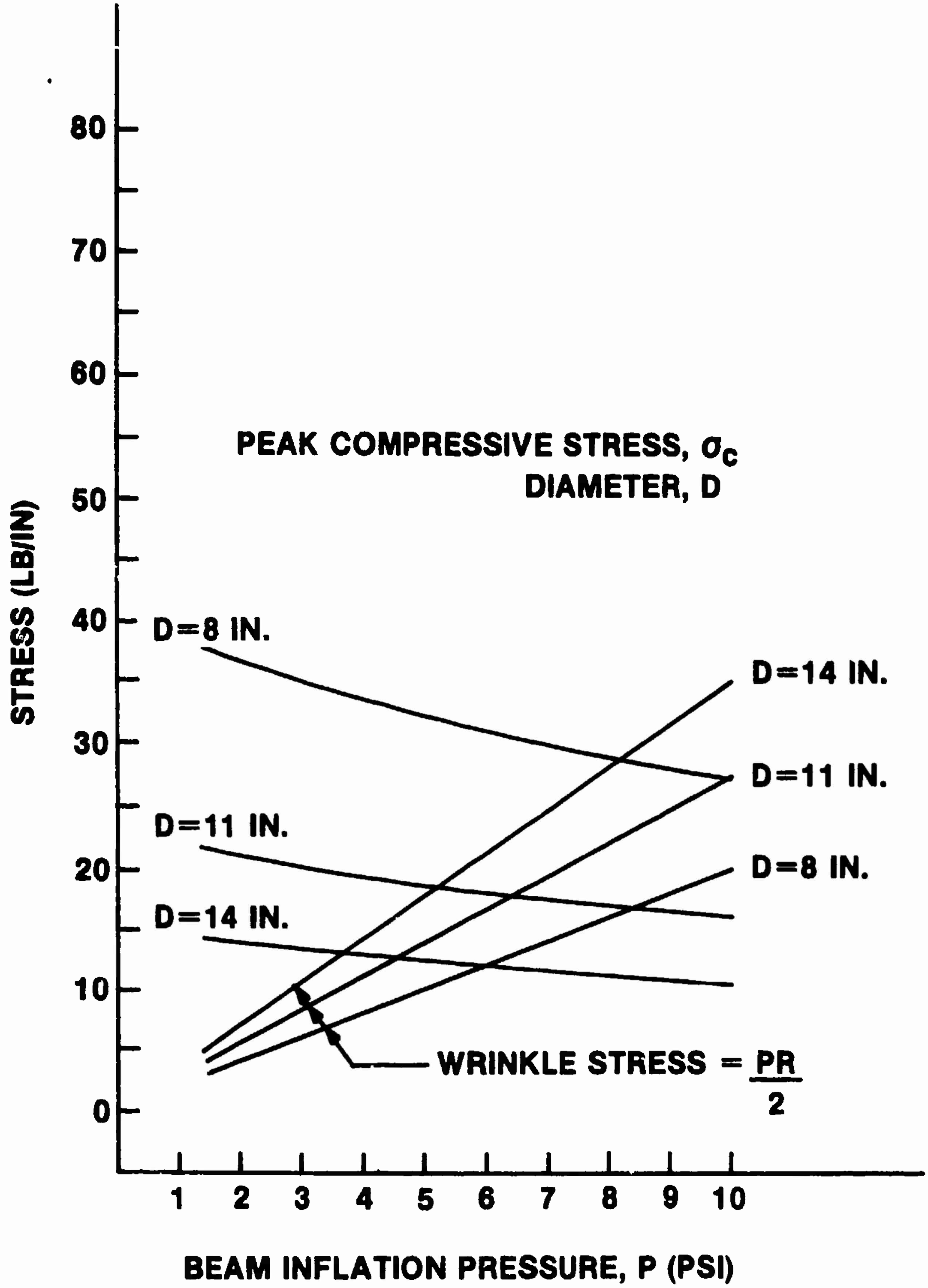

FIGURE C.18: Peak compressive and wrinkle stress vs. inflation pressure for 300 sq ft Leaning Arch BAS with guylines, 30 mph parallel wind load

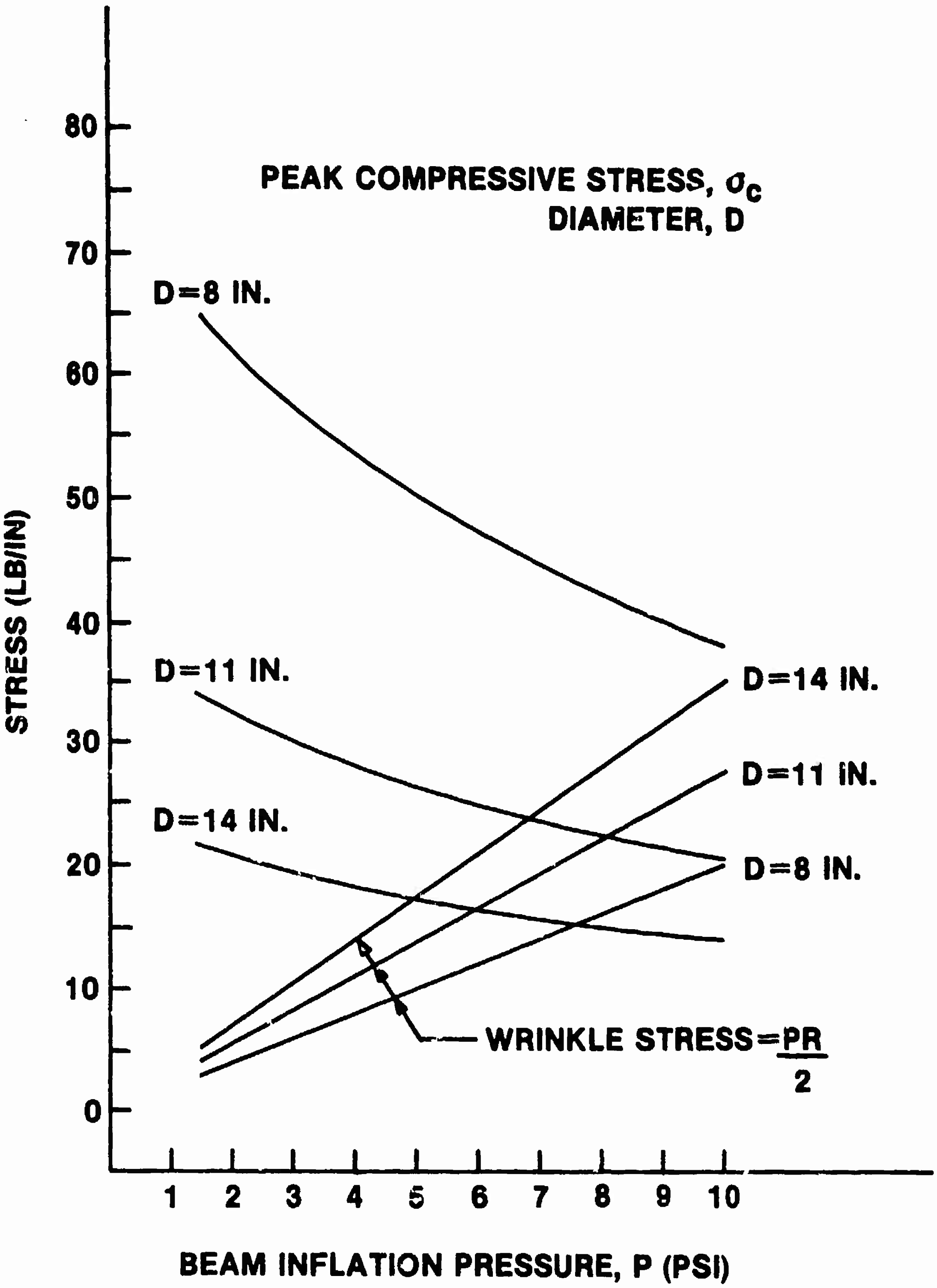

FIGURE C.19: Peak compressive and wrinkle stress vs. inflation pressure for 300 sq ft Vertical Arch BAS, 10 psf snow load

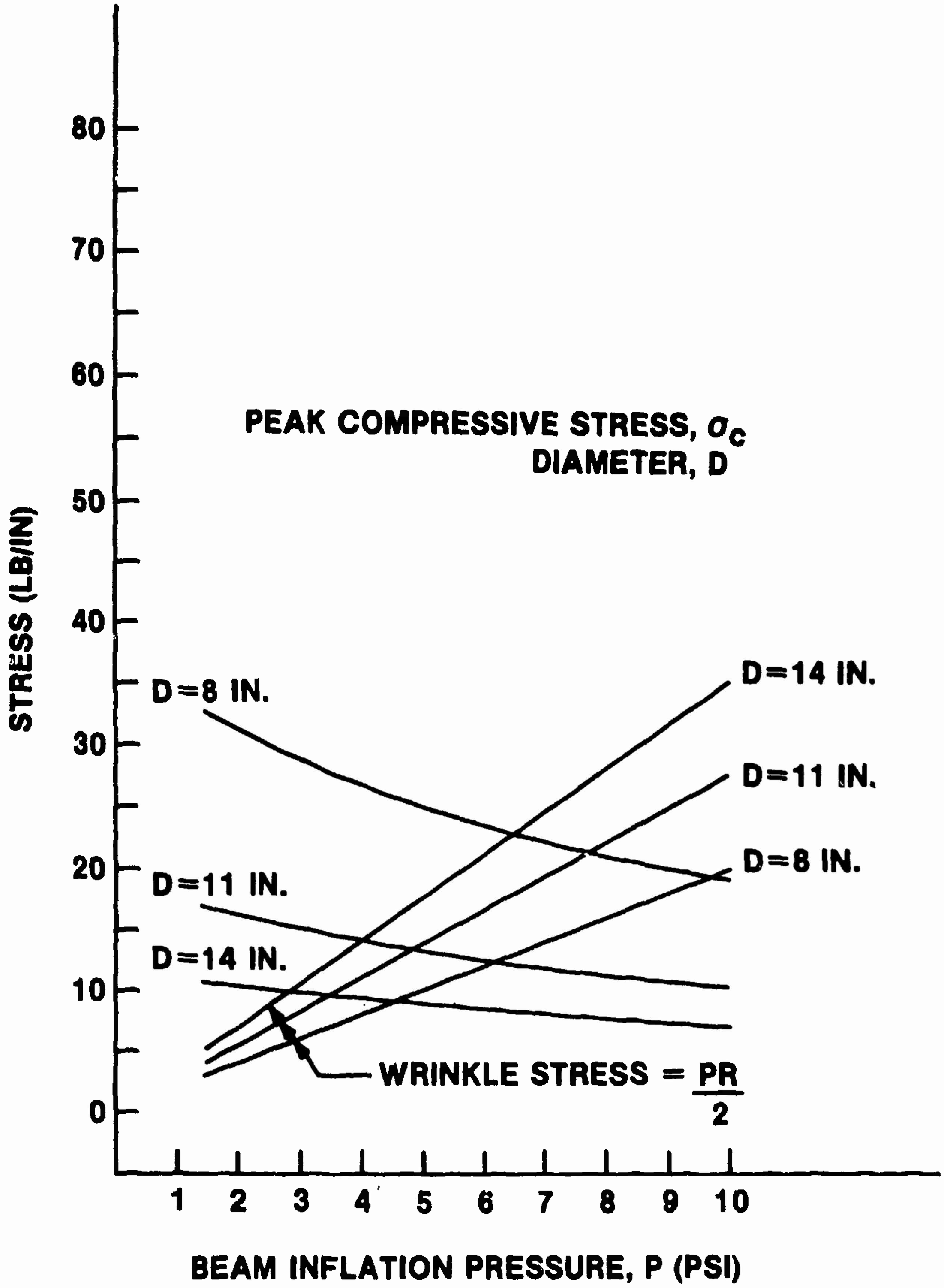

FIGURE C.20: Peak compressive and wrinkle stress vs. inflation pressure for 300 sq ft Vertical Arch BAS, 5 psf snow load

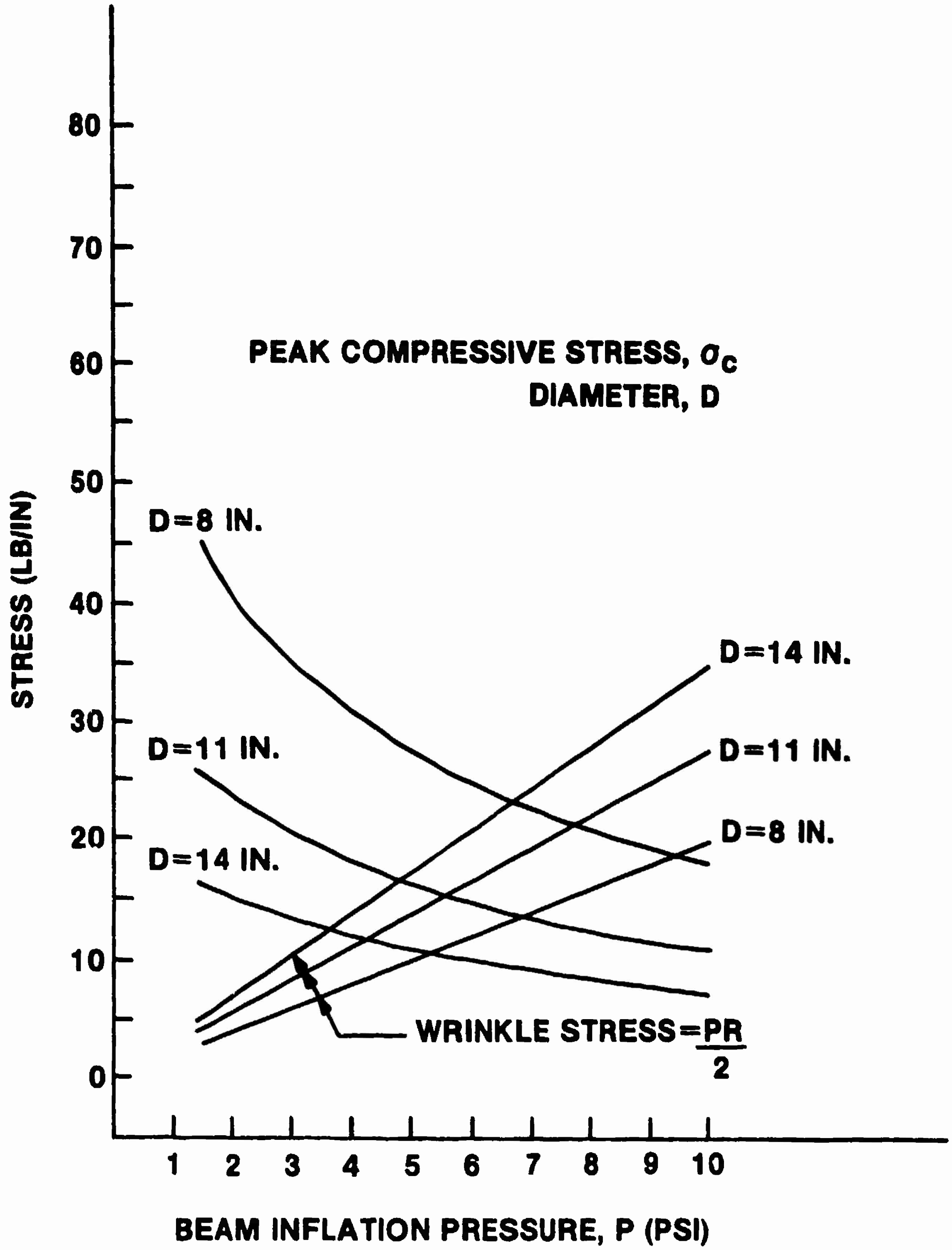

FIGURE C.21: Peak compressive and wrinkle stress vs. inflation pressure for 300 sq ft Vertical Arch BAS, 30 mph wind load

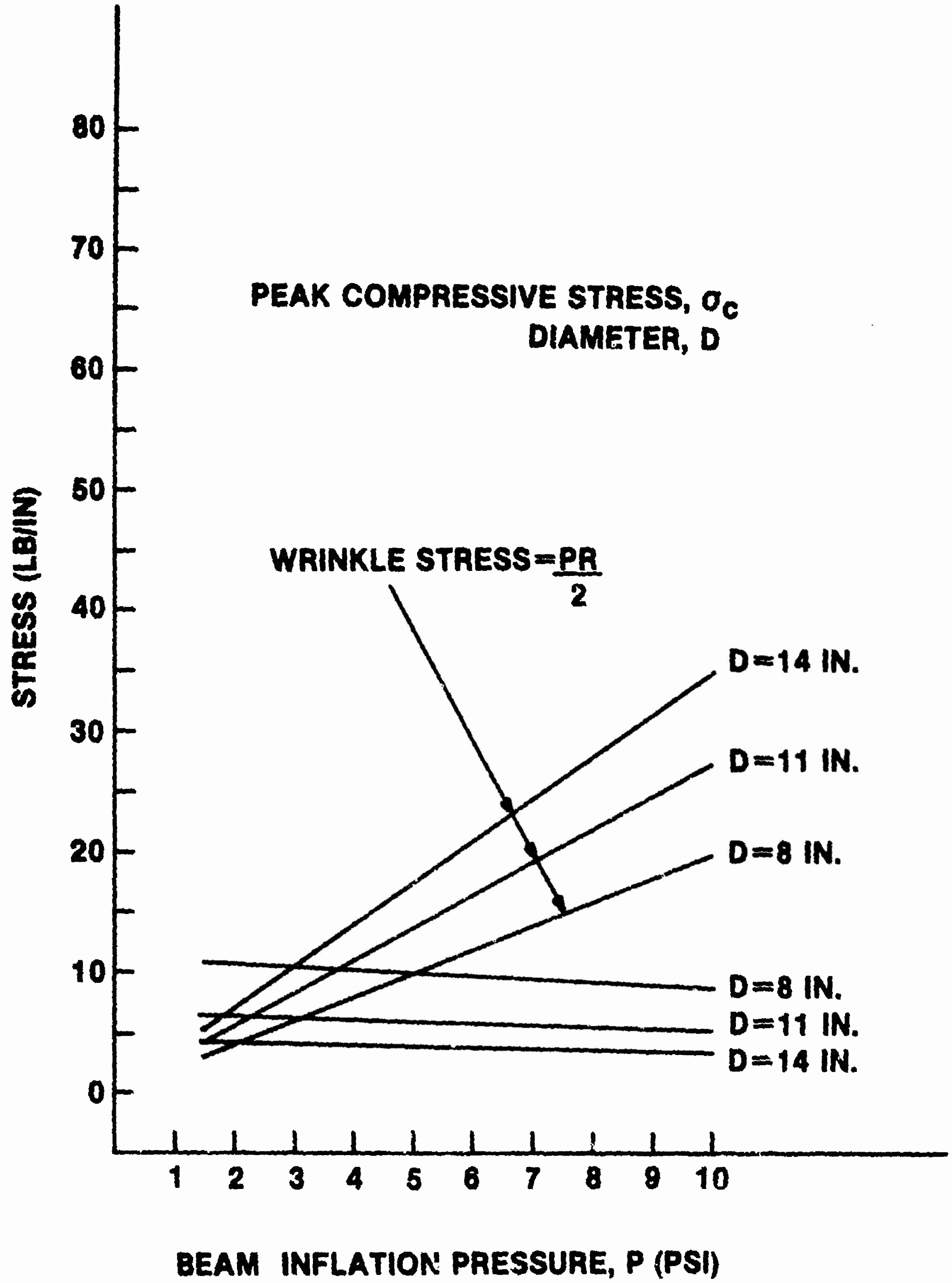

FIGURE C.22: Peak compressive and wrinkle stress vs. inflation pressure for 300 sq ft Vertical Arch BAS with guylines, 30 mph wind load

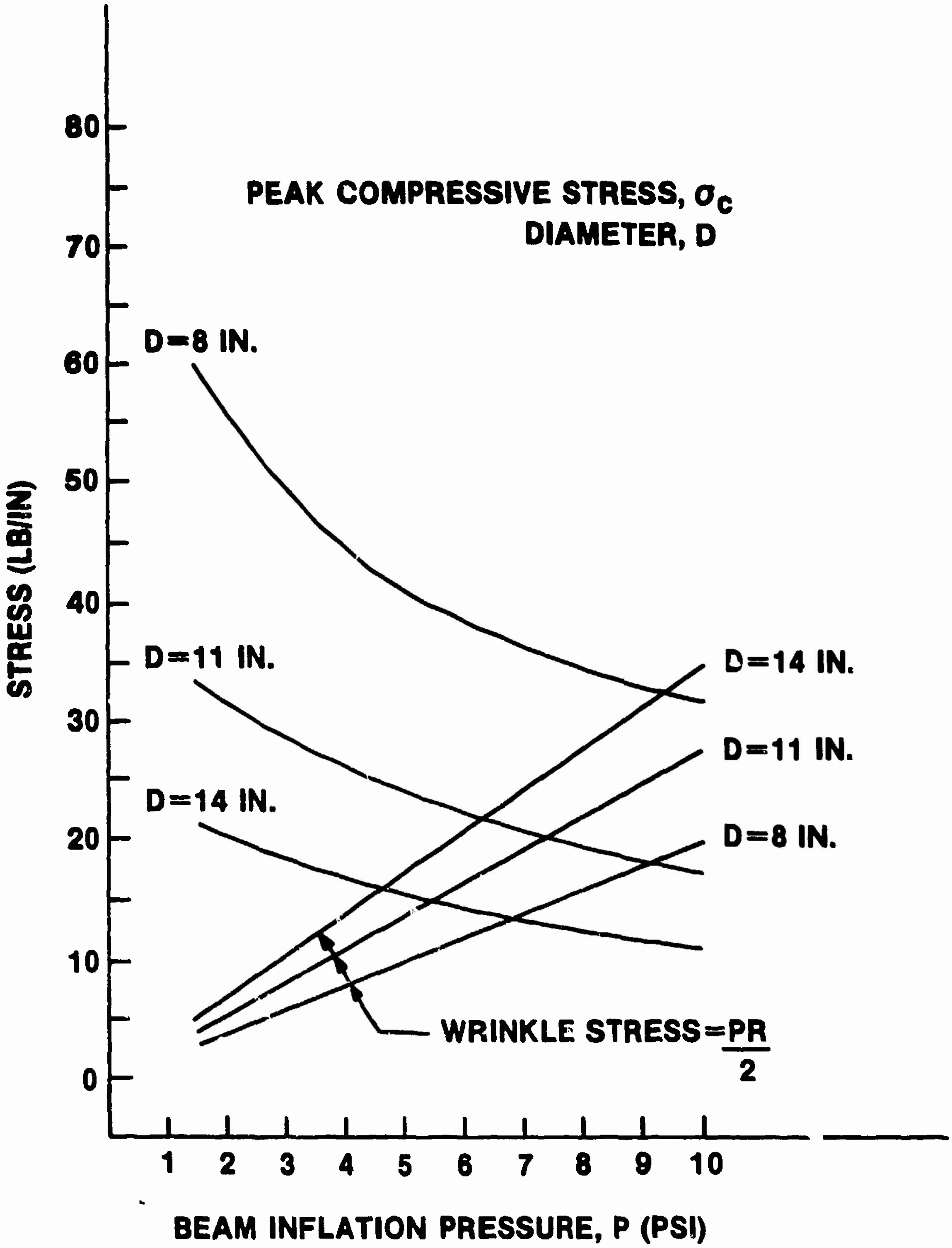

FIGURE C.23: Peak compressive and wrinkle stress vs. inflation pressure for 300 sq ft Vertical Arch BAS, 30 mph parallel wind load

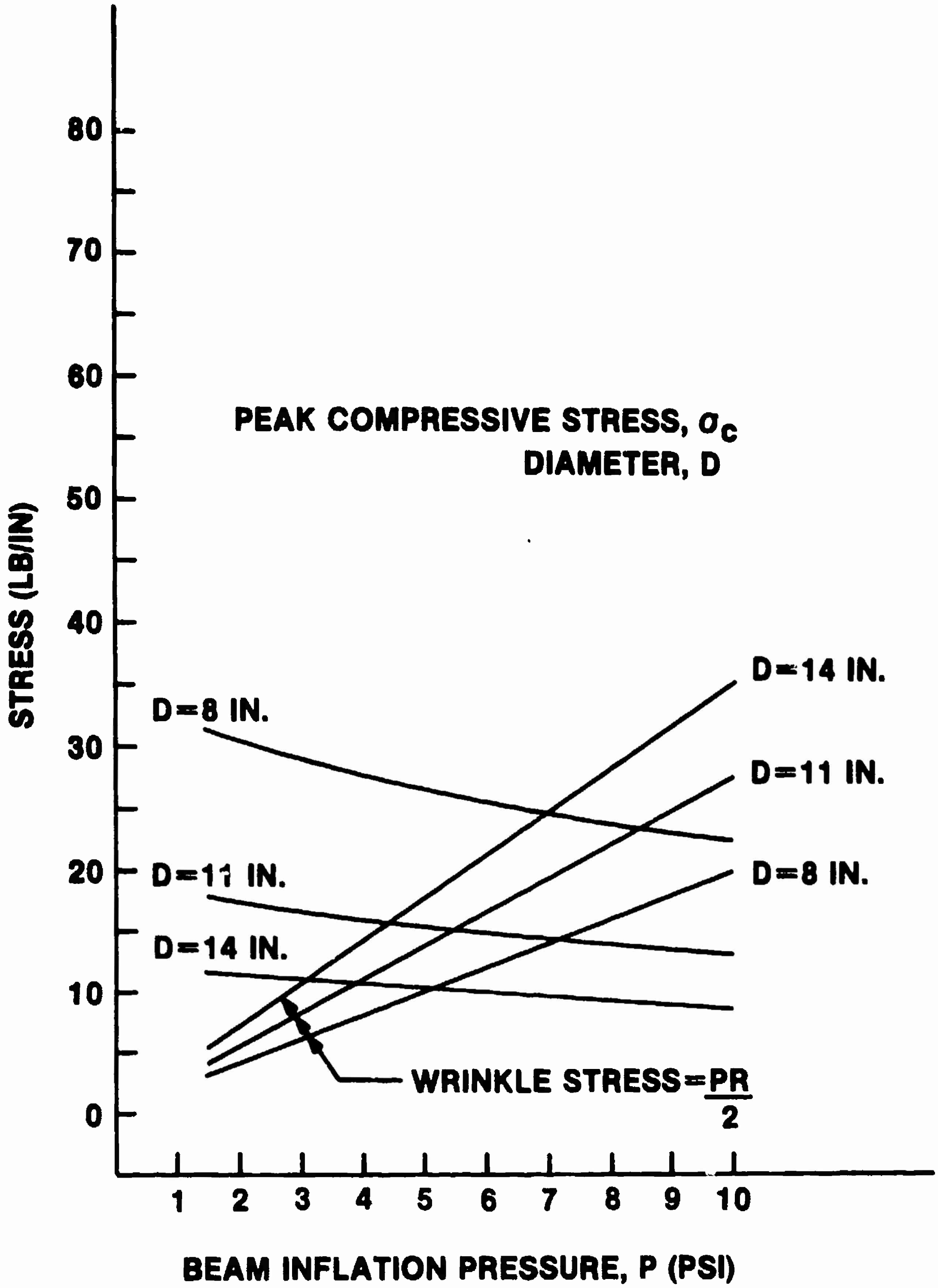

FIGURE C.24: Peak compressive and wrinkle stress vs. inflation pressure for 300 sq ft Vertical Arch BAS with guylines, 30 mph parallel wind load

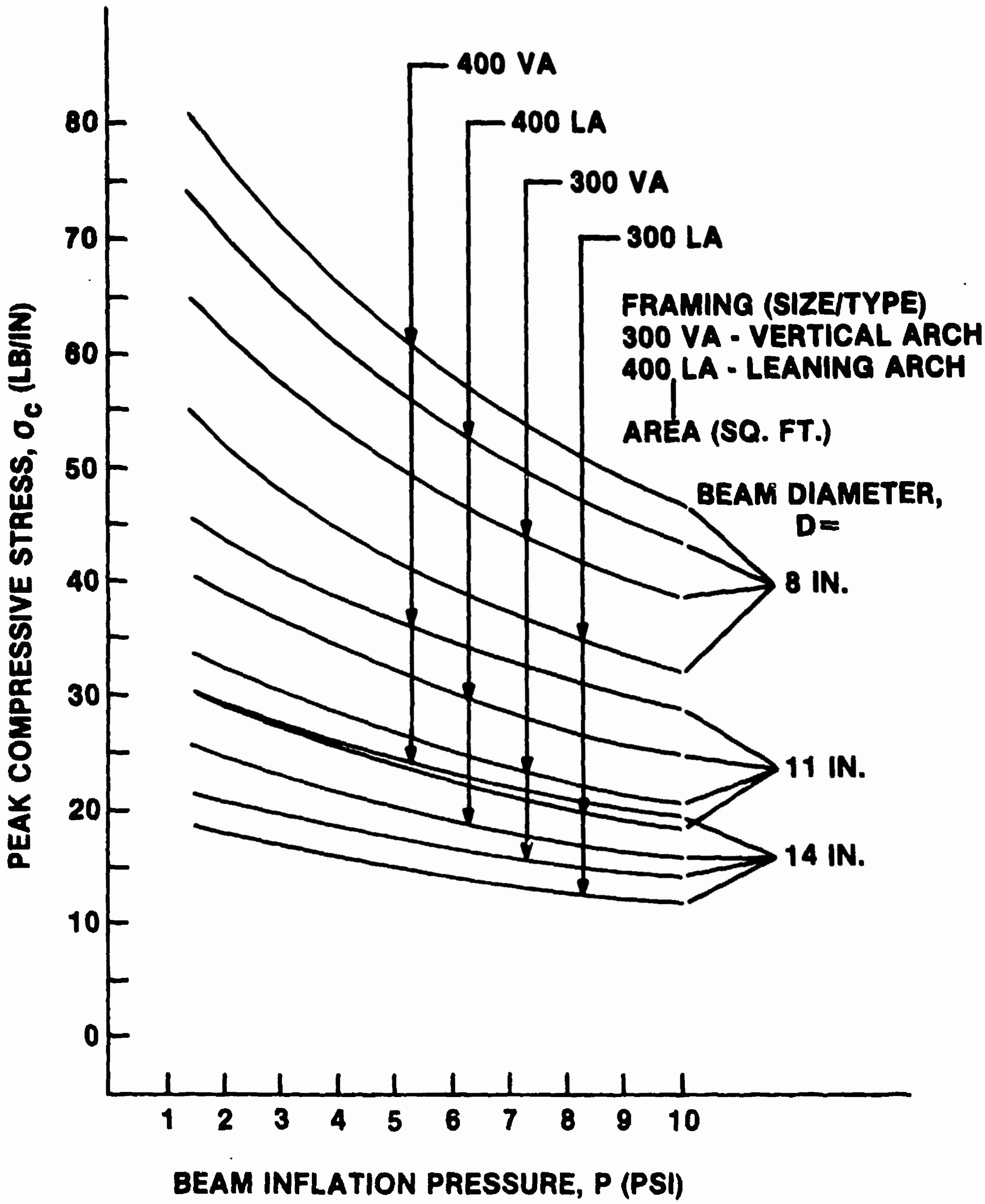

FIGURE C.25: <u>Peak compressive stress vs. beam inflation pressure for 10 psf snow load</u>

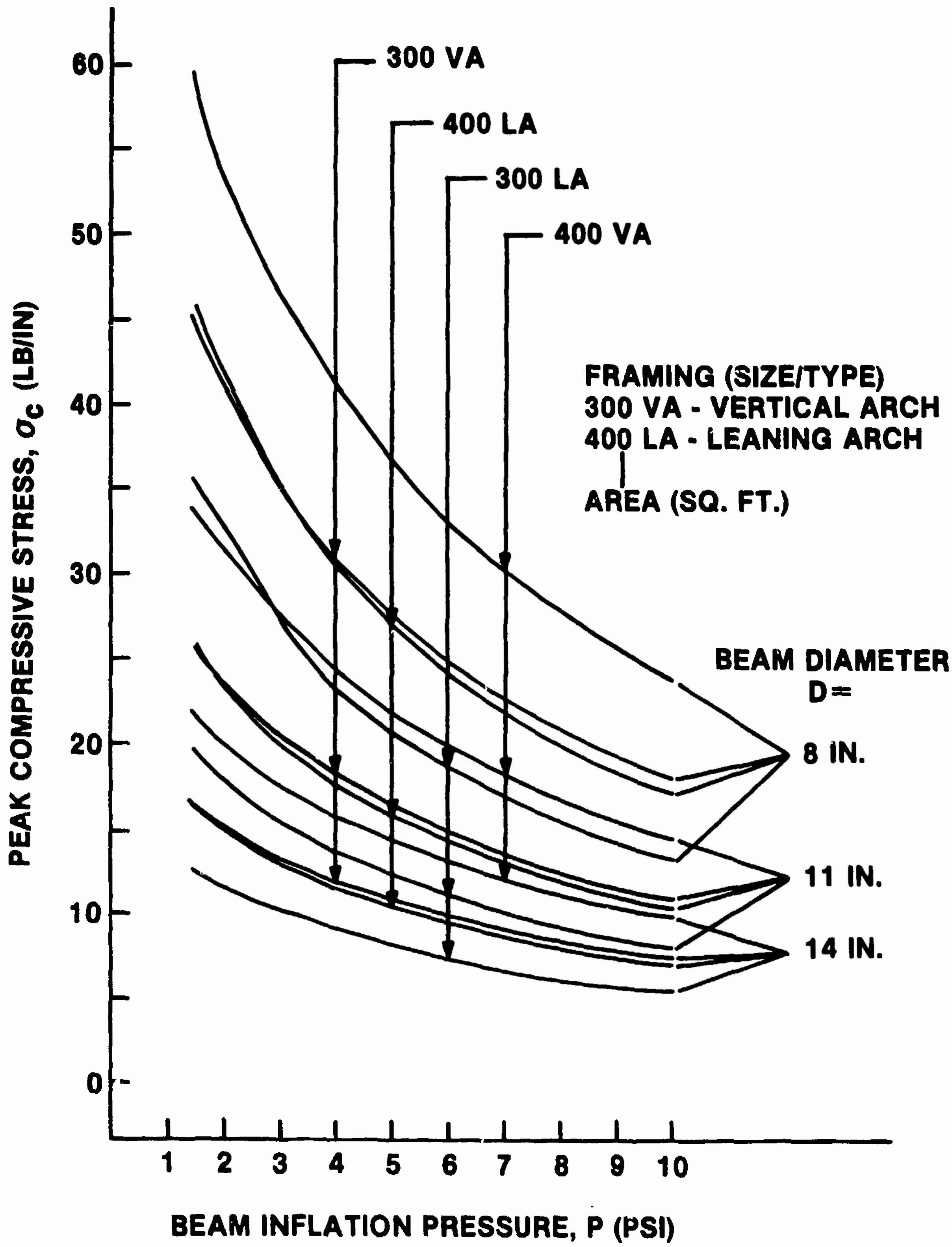

FIGURE C.26: Peak compressive stress vs. beam inflation pressure for 30 mph wind load

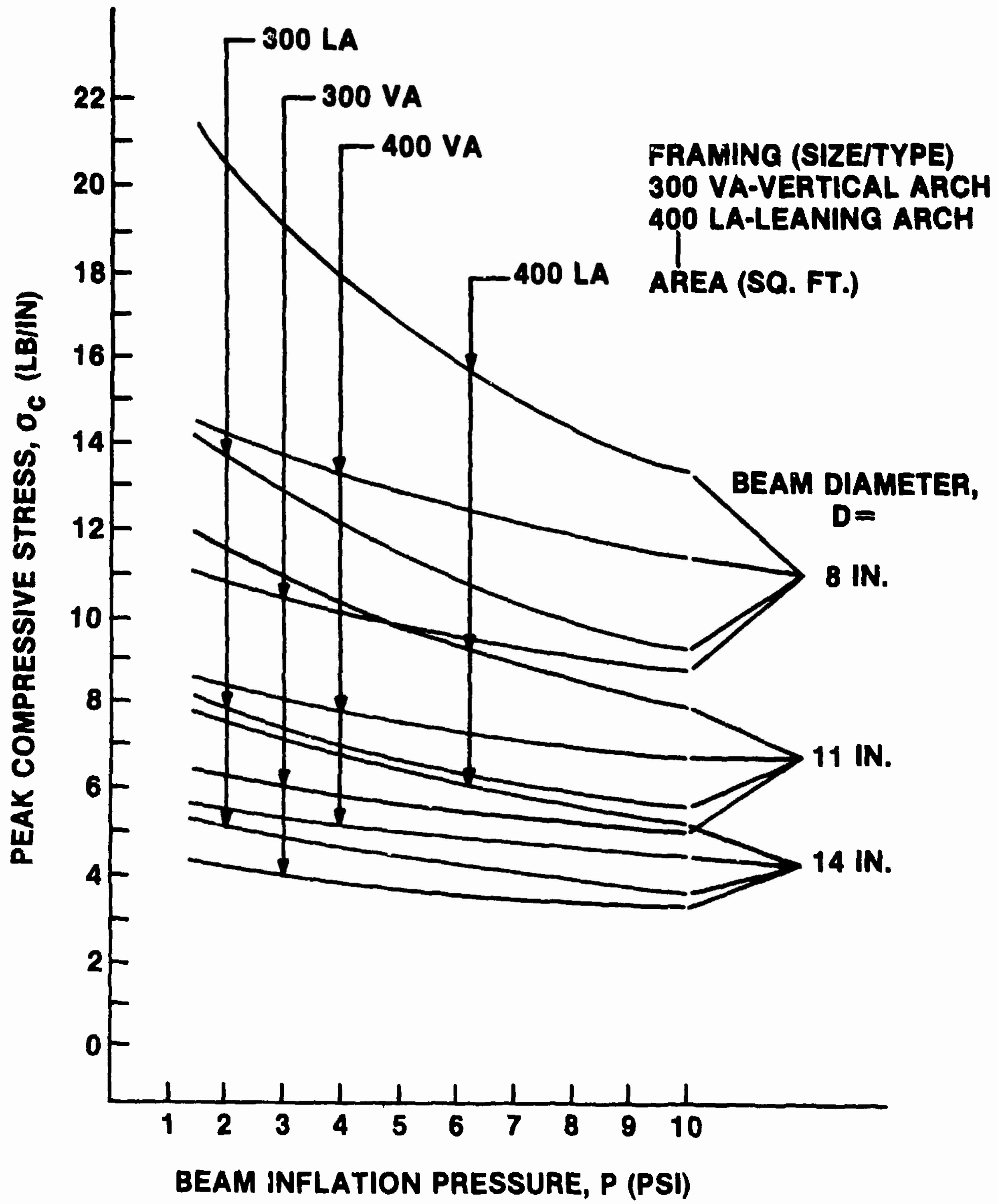

FIGURE C.27: Peak compressive stress vs. beam inflation pressure for 30 mph wind load (with guylines)

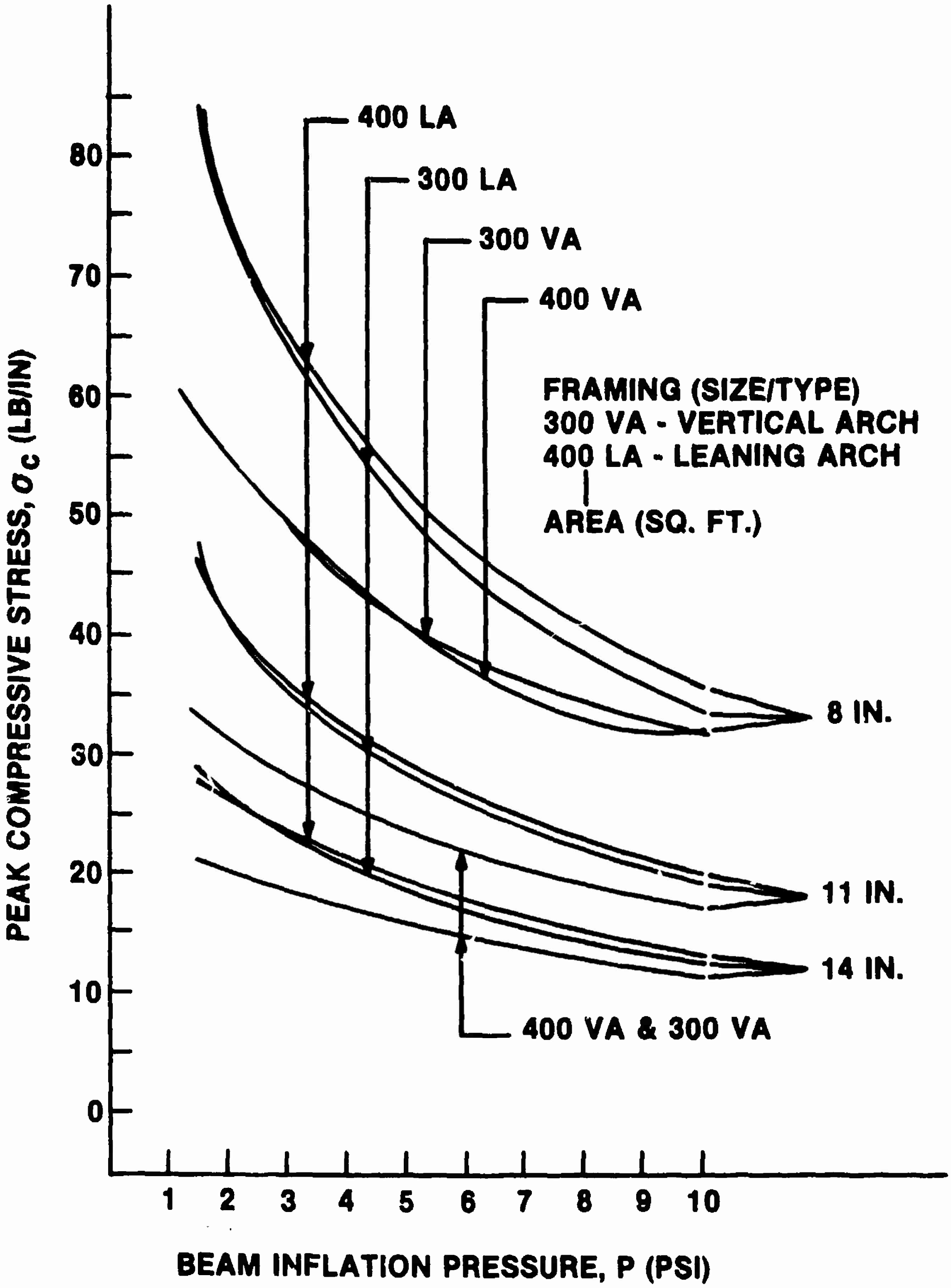

FIGURE C.28: Peak compressive stress vs. beam inflation pressure for 30 mph parallel wind load

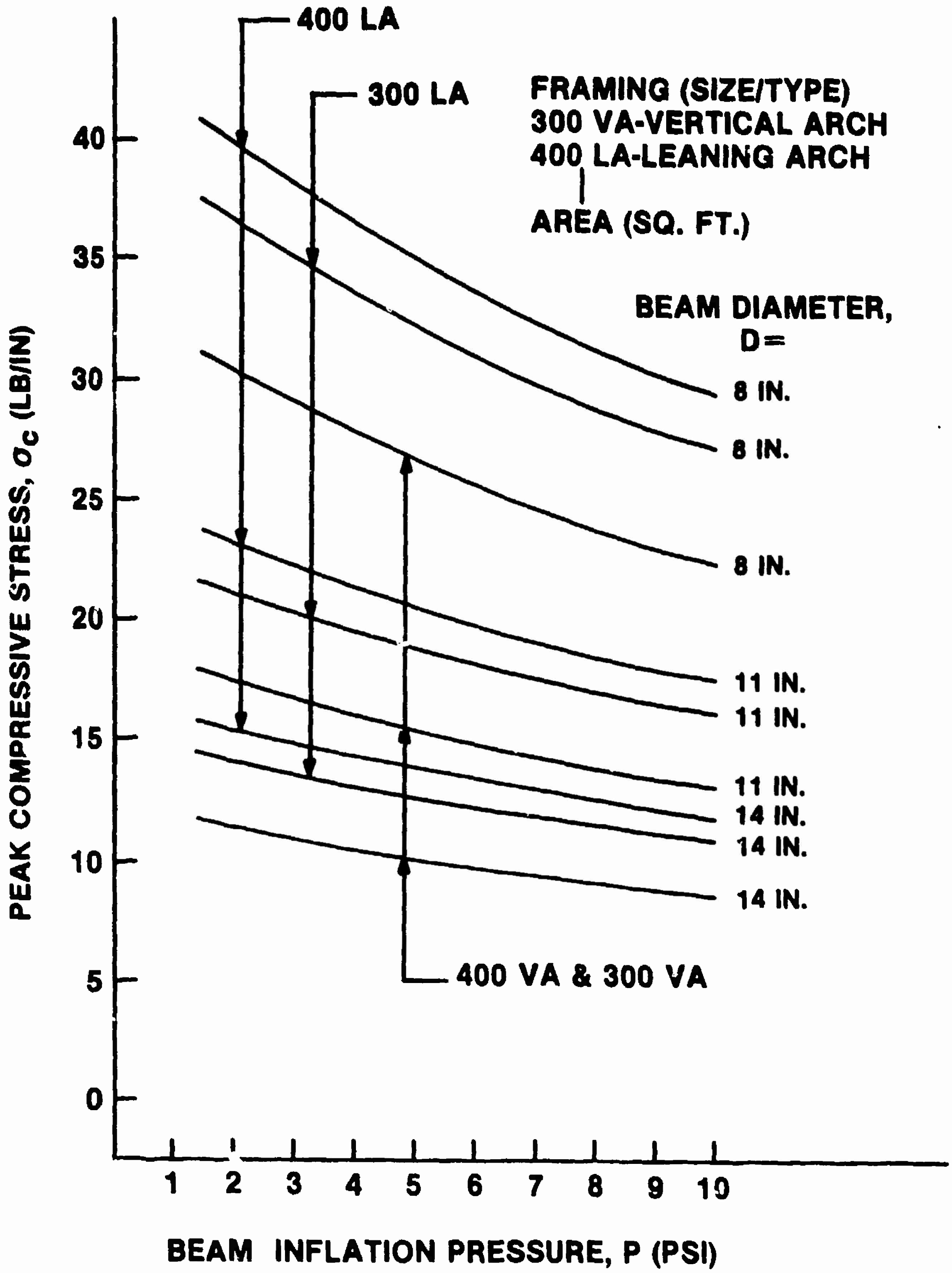

FIGURE C.29: Peak compressive stress vs. beam inflation pressure for 30 mph parallel wind load (with guylines)

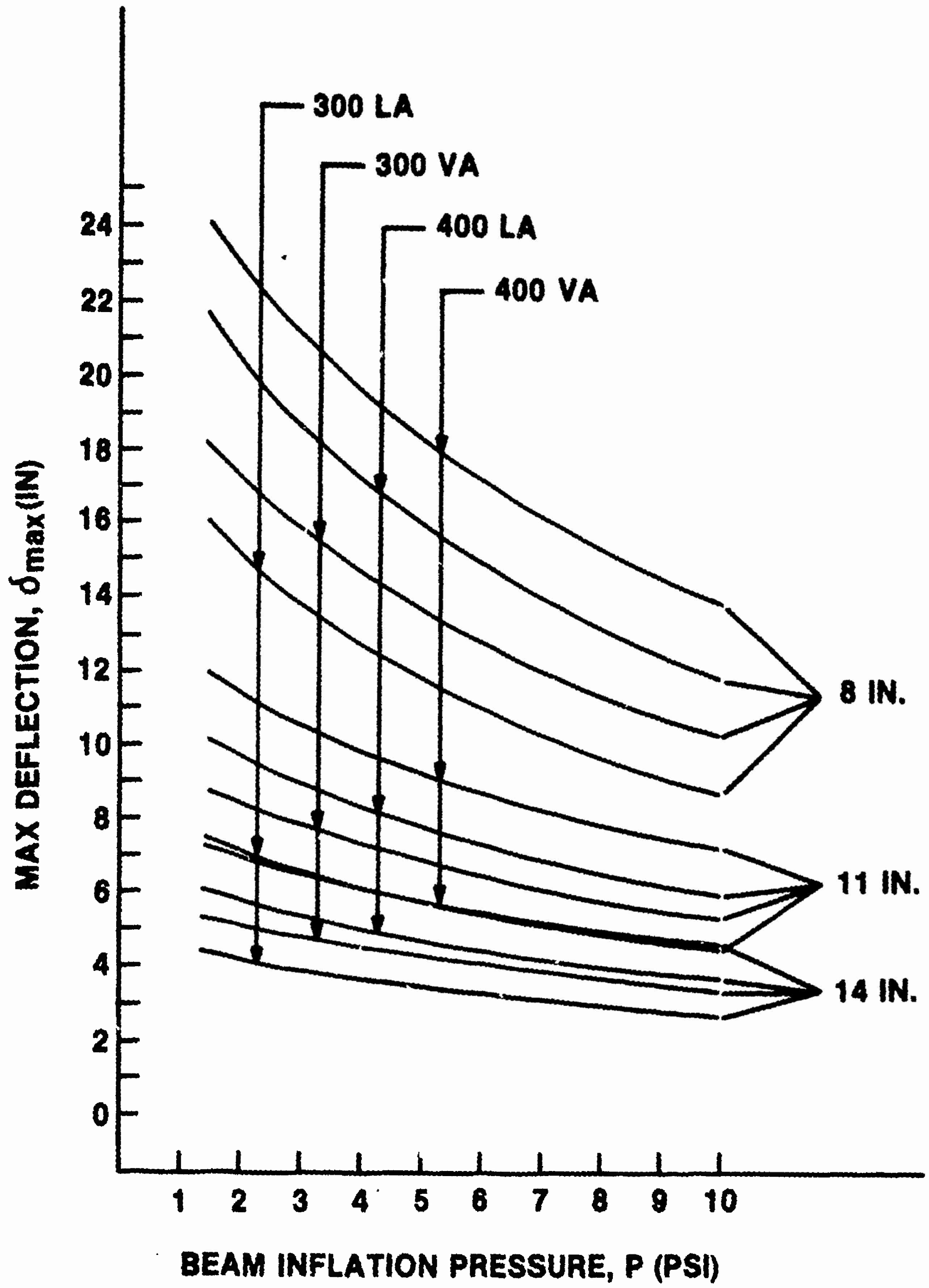

FIGURE C.30: Maximum deflection vs. beam inflation pressure for 10 psf snow load

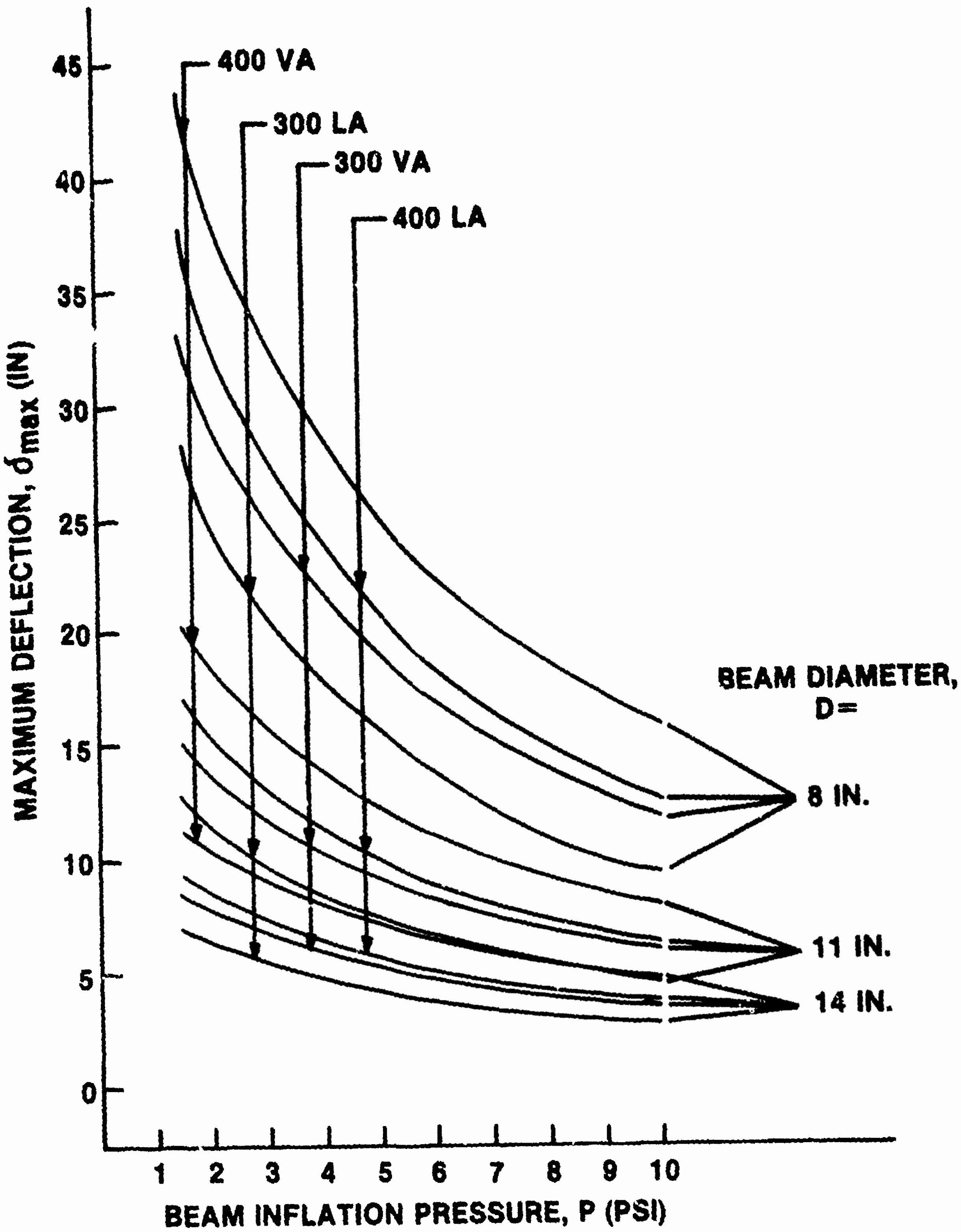

FIGURE C.31: Maximum deflection vs. beam inflation pressure for 30 mph wind load

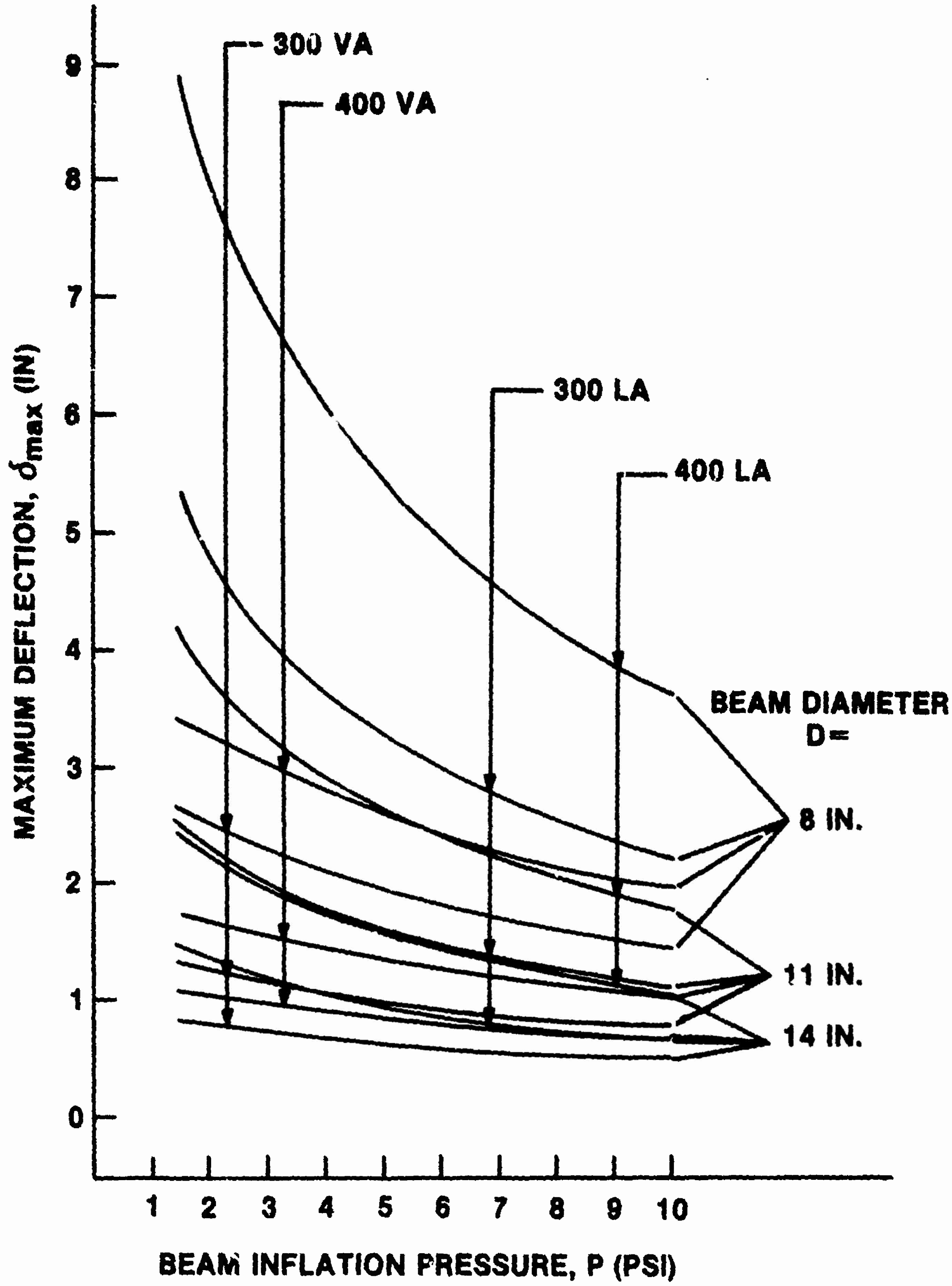

FIGURE C.32: Maximum deflection vs. beam inflation pressure for 30 mph wind load (with guylines)

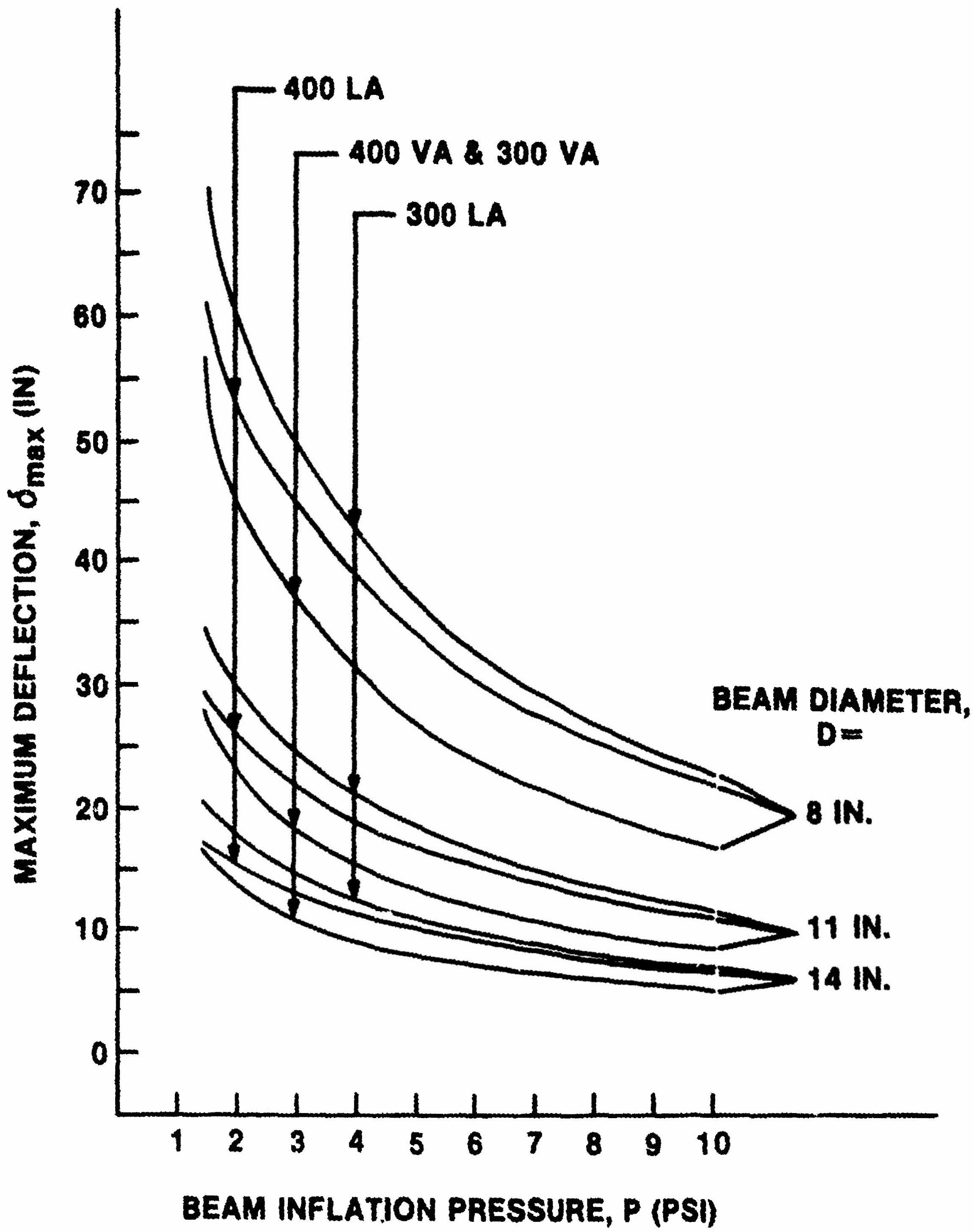

FIGURE C.33: Maximum deflection vs. beam inflation pressure for 30 mph parallel wind load

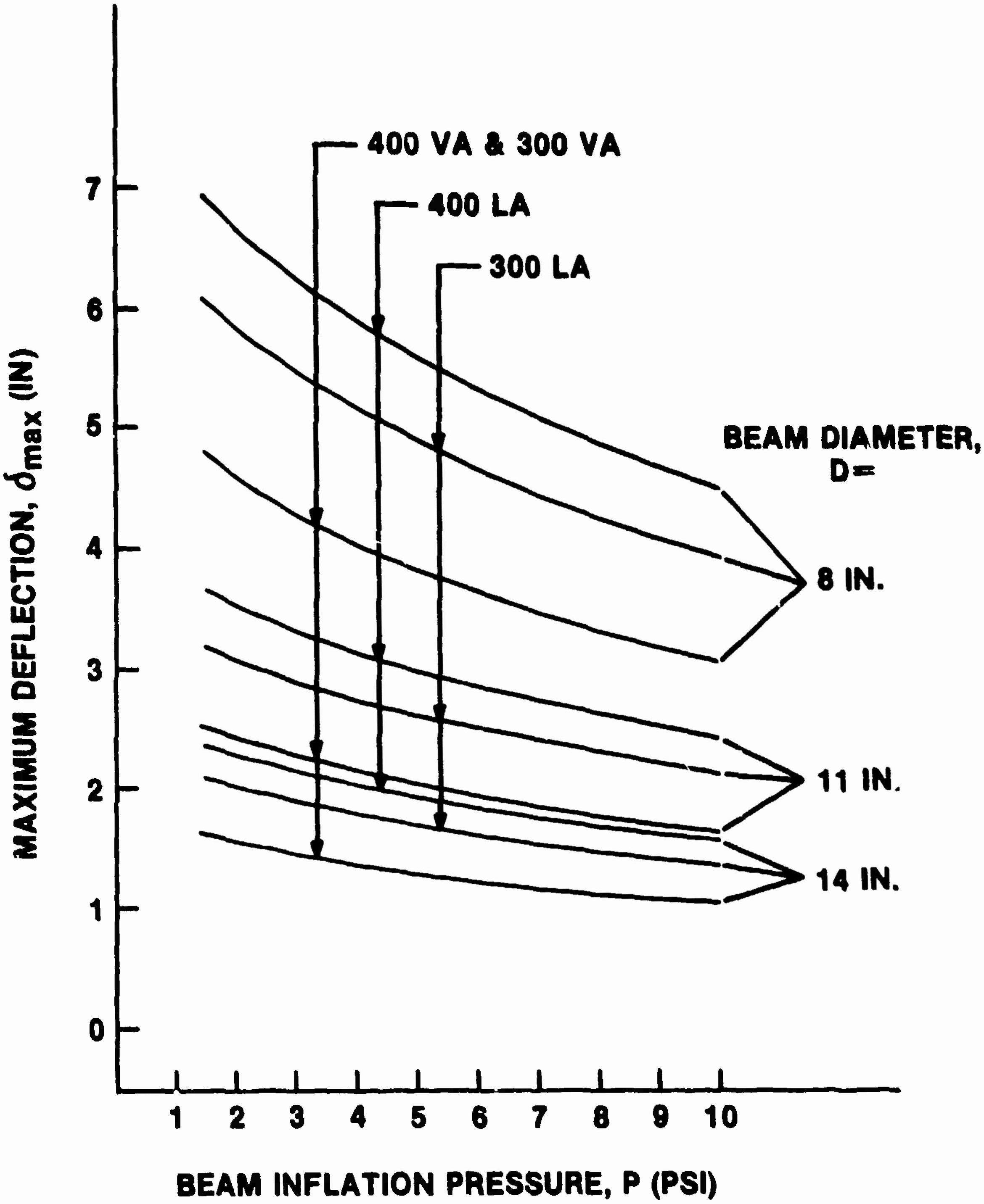

FIGURE C.34: Maximum deflection vs. beam inflation pressure for 30 mph parallel wind load (with guylines)

APPENDIX D

Tables of Minimum Required Pressure, Maximum Compressive Stress and Maximum Deflection vs. Beam Diameter For Each Load and Arrangement

TABLE D.1: 10 psf snow load, Minimum required pressure, maximum compressive stress, maximum deflection vs. beam diameters, D = 8, 11, 14 inches, for all arrangements

Framing Concept	Beam Diameter (in)	Minimum Required Pressure (psi)	Maximum Compressive Stress (lb/in)	Maximum Deflection (in)
400 sq ft Leaning Arch	8	-	-	-
	11	9.3	25.5	6.1
	14	5.6	19.5	4.5
400 sq ft Vertical Arch	8	-	-	-
	11	10.5	28.5	7.2
	14	6.5	22.8	5.4
300 sq ft Leaning Arch	8	-	-	-
	11	7.5	20.6	5.0
	14	4.45	15.7	3.6
300 sq ft Vertical Arch	8	-	-	-
	11	8.15	22.3	5.7
	14	5.0	17.6	4.2

TABLE D.2: 5 psf snow load, Minimum required pressure, maximum compressive stress, maximum deflection vs. beam diameters, D = 8, 11, 14 inches, for all arrangements

Framing Concept	Beam Diameter (in)	Minimum Required Pressure (psi)	Maximum Compressive Stress (lb/in)	Maximum Deflection (in)
400 sq ft Leaning Arch	8	-	-	-
	11	5.6	15.3	3.75
	14	3.2	11.3	2.65
400 sq ft Vertical Arch	8	-	-	-
	11	6.25	17.2	4.3
	14	3.75	13.1	3.1
300 sq ft Leaning Arch	8	8.6	17.2	4.67
	11	4.4	12.1	3.0
	14	2.5	8.9	2.05
300 sq ft Vertical Arch	8	9.7	19.4	5.2
	11	4.9	13.5	3.45
	14	2.8	10.0	2.4

TABLE D.3: 30 mph wind load, Minimum required pressure, maximum compressive stress, maximum deflection vs. beam diameters, D = 8, 11, 14 inches, for all arrangements

Framing Concept	Beam Diameter (in)	Minimum Required Pressure (psi)	Maximum Compressive Stress (lb/in)	Maximum Deflection (in)
400 sq ft Leaning Arch	8	9.1	18.2	13.6
	11	5.5	15.2	9.4
	14	3.55	12.3	6.8
400 sq ft Vertical Arch	8	-	-	-
	11	6.8	18.7	10.2
	14	4.35	15.4	7.6
300 sq ft Leaning Arch	8	7.8	15.6	11.25
	11	4.65	12.8	7.75
	14	2.9	10.2	5.6
300 sq ft Vertical Arch	8	9.4	18.8	12.5
	11	5.6	15.5	8.6
	14	3.6	12.6	6.25

TABLE D.4: 30 mph wind load, Minimum required pressure, maximum compressive stress, maximum deflection vs. beam diameters, D = 8, 11, 14 inches, for all arrangements with guylines

Framing Concept	Beam Diameter (in)	Minimum Required Pressure (psi)	Maximum Compressive Stress (lb/in)	Maximum Deflection (in)
400 sq ft Leaning Arch	8	7.5	15.0	4.35
	11	3.75	10.4	3.0
	14	2.1	7.5	2.2
400 sq ft Vertical Arch	8	6.2	12.3	2.4
	11	2.9	8.0	1.55
	14	1.6	5.8	1.08
300 sq ft Leaning Arch	8	5.6	11.2	3.1
	11	2.65	7.3	2.08
	14	1.5	5.19	1.46
300 sq ft Vertical Arch	8	4.85	9.7	1.97
	11	2.25	6.3	1.23
	14	1.5	4.22	0.81

TABLE D.5: 30 mph parallel wind load, Minimum required pressure, maximum compressive stress, maximum deflection vs. beam diameters, D = 8, 11, 14 inches, for all arrangements

Framing Concept	Beam Diameter (in)	Minimum Required Pressure (psi)	Maximum Compressive Stress (lb/in)	Maximum Deflection (in)
400 sq ft Leaning Arch	8	-	-	-
	11	8.2	22.4	13.4
	14	5.2	18.2	10.0
400 sq ft Vertical Arch	8	-	-	-
	11	7.3	20.0	10.5
	14	4.55	16.1	8.3
300 sq ft Leaning Arch	8	-	-	-
	11	7.9	21.8	13.5
	14	5.1	18.0	10.9
300 sq ft Vertical Arch	8	-	-	-
	11	7.3	20.2	10.5
	14	4.55	16.1	8.3

TABLE D.6: 30 mph parallel wind load, Minimum required pressure, maximum compressive stress, maximum deflection vs. beam diameters, D = 8, 11, 14 inches, for all arrangements with guylines

Framing Concept	Beam Diameter (in)	Minimum Required Pressure (psi)	Maximum Compressive Stress (lb/in)	Maximum Deflection (in)
400 sq ft Leaning Arch	8	-	-	-
	11	7.0	19.2	2.75
	14	4.0	14.1	2.05
400 sq ft Vertical Arch	8	-	-	-
	11	5.5	15.2	2.0
	14	3.1	11.0	1.46
300 sq ft Leaning Arch	8	-	-	-
	11	6.45	17.9	2.48
	14	3.7	13.2	1.82
300 sq ft Vertical Arch	8	-	-	-
	11	5.5	15.1	2.0
	14	3.15	11.0	1.46